Maize (*Zea mays* L.) nucleoskeletal proteins regulate nuclear envelope remodeling and function in stomatal complex development and pollen viability.

McKenna JF*†, Gumber HK*, Turpin ZM, Jalovec AM, Kartick AC, Graumann K#, and Bass HW#

*co-first authors, equal contributions

co-corresponding authors

email addresses:

Joseph F. McKenna, josephmckenna@brookes.ac.uk, Department of Biological and Medical Sciences, Oxford Brookes University, Oxford, UK

† Current address: Joe.McKenna@Warwick.ac.uk, School of Life Sciences, University of Warwick, Coventry, CV4 7AL, UK, ORCID 0000-0003-4838-6048

Hardeep K. Gumber, hkg12@my.fsu.edu, Department of Biological Science, Florida State University, Tallahassee, FL, USA, ORCID 0000-0001-5250-7207

Zachary M. Turpin, zmt11@my.fsu.edu, Department of Biological Science, Florida State University, Tallahassee, FL, USA

Alexis M. Jalovec, amj13e@my.fsu.edu, Department of Biological Science, Florida State University, Tallahassee, FL, USA

Andre C. Kartick, ack17@my.fsu.edu, Department of Biological Science, Florida State University, Tallahassee, FL, USA

Katja Graumann, kgraumann@brookes.ac.uk, Department of Biological and Medical Sciences, Oxford Brookes University, Oxford, UK

Hank W. Bass, bass@bio.fsu.edu, Department of Biological Science, Florida State University, Tallahassee, FL, USA, ORCID 0000-0003-0522-0881

Author Approval: All authors approve of this manuscript for preprint server biorxiv.

Competing Interests: All the authors declare no competing interest.

ABSTRACT

In eukaryotes, the nuclear envelope (NE) encloses chromatin and separates it from the rest of the cell. The Linker of Nucleoskeleton and Cytoskeleton (LINC) complex physically bridges across the NE, linking nuclear and cytoplasmic components. In plants, these LINC complexes are beginning to be ascribed roles in cellular and nuclear functions, including chromatin organization, regulation of nuclei shape and movement, and cell division. Homologs of core LINC components, KASH and SUN proteins, have previously been identified in maize. Here, we characterized the presumed LINC-associated maize nucleoskeletal proteins NCH1 and NCH2, homologs of members of the plant NMCP/CRWN family, and MKAKU41, homologous to AtKAKU4. All three proteins localized to the nuclear periphery when transiently and heterologously expressed as fluorescent protein fusions in *Nicotiana benthamiana*. Overexpression of MKAKU41 caused dramatic changes in the organization of the nuclear periphery, including nuclear invaginations that stained positive for non-nucleoplasmic markers of the inner and outer NE, and the ER. The severity of these invaginations was altered by changes in LINC connections and the actin cytoskeleton. In maize, MKAKU41 appeared to share genetic functions with other LINC components, including control of nuclei shape, stomatal complex development, and pollen viability. Overall, our data show that NCH1, NCH2, and MKAKU41 have characteristic properties of LINC-associated plant nucleoskeletal proteins, including interactions with NE components suggestive of functions at the nuclear periphery that impact the overall nuclear architecture.

Keywords (4-6): Nucleus, Nuclear Envelope, Maize, Lamin, Nucleoskeleton, kaku4, Peripheral Nucleoplasm

INTRODUCTION

In plant cells, as with all eukaryotes, the nucleus is a conspicuous and characteristic organelle, housing the DNA (reviewed by (Meier et al. 2017)). The nucleus itself is a dynamic structure, organized largely by its enclosing membrane system - the nuclear envelope (NE). The NE is a double-membraned structure composed of an outer nuclear membrane (ONM) and an inner nuclear membrane (INM) connected at nuclear pores (reviewed by (Hetzer 2010; Graumann and Evans 2017). The functional properties of the NE are mediated by protein complexes linked to myriad cellular and nuclear processes, including cell division and gene expression (Kim et al. 2015; Meier et al. 2017; De Magistris and Antonin 2018; Pradillo et al. 2019). A major conserved NE complex is the linker of nucleoskeleton and cytoskeleton (LINC) complex (Crisp et al. 2006), known for it involvement in processes such as the maintenance of nuclear architecture and mechanical structures, signalling, nuclear motility, and nuclear positioning (reviewed by (Rothballer and Kutay 2013), (Chang et al. 2015; Tamura et al. 2015; Pradillo et al. 2019; Starr 2019). Well beyond the historically recognized role of compartmentalization, NE investigations increasingly address how the NE contributes to both general and specialized functions in plant growth and development. The underlying molecular mechanisms coordinating and regulating these fundamental NE processes remain, however, largely unknown.

The hallmark of LINC complexes is their ability to form direct connections bridging the cytoplasm and the nucleoplasm. This is accomplished by a core complex of two groups of proteins, residing on the two separate membranes of the NE. The INM

houses the Sad1/UNC84 homology (SUN) domain proteins and the ONM houses the Klarsicht/ANC-1/Syne homology (KASH) proteins (Hagan and Yanagida 1995; Malone et al. 1999; Starr 2002; Murphy et al. 2010). As a group, the KASH proteins are numerous and diverse, reflecting their various cytoplasmic binding partners, such as cytoskeletal and motor proteins (Starr and Fridolfsson 2010; Luxton and Starr 2014; Kim et al. 2015; Evans and Graumann 2018; Starr 2019). In contrast, the SUN-domain proteins are less diverse but still exhibit interactions with multiple components of the nucleoplasm, such as nucleoskeletal components and chromatin proteins (Haque et al. 2006; Janin et al. 2017). While cytoskeletal components of LINC complexes and the SUN proteins appear conserved in eukaryotes, plants have evolved unique KASH proteins and nucleoskeletal components. Plant nucleoskeletal components, while lacking sequence homology, share many of the animal lamin features, including interactions with the NE and their ability to impact chromatin structure and gene expression (Masuda et al. 1997; Dittmer et al. 2007; Wang et al. 2013; Ciska and Moreno Dí-az de la Espina 2014; Goto et al. 2014; Zhao et al. 2016; Guo et al. 2017; Choi et al. 2019; Ciska et al. 2019; Hu et al. 2019; Sakamoto 2020).

Plant nucleoskeletal proteins that interact directly or indirectly with the NE fall into two families of proteins. One family, the Nuclear Matrix Constituent Proteins/Crowded Nuclei (NMCP/CRWN) proteins, is found in plants with members encoded by the NMCP genes in carrot (Masuda), CRWN genes in Arabidopsis (Dittmer et al. 2007), and NCH genes in maize (Gumber et al. 2019a). The other family is also found in plants and encoded by the AtKAKU4 gene in Arabidopsis (Goto et al. 2014) and the MKAKU41 and

MKAKU42 genes in maize (Gumber et al. 2019a). Here we refer to these two gene or protein families generally as CRWN and KAKU4.

In Arabidopsis, CRWN1 is located primarily at the nuclear periphery and interacts with SUN-domain proteins (Dittmer et al. 2007; Graumann 2014). CRWN proteins have been implicated in the regulation of nuclear shape, nuclear size, chromatin organization, regulation of gene expression, and nuclear body formation in plants (reviewed in (Sakamoto 2020). KAKU4 was shown to interact with CRWN1 by yeast two-hybrid analysis, supporting their cooperation in the form and function of a plant nucleoskeletal system (Goto et al. 2014). Fluorescent protein fusions driven by native promoter expression and electron microscopy showed that KAKU4 is localized to the inner nuclear membrane. Interestingly, when high-expression stable lines were selected or high-expression transient transformation was performed, KAKU4 appeared to induce nuclear invaginations, which increased significantly when co-expressed with CRWN1 (Goto et al. 2014).

Together, the CRWN and KAKU proteins are known to affect phenotypes in eudicots, yet their roles in crop species are less well understood. Two maize CRWN homologs are known; NCH1 which is most closely related to AtCRWN1-3, and NCH2 which is most closely AtCRWN4. Maize MKAKU41 homologs are encoded by *MKAKU41* and *MKAKU42* (Gumber et al. 2019a). To investigate the functional conservation of these presumed nucleoskeletal proteins in maize, we characterized *NCH1* and *NCH2* and *MKAKU4* using cytological or genetic approaches.

RESULTS

Maize NCH1, NCH2, and MKAKU41 localized to the nucleus, primarily at the nuclear periphery

In order to determine the cellular localization of the maize CRWN homologs NCH1, NCH2, and the KAKU4 homolog MKAKU41, we produced gene constructs with the protein coding region fused to either GFP or mCherry at the N-terminus. We then expressed these constructs transiently in *N. benthamiana* leaf tissue. All three constructs localized to the nuclear periphery with MKAKU41 also exhibiting internal structures as shown in Figure 1 for nuclei counterstained with DAPI. In order to confirm that NCH1 and NCH2 were localized at the nuclear periphery, we performed co-expression of NCH1 or NCH2 with AtCRWN1 (Fig. S1). The co-localization of NCH with CRWN confirmed that NCH1 and NCH2 did localize to the nuclear periphery when transiently expressed in *N. benthamiana*. Interestingly, MKAKU41 showed nuclear envelope labelling and inner nucleus labelling in most cells, including membrane invaginations (Fig. 1B, white arrowheads), as has been described for Arabidopsis KAKU4 when expressed under the control of the 35S promoter (Goto et al. 2014). These included internal structures and circular ring-like invaginations within the nucleus. The structures labelled with MKAKU41 colocalized with brighter DAPI staining regions, implying that MKAKU41 may associate with heterochromatin. The ring-like invaginations lacked internal DAPI staining and therefore appeared devoid of typical nucleoplasmic chromatin. Interestingly, the CRWN1 homolog NCH1 alone also caused these aberrant-looking intranuclear structures (Fig. 1B, white arrow), although to a lesser extent than

MKAKU41. However, NCH2, a CRWN4 homolog (Fig. 1A), did not induce ring-like invaginations. The NCH1 and NCH2 also displayed different mobility proportions at the nuclear periphery (Fig. 1C, S1B and S1C) as determined by Fluorescence Recovery After Photobleaching (FRAP). NCH2 was significantly less mobile (16% mobile fraction) than NCH1 (49% mobility) indicating that they might interact with different protein complexes or structures. The lower mobility of NCH2 compared to NCH1 is consistent with its reduced capacity to remodel the nuclear envelope membrane and cause invaginations (Fig. 1A,C). The large immobile fraction of NCH2, but not NCH1, was comparable to that of AtCRWN1 (Graumann 2014).

It has been demonstrated that the degree of nuclear invagination and deformation is dependent on the expression level of KAKU4 in *A. thaliana* (Goto et al. 2014). We therefore asked if this causal relationship was conserved in the maize genes, MKAKU41, NCH1, and NCH2, using the dose-response transient expression assays summarized in Figure 2. We infiltrated *N. benthamiana* with three different concentrations of Agrobacterium, OD 0.01, 0.05, or 0.1, and then classified live-imaged nuclei (N≥30 per condition) into one of three previously described nuclear periphery cytological image patterns (Goto et al. 2014): type I for normal nuclear periphery localization, type II for minor invagintions or inclusions in the nucleus, and type III for major invaginations and deformation of the nucleus. This classification assisted with a comparative analysis of the severity of changes in nuclear morphology across the various experiments used throughout this study. Increasing the infiltration concentration of NCH1 resulted in progressively increased nuclear deformation illustrated by type II pattern increases and the appearance of type III at the highest transfection dose (Fig.

2A). NCH2 also showed a transfection dose-dependent increase in nuclear aberration coupled to type II increases, but less so and without any type III nuclei even at the highest dose (Fig. 2B). For MKAKU41, increasing the transfecting plasmid concentration led from most nuclei just showing peripheral localization initially to slightly under half showing type III patterns with severe invaginations seen at the highest concentration (Fig. 2C). We interpret these results as establishing that because all three of the proteins tested showed they could cause dose-dependent increases in severity of nuclear deformation patterns, they can all be considered to be part of the same process, one needed to properly organize a nuclear periphery compartment within interphase nuclei.

Co-expression of NCH1 or NCH2 with MKAKU41 showed a synergistic effect on invagination and nuclear deformation phenotypes

The Arabidopsis CRWN1 and KAKU4 have previously been shown to result in increased nuclear deformation and invaginations when co-expressed (Goto et al. 2014). In order to determine whether the maize homologs similarly affect the nuclear organization pathway, we co-expressed MKAKU41 with either NCH1 or NCH2 as presented in Figure 3. Upon co-expression, the nuclear invaginations and deformations were substantially enhanced compared to single-expression (Fig. 3A). Quantifying the most severe phenotype (type III), we observed that NCH1 alone exhibited 7% and MKAKU41 alone exhibited 42%. However, the combination of NCH1 and MKAKU41 exhibited 88% type III, well beyond the combined value of 49%, and thus synergistic for this measurement. Similarly, the NCH2 and MKAKU41 co-expression reached a level of

66% type III nuclei, considerably more than 42% sum of the single-expressed levels. Therefore, NCH proteins appeared to act cooperatively with MKAKU41 to affect nuclear periphery organization as judged by changes in their localization patterns. This cumulative effect on nuclear structure suggests that NCH1/NCH2 and MKAKU41 may act in the same protein complex. We tested this idea by checking for evidence of interaction between NCH and MKAKU41 *in planta* using acceptor photobleaching fluorescence resonance energy transfer (apFRET). A significant rise in FRET efficiencies would indicate interactions and such was measured when NCH1 and NCH2 were co-expressed with MKAKU41, compared to a non-interacting control, calnexin (Fig. 3C). Internal control FRET efficiency % values were very low, as expected for non bleached controls (Table S1). This demonstrated that NCH1 and NCH2 can interact with MKAKU41, and is consistent with their synergistic effect on levels of nuclear deformations. This observation is similar to that observed for Arabidopsis homologs using yeast two-hybrid system and plant expression (Goto et al. 2014). Importantly, our findings provide evidence from live imaging for *in planta* interactions between these proteins at the nuclear periphery.

MKAKU41 overexpression remodeled other inner and outer nuclear membrane proteins

Both AtKAKU4 and MKAKU41 cause deformation of the NE and disruption of nuclei structure when co-expressed with AtCRWN1 (Goto et al. 2014), NCH1, or NCH2 (Fig. 3). To further investigate whether this involves the entire NE, we asked whether overexpression of MKAKU41 can result in the invagination of other proteins not

previously tested but known to localize to either the INM, the ONM, or the ER. For this we used AtSUN2-YFP to mark the INM, ZmMLKP1-GFP to mark the ONM, and calnexin-GFP to mark the ER membrane. Figure 4 shows that each of these markers showed normal nuclear periphery localization when expressed individually. However, upon co-expression with MKAKU41, all of these proteins appeared in aberrant intranuclear structures. Therefore, the expression of MKAKU41 appears to have caused the internalisation of the entire NE, including the calnexin-GFP ER membrane marker, demonstrating that MKAKU41-induced nuclei deformations and invaginations are not limited to nucleoplasmic and INM LINC proteins.

Previously, it has been shown that AtSUN1 and AtSUN2 interact with AtCRWN1, mediated by the SUN N-terminus (Graumann 2014) and that the deletion construct SUN2ΔNterm could disrupt SUN-CRWN interactions (Graumann et al. 2010; Graumann 2014). To investigate more specifically the role of the LINC complex in producing these aberrant nuclear structures, we overexpressed SUN2ΔNterm as a way to abrogate CRWN-SUN binding and thereby possibly reduce the interaction of MKAKU41 with the LINC complex. Notably, SUN2-MKAKU41 co-expression resulted in mostly type III nuclei, whereas the SUN2ΔNterm-MKAKU41 co-expression led to less deformation, with nuclei showing mostly type II phenotype (Fig. 4A). Interestingly, nuclear envelope fluorescent labelling of full-length SUN2 appeared lower than that in SUN2ΔNterm when co-expressed with MKAKU41 (Fig. 4A & 4B). Signal intensity line profiles drawn over the nuclear invagination (Fig. 4A, dashed line) or nuclear envelope (Fig. 4A, solid line) regions showed that the SUN2 full length signal was much stronger within the invaginations but lower at the nuclear envelope when compared to those from

238 SUN2ΔNterm fluorescence (Fig. 4B). We quantified the effect of co-expressed
239 MKAKU41 on the SUN2's tendency for peripheral staining by determining the
240 percentage of the signal in the interior versus the entire nucleus (sub-periphery / whole
241 nucleus/, Fig. S2). For instance, if the signal was entirely peripheral, the percentage
242 would be at or near zero. Figure 4C shows an increase in internal fluorescence for
243 SUN2 in the SUN2 - MKAKU41 co-expression compared to SUN2 alone ($p<0.0001$).
244 Therefore, full length SUN2 is relocated away from the nuclear periphery when
245 coexpressed with MKAKU41. The relative internal nuclear fluorescence also increased
246 upon SUN2ΔNterm coexpression with MKAKU41 ($p<0.001$), but to a lesser extent than
247 for full length SUN2 ($p<0.001$). These observations implicate the LINC complex and
248 more specifically the nucleoplasmic N-terminal domain of the NE protein, SUN2, in the
249 formation of aberrant MKAKU41-dependent intranuclear structures.
250
251 **Impairing Nuclear Actin anchoring enhances nuclear invaginations**
252 In addition to the SUN2 NE protein which spans the INM and has direct contact with the
253 nucleoplasm, we also examined an ONM maker, MLKS2, and its ARM domain deletion
254 derivative previously shown to be impaired for actin binding (Gumber et al. 2019b).
255 Upon co-expression with MKAKU41, the ONM marker MLKS2 also appeared in
256 intranuclear invagination-like structures as shown in Figure 5 (panel A). Upon co-
257 expression of MKAKU4 and MLKS2ΔARM, nuclear deformations and invaginations
258 were observed (Fig. 5A) and found to much more severe and abundant (Fig. 5B)
259 compared to those from co-expression of MKAKU4 and the full length MLKS2.
260 Therefore, the ONM KASH protein MLKS2 is brought moved to intranuclear structures

by MKAKU41 co-expression, and loss of the actin-interacting ARM domain exacerbates the situation and implicates cytoplasmic F-actin in NE and nuclear periphery remodeling.

In order to further probe the interaction between peri-nuclear actin and MKAKU41-induced nuclear deformations, we used Latrunculin-B (LatB) to depolymerise the actin cytoskeleton as described previously (McKenna et al. 2019). Figure 5C shows that upon expression of MKAKU41 at a moderate level (OD0.05), LatB depolymerisation of the actin cytoskeleton resulted in a statistically significant increase in the number of invaginations ($P \leq 0.001$). While this trend existed at lower (OD0.01) and higher transfection concentrations (OD0.1), it was not statistically significant. To further explore the connection between the actin cytoskeleton and MKAKU41 induced nuclear deformations, we examined the interior versus peripheral signal ratios (Fig. S2) and found that actin depolymerization quantitatively shifted the INM NE marker, LBR, towards increased interior signal (Fig. 5D). This same effect was seen and found to be statistically significant for two concentrations of MKAKU41 infiltration, OD0.01 ($P \leq 0.01$) and 0.05 ($P \leq 0.05$). This demonstrates that at the moderate transfection concentration of 0.05OD, actin depolymerization with LatB increases the internalization of peripheral markers. These findings corroborate those from the MLKS2ΔARM experiments in that they implicate F-actin as a possible factor that can provide an opposing force or counterbalance to nucleoskeletal proteins which can invaginate the NE and create inclusion bodies in a concentration-dependent manner.

Transposon disruption of the MKAKU41 gene co-segregates with phenotypic effects on nuclear shape and development.

Having seen that overexpression of maize MKAKU41 in a eudicot species resulted in nuclear architecture disruption and severe nuclear envelope misplacement, we wanted to examine the role of this gene in its native genetic background, maize. From the UniformMu transposon mutagenesis project, we found and characterized a Mutator-tagged allele of *MKAKU41*, allowing for a genetic examination of the biological consequences of gene disruption in maize.

The transposon-tagged allele, here designated *mkaku41*, and its wild-type counterpart, *MKAKU41*, are shown in Figure 6. The wild-type *MKAKU41* gene (Zm00004b040444) from the color-converted W22 inbred is annotated as being associated with three transcript models. The gene structure for transcript model T01 (Fig. 6A) spans 7.9 kb, with 11 exons producing an mRNA with a single large ORF predicted to encode a protein of 579 AA. The transposon insertion site (mu1005806) is located in the 5' UTR (Fig. 6B). The transposon insertion allele was characterized by genomic PCR analysis (Fig. 6C) using various combinations of primers that were flanking the insertion site, and were gene-specific and *Mutator*-specific (Fig. 6A, primers F, T, R). These PCR products were visualized (Fig. 6C) and sequenced (Fig. 6D) from the W22 wild type progenitor (W22+) as well as F2 individuals from families segregating for *mkaku41* (+/+, +/-, or -/-), where the "-" symbol denotes the transposon-insertion allele. These PCR primers and PCR gel products were used for plant genotyping in subsequent analyses.

By inspection of the junction sequences between the wild-type reference W22 genome and the transposon (Fig. 6D, lower case letters), we identified the 9-bp target site duplication as CTCCTCTC (color coded green in Fig. 6). These results confirmed that the transposon was inserted in the 5' UTR at a position 23 bp upstream of the start codon, disrupting the majority of the wild-type 95 bp 5' UTR. The location of this insertion, while not in the protein coding region of the gene, is within the first exon and its location is expected, therefore, to disrupt the expression or transcript structure of the gene. Surprisingly, from transcriptome analysis we found that the gene expression levels for MKAKU41, measured as total normalized reads across the gene model, were similar in libraries made from wildtype and mutant leaf and tassel. We mined the transcript data to investigate the effect of the transposon insertion on the 5' UTR region by searching for the presence of a unique 25 bp 5' UTR sequence located just upstream of the mapped insertion site (Fig. 6D,E, "Query sequence" highlighted in yellow). We found a total of 70 matches to our 25 bp query sequence in our transcriptome, which was sequenced at a depth of over 100M reads per tissue-genotype combination (Fig. 6E). All 70 occurrences of the query sequence were from the wildtype libraries except for one, which was on the reverse strand relative to the gene (Fig. 6E). These results indicate that the 5' UTR was indeed disrupted in the mutant plants. In addition to this detailed analysis of MKAKU41, some differentially expressed genes (Table S2) were observed in mutant versus wild-type leaf and meiotic-enriched whole tassel, but gene ontology analysis did not reveal any clear and reproducible enrichments that differed from those of randomized controls.

We next explored the phenotypic consequences of the *mkaku41* transposon insertion on root hair nuclei, stomatal complex, and pollen viability, as summarized in Figure 7. The root hair nuclei in W22+ (normal) and *mkaku41* mutant seedlings 5 days after imbibition were imaged and their shapes were analyzed (Fig. 7A-F). The mutant nuclei were visually and quantitatively more rounded than their wildtype counterparts. The mutant nuclei had an average maximum length of 22 μm whereas their wild-type counterparts averaged 34 μm (Fig. 7G). The mutant nuclei also exhibited a higher circularity index than the wildtype nuclei (Fig. 7H). Both measures (n=50) were statistically significant as determined using T-test, two-tailed with $p<0.0001$.

Next, we analyzed two above-ground phenotypes, the appearances of stomatal complexes and pollen. In W22+ plants, a normal stomatal complex is composed of two guard cells flanked by two subsidiary cells as shown for W22+ (Fig. 7I). In contrast, mutant plants showed irregular stomatal complexes composed of two normal-looking guard cells flanked by one or two extra and irregularly positioned subsidiary cells (arrows, Fig.7 J-N). For the pollen phenotypes, we assayed viability and shape (Fig. 7O-R). Using the modified Alexander's differential staining method, we found that the percent of viable pollen was dramatically reduced in the mutant, from 84% to 46%. The shape of the pollen was also affected in the mutant, where the average degree of roundness decreased from 0.93 to 0.7. Both measures ($n>1,000$ for staining, $n=100$ for roundness) were statistically significant as determined using a two-tailed T-test with $p<0.0001$.

Taken together, these findings show that the *mkaku41* mutation was associated with multiple phenotypes including root hair nuclear shape, stomatal complex

development, and pollen viability. Therefore, MKAKU41 appears to act in some of the same genetic pathways as the NE-associated LINC complex proteins such as SUN and KASH. This genetic data in maize is interesting when considered with our findings that heterologous overexpression phenotypes and actin perturbations (Figs. 1-5) disrupt nuclear architecture and nuclear envelope organization. Taken together, all of these experiments establish biological roles for MKAKU41, NCH1, and NCH2 as nucleoskeletal proteins that regulate fundamental nuclear processes in cellular structure and function.

DISCUSSION

Regulation of nucleus size and shape is important for many fundamental cellular processes in all eukaryotes. Nuclear architecture is controlled by multiple interactions involving the NE, NE-associated complexes, and the nucleoskeleton. Here, we characterized multiple maize nucleoskeletal proteins, which, like their animal counterparts, controlled nuclear dynamics. An overarching goal motivating this study is to establish the general rules that apply across the plant domain, an evolutionarily vast space. Towards this goal, we have utilized the tobacco transient heterologous expression assay as a powerful and versatile experimental platform for plant nuclear envelope research. In this study and previously, we have established cellular localization, protein-protein interactions, dose-response phenotypes, and live cell imaging that allows for kymographic analysis, mobility via FRAP, and interactions via

373 AP-FRET, all of which have enabled and accelerated our understanding of grass and
374 model crop NE biology (Gumber et al. 2019b, a).

375 The maize nucleoskeletal proteins examined in this study are NCH1, NCH2 and
376 MKAKU41, each of which has one or more homologs (Fig. 1A) in eudicot species
377 (Gumber et al. 2019a) and all of which exhibit nuclear localization and NE enrichment in
378 heterologous expression systems. Interaction data from this (Fig. 3C) and prior studies
379 further indicate that these proteins are coupled to the NE via the LINC complex. These
380 findings, together with those from other plant species, point to the broad conservation of
381 plant nucleoskeletal proteins across angiosperms (Goto et al. 2014; Meier et al. 2017;
382 Ciska et al. 2019; Sakamoto 2020). The functional conservation of these components is
383 evidenced by previously reported cross-species functional rescue (Gumber et al. 2019b)
384 and by the current study where we show that the maize MKAKU41 (Fig. 4) interacts with
385 Arabidopsis AtSUN2, causing altered nuclear localization of the Arabidopsis AtSUN2.

386 Multiple lines of evidence for conservation of plant LINC complexes are also
387 seen at the organismal and phenotypic level. For instance, we (Fig. 7) and others found
388 that mutant phenotypes commonly include the rounding up of root hair nuclei, disruption
389 of stomatal complex development, and effects on pollen shape and viability (Dittmer et
390 al. 2007; Goto et al. 2014, 2020; Zhou et al. 2014; Gumber et al. 2019b; Newman-Griffis
391 et al. 2019). The nuclear shape defects in root hairs have become a hallmark of LINC
392 defects in plants, and as such were predicted. However, the stomatal complex and
393 pollen shape phenotypes have not been previously observed for plant mutants of
394 MKAKU4 genes, but they resemble to some extent those of the plant KASH mutant,
395 *mlks2* (Gumber et al. 2019b). To gain genetic insight into these nucleoskeletal proteins

in the crop species maize, we searched for transposon-disrupted alleles of MKAKU41, NCH1, and NCH2. Of these, we found that the *MKAKU41* gene was reported to have a Mutator insertion (McCarty and Meeley 2009), described here as the first known mutant allele, *mkaku41*. The insertion site was in the 5'-UTR (Fig. 6), a common hot-spot for Mu insertion (Zhang et al. 2020). The transcript abundance was not significantly reduced in the mutants, but the mutant allele produced an extremely truncated 5' UTR of 23 bp or less. Given that the median 5' UTR length in maize was recently determined to be 132 bp (Leppek et al. 2018), such an extremely short 5’ UTR in the *mkaku41* mutants may abolish or greatly decrease the ability of the cell to utilize the native start codon for translation of the full-length protein. If the mutant 5' UTR is too short for efficient ribosome assembly and scanning, the next in-frame start codon is considerably farther downstream, which would result in a loss of the first 125 AA. Additionally, the mutant 5'UTR may lack regulatory mRNA sequences in the first ~70 bases of the full-length transcript. Further genetic and experimental analyses with new alleles, gene editing, or application of specific biotic or abiotic stresses will be needed to gain a better understanding of how these plant nucleoskeletal proteins functionally interact with the genomes they help to organize.

The regulation of nuclear morphology and intra-nuclear organization was further explored to gain mechanistic insight, using the tobacco transient expression assay with fluorescently tagged proteins and quantitative microscopic analyses. We used this approach to explore multiple aspects of the remarkable nuclear architecture disruption caused by overexpression of each of the three maize nucleoskeletal proteins examined. The severity of the nuclear disruption and of the NE invaginations was increased by co-

overexpression of two components (e.g. MKAKU41 with NCH1 or NCH2), or by increasing the transfecting plasmid concentration, expected to increase their expression levels. These findings (Fig. 2) and previous studies from plants and animals reveal that proper nucleoskeleton protein concentration may be a primary determinant for overall nuclear architecture (Legartová et al. 2014; Goto et al. 2014; Jorgens et al. 2017).

In addition to protein abundance, components of the nuclear invaginations were tested for the presence of LINC and ER proteins. Knowing that SUN proteins interact with ONM KASH proteins as part of the core LINC complex, we tested whether the intranuclear foci of MKAKU41-FP reflected protein aggregates of entire NE, checking for colocalization with two types of markers, those in the NE but not the LINC complex or those in the ER membrane. All of these, including multiple ONM markers, colocalized with the aberrant intranuclear structures (Figs. 4 and 5), demonstrating that these intranuclear structures contain components from both the INM and ONM of the nuclear envelope. These plant nuclei invaginations may contain, therefore, the entire NE proteome as well as NE-associated chromatin that would normally be limited to the nuclear periphery. Such invaginations are known to occur in plants and animals, which can show grooves, deformations, actin, or ER in stable structures seen as deep invaginations (Collings et al. 2000; Schermelleh et al. 2008). Interestingly, the membrane invaginations and deformations caused by MKAKU41 also resemble to some extent animal nuclear deformations associated with Lamin-A mis-expression (Lammerding et al. 2004; Schreiber and Kennedy 2013; Swift et al. 2013; Legartová et al. 2014).

In our experimental set up, we disrupted the LINC complex at two different connections to investigate the effect of these disruptions on the NE structure. The first, a SUN2ΔN, severed the LINC-to-nucleoskeleton connection; the second MLKS2ΔARM, severed the LINC-to-cytoskeleton connection. It is quite interesting that these two disruptions exhibited contrasting effects on the severity of invaginations. Our domain-deletion analyses showed that perturbation of the LINC-to-nucleoskeleton connection *reduced* the severity (Fig. 4A), whereas preventing the LINC-to-cytoskeleton connection *increased* the severity of invaginations (Fig. 5). This has important mechanobiological implications for the idea that plant nuclear shape involves a balance of forces between actin-nucleus interactions and nucleoskeletal components. Interestingly, AtKAKU4, arabidopsis KASH proteins WIPs, and NE-associated myosin are all involved in nuclear migration in various cellular processes, such as in pollen-tube growth (Goto et al., 2020, Meier et al., 2017), which also involves changes in actin dynamics.

Moving the nucleus exerts physical stress on the NE and the opposing forces of the LINC components (nucleoskeletal and cytoskeletal) are expected to be, therefore, important for maintaining NE integrity and stability (Enyedi and Niethammer 2017). The contrasting effects on NE integrity that we observe in this study are an indicator that maize nucleoskeletal components may be functionally associated with just such a tug-of-war process that manifests as regulation of nuclear shape. Multiple lines of evidence are consistent with this idea, including the change to spherical nuclei caused by genetic knockouts of a nuclear-envelope-localized myosin (Tamura et al. 2013) and the rounding up of root hair nuclei caused by the maize *mlks2* mutation (Gumber et al. 2019b). Along these lines, our study adds to the growing body of evidence that plants

464 deploy a general mechanism for nuclear shape in which a balance of forces is achieved
465 through LINC-interacting components on both sides of the NE, ensuring its structure
466 and function as a flexible cellular partition. In the current study, we note multiple
467 indications (Fig. 5) that support this tug-of-war type arrangement. These ideas align
468 with results from mammalian studies that identify roles for the LINC complex in
469 mediating mechanical crosstalk between the cytoplasm and nucleus (Alam et al. 2016;
470 Jorgens et al. 2017; Hieda 2019; Agrawal and Lele 2019; Bouzid et al. 2019).
471 Previous investigations of CRWN and KAKU4 have focused on chromatin
472 structure and nuclear architecture (Dittmer et al. 2007; Grob et al. 2014; Hu et al. 2019),
473 but our studies indicate that nucleoplasmic disruptions can also affect normal
474 developmental processes, an important finding for crop species. In animals, the
475 interplay between cellular-level structural integrity and genomic responses to
476 environmental and developmental processes is increasingly recognized as a complex
477 process involving lamins as central players (Gerbino et al. 2018). This study advances
478 our knowledge of the plant nucleoskeleton by identifying the components and their roles
479 in regulating fundamental dynamic processes of the plant nuclear envelope.
480
481
482 **METHODS**
483
484 **Cloning**
485 Maize gene constructs and sequence information for the clones used in this study are
486 listed in Table S3. NCH1 ORF was custom-synthesized with *Bam*HI and *Sbf*I at the 5'

and 3' ends, respectively (Genscript Biotech Corporation, NJ). The *Bam*HI-NCH1-*Sbf*I construct was sub-cloned by restriction cloning into an ECGFP donor vector containing eGFP-FLAG-HA (Gumber et al. 2019, JCB), to create the eGFP-FLAG-HA-NCH1 entry vector, named NCH1ec. Similarly, the *Bam*HI-NCH2-*Pst*I construct was custom synthesized and sub-cloned into an ECGFP donor vector to create the eGFP-FLAG-HA-NCH2 entry vector, named NCH2ec. For construction of the mKAKU41vector, *Bam*HI-mCherry-FLAG-HA-MKAKU41-*Bam*H1 was synthesized by Genscript and cloned in pUC18 at the *Bam*HI restriction site. From this cloning vector, the mCherry-FLAG-HA-MKAKU41 gene construct was amplified using KAKUattF (5'-GGGGACAAGTTTGTACAAAAAAGCAGGCTTCATGGTTAGCAAGGGAGAAGAGG-3') and KAKUattR (5'-GGGGACCACTTTGTACAAGAAAGCTGGGTCTCACGTAGCCCGTCCCCGT-3') primers and inserted into pDONR221 vector by BP cloning (Invitrogen), to generate the MKAKU41 entry clone, named MKAKU41ec. For the generation of plant expression vectors, the fluorescent fusion protein constructs from these three entry clones were then transferred individually to the destination vector pH7WG2 (Karimi et al. 2002) by Gate LR recombination (Invitrogen).

For production of the p35S::SP-mCherry-GFP-HDEL positive control for apFRET, mCherry was PCR amplified with Q5 polymerase (NEB) using primers JM403 (5'-GGGGACAAGTTTGTACAAAAAAGCAGGCTACAATGAAAGCCTTCACACTCGCTCTCTTCTTAGCTCTTTCCCTCTATCTCCTGCCCAATCCAGCCATGGTGAGCAAGGGCGAGGAGG-3') & JM404 (5'-acctccactgccaccCTTGTACAGCTCGTCCATGCCG-3'). The primers included both the Gateway cloning attB1 site and secretion signal at the 5' end,

and a 15nt overhang for Gibson assembly at the 3' end, which contained a GGSGG amino acid linker between mCherry and GFP upon fusion. GFP was amplified using primers JM367 (5'GGGGACCACTTTGTACAAGAAAGCTGGGTGtcataattcatcatGCTTGTACAGCTCGTCCATGCCGAGAG-3') & JM405 (5'GTACAAGggtggcagtggaggtATGGTGAGCAAGGGCGAGGAGC-3') which contained the GGSGG linker at the 5' end, and the HDEL ER retention motif, an attB2 site, and a stop codon at the 3' end. These two products were fused together using the NEB HIFI Gibson assembly enzyme mix and incubated at 50°C for one hour. A Gateway BP reaction into pDONR221 and subsequent LR reaction into pB7FWG2 was then performed to produce the final vector. All steps confirmed by colony PCR and sequencing.

Agrobacterium transformation

Constructs were transformed into A. tumefaciens GV3101. Transformation was performed by incubating plasmid DNA and chemically competent agrobacterium on ice for 30 minutes, followed by 5 minutes cold shock in liquid nitrogen, then 5 minutes heat shock at 37□ in a rotating incubator. After heat shock, 200µL LB media was added and cells incubated at 28□ for two hours. Cells were then plated in LB plates containing Spectinomycin (50µg/mL), Gentamycin (10 µg/mL) and Rifampicin (25 µg/mL) and incubated for two days at 28°C. Individual colonies were then picked, grown O/N and transformed into *N. benthamiana*.

Plant growth conditions

N. benthamiana plants were grown in 16:8h light:dark cycle in a greenhouse maintained at 21 °C. Infiltrated plants were 5-6 weeks old.

Live cell imaging

Fluorescently tagged proteins of interest were transiently transformed into *N. benthamiana* as described previously (Sparkes et al. 2006). Protein expression constructs first reported here are p35S::NCH1-GFP, p35S::NCH2-GFP and p35S::MKAKU41-mCherry. All other markers have been previously published: p35S::GFP-CNX (Irons et al. 2003), p35S::LBR-GFP (Irons et al., 2003), p35S::MLKP1-GFP (Gumber et al. 2019a), p35S::YFP-AtSUN2 (Graumann et al. 2010), p35S::YFP-AtSUN2ΔNterm (Graumann et al. 2010), p35S::MLKS2-GFP and p35S::MLKS2ΔARM-GFP (Gumber et al. 2019b). An agrobacterium culture of OD 0.1 was used in all conditions unless otherwise stated and cells were imaged three days after transformation. The GFP / mCherry combinations were imaged using a Zeiss LSM 800 confocal microscope with line switching, 488nm and 561 nm excitation, and 500-550nm and 565-620nm emissions, collected for GFP and mCherry respectively. For GFP / YFP and YFP / mCherry imaging, a Zeiss LSM 880 was used with frame switching. For GFP / YFP imaging, 488nm and 514nm excitation was used with emission collected between 500-550 and 525-560 for GFP and YFP respectively. For YFP / mCherry imaging, 514nm and 561nm excitation was used, and emission collected between 517-560nm and 561-624 nm respectively. An image size of 512x512 pixels with a scan zoom of 4 and a 63x 1.4NA lens was used for all imaging described above. All combinations were

performed with three independent experimental repeats; representative images are shown. For Fluorescence recovery after photobleaching (FRAP) a 100x 1.4NA lens was used with a 4µm ROI in the center of the image, encompassing the nucleus. Five scans were taken pre-bleach and then the 488nm laser bleached the ROI by using 100% transmission for 20 iterations. Recovery Images were then collected for one minute to monitor recovery. Data was normalised and FRAP curves produced as described previously (Martiniere et al. 2012).

For acceptor photobleaching förster resonance energy transfer (apFRET) a 100x 1.4NA lens was used with a 4µm ROI in the center of the image, encompassing the nucleus. Five scans were performed with both GFP and mCherry emission / excitation, and then the mCherry construct was bleached in the ROI by the 561nm laser at 100% transmission for 20 iterations. Following this, five post-bleach scans were taken. Data was normalized and apFRET efficiency (%) calculated as previously (Graumann et al. 2010; Graumann 2014; Pawar et al. 2016). A minimum of 30 nuclei per condition were used for apFRET across three experimental repeats. A one-way ANOVA was performed to determine statistically significant differences between samples. For Latrunculin-B (LatB) treatment for depolymerisation of the actin cytoskeleton, samples were incubated with 25 µM LatB for one hour, as this has previously been shown to depolymerise the actin cytoskeleton sufficiently (McKenna et al. 2019). Graphs were generated with graphpad and as described in the figure legends.

Maize plant material and genotyping

The wild-type W22 used in this study is a color-converted W22 line obtained from Hugo Dooner (Waksman Inst., Rutgers, New Jersey, USA) derived by (Brink 1956). The UF-Mu-00395 seed stock was obtained from the Maize Genetics Cooperation Stock Center (http://maizecoop. cropsci.uiuc.edu/). The plants were grown at the Florida State University Mission Road Research Facility (Tallahassee, FL, USA) during summer 2017 and 2018, and propagated by out- crossing to W22. In the fall of 2018, the progeny seeds were grown in the greenhouse in the King Life Sciences Building (Biological Science Dept, Florida State University, Tallahassee, FL, USA). The segregating plants were self-crossed to obtain mutant plants from among the progeny.

DNA was isolated from 4-week old seedlings as described previously in (Gumber et al. 2019b). PCR genotyping was carried out using a combination of gene-specific forward (F, 5'-CCCGTGAAGCCGAAGGCAGA-3') and reverse (R, 5'-CGCCTCACGCTCACGCTCAC-3') primers, or transposon-specific Tir6 primer (5'-AGAGAAGCCAACGCCAWCGCCTCYATTTCGTC-3') in combination with F or R primer. The PCR products were resolved by agarose gel electrophoresis and cloned in pCRTM4Blunt-TOPO® Vector (Invitrogen cat # K2875-20) by TA cloning. The clones were sequenced and the insert sequences were verified using M13F and M13R vector primers at the Molecular Cloning Facility, Department of Biological Sciences, Florida State University. The sequences were aligned with the W22v2 reference genome to validate the transposon insertion site.

599 **Microscopy in maize**

600 Maize root hair imaging was carried out as described in (Gumber et al. 2019b). Briefly,
601 roots were harvested from 5-day old seedlings and fixed for 1 hour in Buffer A (Howe et
602 al. 2013) supplemented with 4% paraformaldehyde. Small sections of root tissue
603 containing root hair were stained with 3 µg/mL DAPI for 20 min at room temperature,
604 mounted with VECTASHIELD, and imaged on an EVOS fluorescence microscope
605 (Thermo Fisher Scientific). The images were processed using the Analyze Particle
606 function of ImageJ to measure the longest diameter and circularity of the nuclei.

607 For stomatal complex imaging, plants were grown in the greenhouse and the 4th
608 leaf was harvested at its first appearance. The harvested leaf was fixed in Buffer A with
609 4% paraformaldehyde for an hour at room temperature with rotation. The tissue was
610 rinsed thrice with and stored in Buffer A at 4C, until further use. The leaf tissue was
611 placed on a glass slide, chopped into small pieces and stained with 3 µg/mL DAPI for
612 20 min at room temperature, mounted with VECTASHIELD, and imaged on an EVOS
613 fluorescence microscope (Thermo Fisher Scientific).

614 Pollen grain staining was carried out as previously described in (Gumber et al.
615 2019b). Briefly, male flowers were harvested before dehiscence and fixed in Carnoy's
616 fixative (6 alcohol:3 chloroform:1 acetic acid) for a minimum of 2 hours at room
617 temperature. Anthers were extruded from flowers with the help of a micro scalpel and
618 forceps on a glass slide. Staining was carried out with modified Alexander's stain
619 containing Malachite green (0.01%), Acid Fuchsin (0.05%) and Orange G (0.005%) as
620 described to differentiate viable (magenta) pollen grains from aborted (green) pollen
621 grains. Bright field images of the pollen grains were collected on Revolve microscope

(Echo Labs). At least 300 pollen grains each from 3 plants of every genotype were counted to calculate pollen viability. Pollen roundness was carried out using Fiji.

RNA isolation and library preparation

Segregating wildtype and mutant mkaku41 plants were grown in the greenhouse. From two week-old plants, fourth leaves were harvested and from 6-8 week old plants, mid-prophase meiotic-staged male flowers were harvested. The tissues were immediately stored in liquid nitrogen. RNA was isolated from three biological replicates for each genotype using Qiagen RNeasy Plant mini kit per manufacturer's instructions. Integrity of the RNA was tested using the Bioanalyzer (Agilent) system. For library preparation, sample input was 400 ng total RNA (determined by Qubit RNA HS reagents, Thermo) with RIN >7 (Bioanalyzer RNA Nano, Agilent). Libraries were prepared with the Biomek 400 Automated Workstation (Beckman Coulter), using the NEBNEXT Ultra II RNA Library Prep kit for Illumina (New England Biolabs) according to manufacturer's instructions, with an RNA fragmentation time of 15 minutes, a 1/10th dilution of NEB adaptor and 11 cycles of PCR amplification with dual-indexing primers. Amplified libraries were initially quantified by Qubit DNA HS reagents, checked for size and artifacts using Bioanalyzer DNA HS reagents, and KAPA qPCR (KAPA Biosystems) was used to determine molar quantities of each library. Individual libraries were diluted and pooled equimolar, and the pool was again checked by Bioanalyzer and KAPA qPCR before submission for sequencing.

644 **RNA sequencing and data analysis**

645 RNA-seq libraries were sequenced on a Novaseq 6000 at the Translational Science
646 Lab, College of Medicine, Florida State University. Approximately 40 million single-end
647 100 base reads were obtained for each biological replicate in this experiment and are
648 available from NCBI sequence read archive project, accession number PRJNA675860.
649 Contaminating 3' adapter sequences were trimmed from the demultiplexed raw reads
650 using cutadapt version 1.16. Raw and trimmed reads were subjected to quality control
651 testing with fastqc. Trimmed reads were aligned to the W22 genome assembly "Zm-
652 W22-REFERENCE-NRGENE-2.0" using the splice-aware aligner hisat2. Briefly, Hisat2
653 indices were constructed from known exons, and splice sites extracted from the W22
654 genome annotation (Zm00004b) and the reference genome assembly (Zm-W22-
655 REFERENCE-NRGENE-2.0.fasta). Trimmed reads were then aligned to the resulting
656 splice-aware hisat2 index using the following optional arguments: --rna-strandness R, --
657 dta-cufflinks, --summary-file. Predicted novel transcripts were assembled and merged
658 across replicates and samples using stringtie2 in "conservative" mode. Per-transcript
659 coverage tables were prepared by stringtie2 in "ballgown" format. Resulting coverage
660 tables were converted into count tables suitable for differential expression analysis by
661 DEseq2 in R using the tximport package. Differential expression analysis was
662 performed separately for each tissue group i.e (leaf mutant vs. WT and tassel mutant
663 vs. WT). Briefly, genes with fewer than 10 counts across all replicates were discarded
664 and DEseq2 results were generated for both tissue groups such that log2(fold-change)
665 estimates were reported for (mutant/WT) ratios. Statistically significant differentially

666 expressed (adjusted p-value <0.05) genes were subsequently extracted from each of
667 the resulting DEseq2 tables for further analysis (Table S2).
668
669 **Acknowledgments**
670
671 We would like to acknowledge the Bioimaging unit at Oxford Brookes for access to the
672 confocal microscopes. This work was performed as part of the Cost action # CA16212
673 'INDEPTH' whose members are appreciated for their fruitful discussions. This work was
674 supported in part by a grant to HWB from the National Science Foundation (NSF IOS
675 1444532).
676
677 ## FIGURE LEGENDS
678
679 **Figure 1: The maize proteins NCH1, NCH2 and MKAKU41 localize to the nuclear**
680 **envelope.** (A) Maximum likelihood phylogenetic tree showing maize NCH1 and NCH2
681 along with homologous proteins CRWN1-4 from Arabidopsis. (B) Confocal imaging of *N.*
682 *benthamiana* transiently expressing NCH1, NCH2 and MKAKU41 as fluorescent protein
683 fusions (green / magenta) and nuclei labelled with DAPI (blue). Both MKAKU41 and
684 NCH1 show nuclear invaginations (white arrowheads) and labelling at the nuclear
685 envelope (white boxes). NCH2 shows predominantly nuclear peripheral localization.
686 Scale bar denotes 5μm. (C) FRAP analysis demonstrates that NCH1 has a larger

687 mobile fraction than NCH2 at the nuclear periphery. N ≥ 30 nuclei imaged across three
688 experimental replicates.
689
690 **Figure 2: The concentration of NCH1, NCH2 and MKAKU41 affects the level of**
691 **nuclei invagination and disruption.** Confocal live cell imaging of NCH1, NCH2 and
692 MKAKU41 shows that increasing the concentration of NCH1 and MKAKU41 increases
693 nuclei disruption. Nuclei were classified as per (Goto et al. 2014) into Type I, Normal
694 nuclear envelope localization; Type II, Minor invaginations and predominantly nuclear
695 envelope localization; or Type III, major disruption of nuclei structure . (A) NCH1, (B)
696 NCH2 and (C) MKAKU41. Scale bar denotes 5μm. N≥ 30 nuclei imaged across three
697 experimental replicates.
698
699 **Figure 3: Coexpression of NCH1 or NCH2 with MKAKU41 enhances nuclear**
700 **invaginations and NCH1 and NCH2 interact with MKAKU41.** (A) Confocal images of
701 *N. benthamiana* coexpressing NCH1 or NCH2 with MKAKU41. (B) Quantification of
702 nuclear morphologies for nuclei expressing single MKAKU41, NCH1, NCH2; or co-
703 expression of NCH1 or NCH2 with MKAKU41; classified into types I, II, or III as
704 described in Figure 2. Scale bar denotes 5μm. (C) The apFRET efficiency (%)
705 demonstrates *in planta* interactions of NCH1 and NCH2 with MKAKU41 in comparison
706 with control (CNX). Solid lines underneath plots denote negative controls, hashed
707 positive control. Key statistical comparisons shown and more fully tabulated in Table
708 S1. Red line denotes mean, blue standard deviation. One-way ANOVA statistical test

709 performed. **** = P ≤ 0.0001. N≥ 30 nuclei imaged across three experimental replicates
710 for all experiments described.
711
712 **Figure 4: MKAKU41-induced nuclear invaginations incorporate other nuclear**
713 **envelope- and ER-localized proteins.** (A) Confocal imaging showing that the outer
714 nuclear Maize membrane markers MLKP1, Arabidopsis nuclear envelope proteins
715 SUN2 and SUN2ΔNterm, and the ER membrane marker CNX are incorporated into
716 invaginations when co-expressed with MKAKU41. Next to confocal images are
717 percentages of nuclei which show deformations as classified previously. (B) SUN2 and
718 SUN2ΔNterm show different incorporation into MKAKU41 induced nuclear
719 invaginations. Graphs show 4μm normalised line profiles over SUN2 or SUN2ΔNterm
720 Invaginations (solid white lines) and nuclear membrane (dotted white lines). Locations
721 of line profiles can be seen in confocal micrographs. (C) Ratio of Sub-periphery/whole
722 nuclei fluorescence of SUN2 and SUN2ΔNterm when expressed on their own or with
723 MKAKU41. **** = P ≤ 0.0001. N ≥ 30 for each condition.
724
725 **Figure 5: Nuclear actin anchoring is important for regulating nuclei deformations**
726 **upon MKAKU41 overexpression. (**A) Confocal live cell imaging of MLKS2 and
727 MLKS2ΔARM single and co-expresssion with MKAKU41. (B) All nuclei imaged were
728 categorised on the level of disruption as described previously. (C) Number of nuclei
729 invaginations at different MKAKU41 expression levels with actin depolymerised (LatB).

730 (D) Sub-periphery / whole nuclei fluorescence ratio from nuclei expressing different
731 levels of MKAKU41 (MK, from 0 to 0.1) with and without actin depolymerisation (LatB).
732 Nuclei were imaged with the NE marker LBR-GFP. Scale bar denotes 5μm. N≥ 30
733 nuclei imaged across three experimental replicates for panel A & B). For Panel C & D ≥
734 60 across three biological replicates.
735
736 **Figure 6. Gene structure of wild-type and transposon-tagged alleles of *MKAKU41*.**
737 (A) Gene model of MKAKU41 (transcript model "T01") showing the positions of exons
738 (black boxes), introns (grey), the 5' and 3' UTRs, the transposon-insertion (Mu),
739 transposon-specific Tir6 PCR primers (T arrows), and the Mu-flanking gene-specific
740 PCR primers (F, R arrows). (B) Diagram of the MuDR insertion site within the 95 bp 5'
741 UTR, showing the locations of the 9 bp target site repeat (green, bp 64-72 in the
742 mkaku41-T01 transcript model) and a 25 bp query sequence (yellow) used for transcript
743 analysis. (C) PCR Genotyping for presence or absence of the Mu-tagged allele. The
744 PCR products using various pairings of gene-specific (F, R) or transposon-specific
745 primer pairs (T). Ethidium bromide-stained agarose gel 100 bp size marker (lane M) and
746 single-plant PCR products (other lanes) from W22+ or select *mkaku41* F2 siblings to
747 illustrate wildtype (+/+), heterozygous (+/-), or mutant (-/-) PCR genotype patterns from
748 the PCR (arrows at right of gel). (D) Sequence of cloned and sequenced amplicons are
749 aligned and show the progenitor W22 (W22 reference) and F2 segregants. The +/+
750 individuals from the transposon mutagenesis stocks were found to be heterozygous for
751 a 2 bp indel (--). The sequences corresponding to a 25 bp query sequence (yellow
752 highlight), the 9 bp insertion site (green highlight), the transposon (lowercase, garnet

753 text), and the start codon (underlined ATG) are indicated. The Mu insertion occured in
754 the allele with the 2bp deletion and produced a flanking 9bp target site duplication. (E)
755 Strand-specific transcriptome analysis is summarized for perfect match occurrences of
756 the query sequence in libraries made from wildtype (top) or mutant (bottom) plants. All
757 of the sense transcripts from the mutant allele had an extremely short (~21 bp or less)
758 5'UTR.
759
760 **Figure 7. Somatic phenotypes of *mkaku41*.** DAPI-stained root hair nuclei in W22+ (A-
761 C) and mkaku41 (D-F) seedlings. (G) Longest diameter of W22+ and mkaku41 root hair
762 nuclei (n=50). (H) Nuclear circularity index measurements using $4\pi(\text{area}/\text{perimeter}^2)$,
763 where 1= perfect circle, of W22+ and mkaku41 root hair nuclei calculated using Fiji. (I)
764 Mature stomatal complex in W22+ DAPI-stained leaf where two central dumbbell-
765 shaped guard cells (GC) are surrounded by two subsidiary cells (SC). (J-N)
766 Representative images of stomatal complexes in *mkaku41* DAPI-stained leaves. Arrows
767 point to extra or irregularly-placed subsidiary cells. Scale bars are 10 μm. *****Student's
768 t-test two-tailed, $p < 0.0001$. (O-Q) Differential staining of anthers for testing pollen
769 viability from W22+ (O) and mkaku41 -/- (P,Q) tassels stained with modified Alexander's
770 stain where viable pollen grains appear magenta and aborted pollen grains appear
771 green. (R) Quantification of pollen viability, n>1000 per genotype. (S) Degree of pollen
772 roundness 4*area/(π*major_axis^2) calculated for W22+ and mkaku41-/- anthers using
773 Fiji. Scale bars are 50 μm. *****Student's t-test two-tailed, $p < 0.0001$.
774

Legends for Supplemental Figures

Figure S1: The Maize NCH1 and NCH2 proteins co-localize with their Arabidopsis homolog CRWN1. Confocal live cell imaging of cells co-expressing either NCH1 or NCH2 with Arabidopsis CRWN1 shows colocalization. B) Scatter dot plot of plateau recovery values from NCH1 and NCH2 FRAP time course experiment. C) Scatter dot plot of halftime recovery values from NCH1 and NCH2 FRAP time course experiment. Scatter dot plot of NCH2 Scale bar denotes 5μm. N≥ 30 nuclei imaged across three experimental replicates.

Figure S2: Description of Sub-periphery / whole nuclei fluorescence ratio measurement. Diagram describing how the sub-periphery over whole nuclei measurement was determined using image J. Two regions of interest (ROIs) were generated, one encompassing the whole nuclei and one only sub-periphery nuclear fluorescence (yellow ROIs with hashed boundaries). The sub-periphery fluorescence value was then divided by the whole nuclei fluorescence value in order to obtain the ratio. If the majority of fluorescence is located at the periphery / nuclear envelope, this would result in a low ratio, conversely if most fluorescence was internal, this would result in a higher ratio.

Figure S3: Multiple Seq Alignment of Transcripts. A) The 5' UTR region and a small portion of the CDS are diagrammed as shown in Figure 5, and reversed (bottom

797 configuration) as aligned in the multiple sequence alignment. B) The multiple sequence
798 alignment displays all of the RNA-seq reads with a perfect match to the 25 bp query
799 sequence (yellow) using grep of the fastq files. All matches were converted to FASTA
800 sequences for multiple sequence alignment. The reference genome sequence is shown
801 at top for comparison. The sequence identifiers start with single characters for tissue
802 ("L" for leaf; "T" for tassel), genotype ("1" for wildtype, "2" for mkaku41 homozygous
803 mutant), or bioreplicate ("A", "B", or "C" for bioreplicate 1, 2, or 3, respectively), followed
804 by unique identifier from Illumina sequence read name. The strandedness is indicated
805 relative to the gene model, with all antisense RNAs indicated (ANTISENSE, red text).
806
807 **Supplementary Tables:**
808
809 **Table S1: Values for apFRET efficiency with Internal controls and multiple**
810 **comparisons of all treatments.**
811 A) All apFRET efficiency % values for data presented in figure 3C including internal
812 control values. B) Tukey multiple comparison one way Anova dataset from all apFRET
813 data presented, including that presented in figure 3C.
814 **Table S2: Differentially expressed genes between *mkaku41* mutant versus**
815 **wildtype plants for maize leaf and tassel.**
816 **Table S3: Plasmid information and Addgene IDs.**
817
818

819

820 # References

821

822 Agrawal A, Lele TP (2019) Mechanics of nuclear membranes. J Cell Sci 132:jcs229245.
823 https://doi.org/10.1242/jcs.229245
824 Alam SG, Zhang Q, Prasad N, et al (2016) The mammalian LINC complex regulates genome
825 transcriptional responses to substrate rigidity. Sci Rep 6:38063.
826 https://doi.org/10.1038/srep38063
827 Bouzid T, Kim E, Riehl BD, et al (2019) The LINC complex, mechanotransduction, and
828 mesenchymal stem cell function and fate. J Biol Eng 13:68.
829 https://doi.org/10.1186/s13036-019-0197-9
830 Brink RA (1956) A Genetic Change Associated with the R Locus in Maize Which Is Directed and
831 Potentially Reversible. Genetics 41:872–889
832 Chang W, Worman HJ, Gundersen GG (2015) Accessorizing and anchoring the LINC complex
833 for multifunctionality. J Cell Biol 208:11–22. https://doi.org/10.1083/jcb.201409047
834 Choi J, Strickler SR, Richards EJ (2019) Loss of CRWN Nuclear Proteins Induces Cell Death
835 and Salicylic Acid Defense Signaling. Plant Physiol 179:1315–1329.
836 https://doi.org/10.1104/pp.18.01020
837 Ciska M, Hikida R, Masuda K, Moreno Díaz de la Espina S (2019) Evolutionary history and
838 structure of nuclear matrix constituent proteins, the plant analogues of lamins. J Exp Bot
839 70:2651–2664. https://doi.org/10.1093/jxb/erz102
840 Ciska M, Moreno Dí-az de la Espina S (2014) The intriguing plant nuclear lamina. Front Plant
841 Sci 5:. https://doi.org/10.3389/fpls.2014.00166
842 Collings DA, Carter CN, Rink JC, et al (2000) Plant Nuclei Can Contain Extensive Grooves and
843 Invaginations. 16. https://doi.org/10.1105/tpc.12.12.2425
844 Crisp M, Liu Q, Roux K, et al (2006) Coupling of the nucleus and cytoplasm: Role of the LINC
845 complex. J Cell Biol 172:41–53. https://doi.org/10.1083/jcb.200509124
846 De Magistris P, Antonin W (2018) The Dynamic Nature of the Nuclear Envelope. Curr Biol
847 28:R487–R497. https://doi.org/10.1016/j.cub.2018.01.073
848 Dittmer TA, Stacey NJ, Sugimoto-Shirasu K, Richards EJ (2007) *LITTLE NUCLEI* Genes
849 Affecting Nuclear Morphology in *Arabidopsis thaliana*. Plant Cell 19:2793–2803.
850 https://doi.org/10.1105/tpc.107.053231
851 Enyedi B, Niethammer P (2017) Nuclear membrane stretch and its role in mechanotransduction.

852 Nucleus 8:156–161. https://doi.org/10.1080/19491034.2016.1263411
853 Evans DE, Graumann K (2018) THE LINKER OF NUCLEOSKELETON AND CYTOSKELETON
854 COMPLEX IN HIGHER PLANTS. https://doi.org/10.1002/9781119312994.apr0617
855 Gerbino A, Procino G, Svelto M, Carmosino M (2018) Role of Lamin A/C Gene Mutations in the
856 Signaling Defects Leading to Cardiomyopathies. Front Physiol 9:1356.
857 https://doi.org/10.3389/fphys.2018.01356
858 Goto C, Tamura K, Fukao Y, et al (2014) The Novel Nuclear Envelope Protein KAKU4
859 Modulates Nuclear Morphology in *Arabidopsis*. Plant Cell 26:2143–2155.
860 https://doi.org/10.1105/tpc.113.122168
861 Goto C, Tamura K, Nishimaki S, et al (2020) The nuclear envelope protein KAKU4 determines
862 the migration order of the vegetative nucleus and sperm cells in pollen tubes. J Exp Bot
863 71:6273–6281. https://doi.org/10.1093/jxb/eraa367
864 Graumann K (2014) Evidence for LINC1-SUN Associations at the Plant Nuclear Periphery.
865 PLoS ONE 9:e93406. https://doi.org/10.1371/journal.pone.0093406
866 Graumann K, Evans DE (2017) The Nuclear Envelope - Structure and Protein Interactions. In:
867 Roberts JA (ed) Annual Plant Reviews online. John Wiley & Sons, Ltd, Chichester, UK,
868 pp 19–56
869 Graumann K, Runions J, Evans DE (2010) Characterization of SUN-domain proteins at the
870 higher plant nuclear envelope. Plant J 61:134–144. https://doi.org/10.1111/j.1365-
871 313X.2009.04038.x
872 Grob S, Schmid MW, Grossniklaus U (2014) Hi-C Analysis in Arabidopsis Identifies the KNOT,
873 a Structure with Similarities to the flamenco Locus of Drosophila. Mol Cell 55:678–693.
874 https://doi.org/10.1016/j.molcel.2014.07.009
875 Gumber HK, McKenna JF, Estrada AL, et al (2019a) Identification and characterization of genes
876 encoding the nuclear envelope LINC complex in the monocot species *Zea mays*. J Cell
877 Sci 132:jcs221390. https://doi.org/10.1242/jcs.221390
878 Gumber HK, McKenna JF, Tolmie AF, et al (2019b) MLKS2 is an ARM domain and F-actin-
879 associated KASH protein that functions in stomatal complex development and meiotic
880 chromosome segregation. Nucleus 10:144–166.
881 https://doi.org/10.1080/19491034.2019.1629795
882 Guo T, Mao X, Zhang H, et al (2017) Lamin-like Proteins Negatively Regulate Plant Immunity
883 through NAC WITH TRANSMEMBRANE MOTIF1-LIKE9 and NONEXPRESSOR OF PR
884 GENES1 in Arabidopsis thaliana. Mol Plant 10:1334–1348.
885 https://doi.org/10.1016/j.molp.2017.09.008

886 Hagan I, Yanagida M (1995) The Product of the Spindle Formation Gene sadl+Associates with
887 the Fission Yeast Spindle Pole Body and Is Essential for Viability. 15
888 Haque F, Lloyd DJ, Smallwood DT, et al (2006) SUN1 Interacts with Nuclear Lamin A and
889 Cytoplasmic Nesprins To Provide a Physical Connection between the Nuclear Lamina
890 and the Cytoskeleton. Mol Cell Biol 26:3738–3751.
891 https://doi.org/10.1128/MCB.26.10.3738-3751.2006
892 Hetzer MW (2010) The Nuclear Envelope. Cold Spring Harb Perspect Biol 2:a000539–a000539.
893 https://doi.org/10.1101/cshperspect.a000539
894 Hieda M (2019) Signal Transduction across the Nuclear Envelope: Role of the LINC Complex in
895 Bidirectional Signaling. 12
896 Howe ES, Murphy SP, Bass HW (2013) Three-Dimensional Acrylamide Fluorescence In Situ
897 Hybridization for Plant Cells. In: Pawlowski WP, Grelon M, Armstrong S (eds) Plant
898 Meiosis: Methods and Protocols. Humana Press, Totowa, NJ, pp 53–66
899 Hu B, Wang N, Bi X, et al (2019) Plant lamin-like proteins mediate chromatin tethering at the
900 nuclear periphery. Genome Biol 20:87. https://doi.org/10.1186/s13059-019-1694-3
901 Irons SL, Evans DE, Brandizzi F (2003) The first 238 amino acids of the human lamin B
902 receptor are targeted to the nuclear envelope in plants. J Exp Bot 54:943–950.
903 https://doi.org/10.1093/jxb/erg102
904 Janin A, Bauer D, Ratti F, et al (2017) Nuclear envelopathies: a complex LINC between nuclear
905 envelope and pathology. Orphanet J Rare Dis 12:147. https://doi.org/10.1186/s13023-
906 017-0698-x
907 Jorgens DM, Inman JL, Wojcik M, et al (2017) Deep nuclear invaginations are linked to
908 cytoskeletal filaments – integrated bioimaging of epithelial cells in 3D culture. J Cell Sci
909 130:177–189. https://doi.org/10.1242/jcs.190967
910 Karimi M, Inzé D, Depicker A (2002) GATEWAY^{TM} vectors for Agrobacterium-mediated plant
911 transformation. Trends Plant Sci 7:193–195. https://doi.org/10.1016/S1360-
912 1385(02)02251-3
913 Kim DI, Kc B, Roux KJ (2015) Making the LINC: SUN and KASH protein interactions. Biol Chem
914 396:295–310. https://doi.org/10.1515/hsz-2014-0267
915 Lammerding J, Schulze PC, Takahashi T, et al (2004) Lamin A/C deficiency causes defective
916 nuclear mechanics and mechanotransduction. J Clin Invest 113:370–378.
917 https://doi.org/10.1172/JCI200419670
918 Legartová S, Stixová L, Laur O, et al (2014) Nuclear Structures Surrounding Internal Lamin
919 Invaginations: MORPHOLOGY OF INTERNAL LAMINS. J Cell Biochem 115:476–487.

https://doi.org/10.1002/jcb.24681

Leppek K, Das R, Barna M (2018) Functional 5′ UTR mRNA structures in eukaryotic translation regulation and how to find them. Nat Rev Mol Cell Biol 19:158–174. https://doi.org/10.1038/nrm.2017.103

Luxton GG, Starr DA (2014) KASHing up with the nucleus: novel functional roles of KASH proteins at the cytoplasmic surface of the nucleus. Curr Opin Cell Biol 28:69–75. https://doi.org/10.1016/j.ceb.2014.03.002

Malone CJ, Fixsen WD, Horvitz HR, Han M (1999) UNC-84 localizes to the nuclear envelope and is required for nuclear migration and anchoring during C. elegans development. Dev Camb Engl 126:3171–3181

Martiniere A, Lavagi I, Nageswaran G, et al (2012) Cell wall constrains lateral diffusion of plant plasma-membrane proteins. Proc Natl Acad Sci 109:12805–12810. https://doi.org/10.1073/pnas.1202040109

Masuda K Peripheral Framework of Carrot Cell Nucleus Contains a Novel Protein Predicted to Exhibit a Long a-Helical Domain. 9. https://doi.org/10.1006/excr.1997.3531

Masuda K, Xu ZJ, Takahashi S, et al (1997) Peripheral framework of carrot cell nucleus contains a novel protein predicted to exhibit a long alpha-helical domain. Exp Cell Res 232:173–181. https://doi.org/10.1006/excr.1997.3531

McCarty DR, Meeley RB (2009) Transposon Resources for Forward and Reverse Genetics in Maize. In: Bennetzen JL, Hake S (eds) Handbook of Maize. Springer New York, New York, NY, pp 561–584

McKenna JF, Rolfe DJ, Webb SED, et al (2019) The cell wall regulates dynamics and size of plasma-membrane nanodomains in *Arabidopsis*. Proc Natl Acad Sci 116:12857–12862. https://doi.org/10.1073/pnas.1819077116

Meier I, Richards EJ, Evans DE (2017) Cell Biology of the Plant Nucleus. Annu Rev Plant Biol 68:139–172. https://doi.org/10.1146/annurev-arplant-042916-041115

Murphy SP, Simmons CR, Bass HW (2010) Structure and expression of the maize (Zea mays L.) SUN-domain protein gene family: evidence for the existence of two divergent classes of SUN proteins in plants. BMC Plant Biol 10:269. https://doi.org/10.1186/1471-2229-10-269

Newman-Griffis AH, del Cerro P, Charpentier M, Meier I (2019) Medicago LINC Complexes Function in Nuclear Morphology, Nuclear Movement, and Root Nodule Symbiosis. Plant Physiol 179:491–506. https://doi.org/10.1104/pp.18.01111

Pawar V, Poulet A, Détourné G, et al (2016) A novel family of plant nuclear envelope-associated

proteins. J Exp Bot 67:5699–5710. https://doi.org/10.1093/jxb/erw332

Pradillo M, Evans D, Graumann K (2019) The nuclear envelope in higher plant mitosis and meiosis. Nucleus 10:55–66. https://doi.org/10.1080/19491034.2019.1587277

Rothballer A, Kutay U (2013) The diverse functional LINCs of the nuclear envelope to the cytoskeleton and chromatin. Chromosoma 122:415–429. https://doi.org/10.1007/s00412-013-0417-x

Sakamoto Y (2020) Nuclear lamina CRWN proteins regulate chromatin organization, gene expression, and nuclear body formation in plants. J Plant Res 133:457–462. https://doi.org/10.1007/s10265-020-01184-1

Schermelleh L, Carlton PM, Haase S, et al (2008) Subdiffraction Multicolor Imaging of the Nuclear Periphery with 3D Structured Illumination Microscopy. Science 320:1332–1336. https://doi.org/10.1126/science.1156947

Schreiber KH, Kennedy BK (2013) When Lamins Go Bad: Nuclear Structure and Disease. Cell 152:1365–1375. https://doi.org/10.1016/j.cell.2013.02.015

Sparkes IA, Runions J, Kearns A, Hawes C (2006) Rapid, transient expression of fluorescent fusion proteins in tobacco plants and generation of stably transformed plants. Nat Protoc 1:2019–2025. https://doi.org/10.1038/nprot.2006.286

Starr DA (2002) Role of ANC-1 in Tethering Nuclei to the Actin Cytoskeleton. Science 298:406–409. https://doi.org/10.1126/science.1075119

Starr DA (2019) A network of nuclear envelope proteins and cytoskeletal force generators mediates movements of and within nuclei throughout *Caenorhabditis elegans* development. Exp Biol Med 244:1323–1332. https://doi.org/10.1177/1535370219871965

Starr DA, Fridolfsson HN (2010) Interactions Between Nuclei and the Cytoskeleton Are Mediated by SUN-KASH Nuclear-Envelope Bridges. Annu Rev Cell Dev Biol 26:421–444. https://doi.org/10.1146/annurev-cellbio-100109-104037

Swift J, Ivanovska IL, Buxboim A, et al (2013) Nuclear Lamin-A Scales with Tissue Stiffness and Enhances Matrix-Directed Differentiation. Science 341:1240104–1240104. https://doi.org/10.1126/science.1240104

Tamura K, Goto C, Hara-Nishimura I (2015) Recent advances in understanding plant nuclear envelope proteins involved in nuclear morphology. J Exp Bot 66:1641–1647. https://doi.org/10.1093/jxb/erv036

Tamura K, Iwabuchi K, Fukao Y, et al (2013) Myosin XI-i Links the Nuclear Membrane to the Cytoskeleton to Control Nuclear Movement and Shape in Arabidopsis. Curr Biol 23:1776–1781. https://doi.org/10.1016/j.cub.2013.07.035

Wang H, Dittmer TA, Richards EJ (2013) Arabidopsis CROWDED NUCLEI (CRWN) proteins are required for nuclear size control and heterochromatin organization. BMC Plant Biol 13:200. https://doi.org/10.1186/1471-2229-13-200

Zhang X, Zhao M, McCarty DR, Lisch D (2020) Transposable elements employ distinct integration strategies with respect to transcriptional landscapes in eukaryotic genomes. Nucleic Acids Res 48:6685–6698. https://doi.org/10.1093/nar/gkaa370

Zhao W, Guan C, Feng J, et al (2016) The *Arabidopsis CROWDED NUCLEI* genes regulate seed germination by modulating degradation of ABI5 protein: CRWNs regulate seed germination. J Integr Plant Biol 58:669–678. https://doi.org/10.1111/jipb.12448

Zhou X, Graumann K, Wirthmueller L, et al (2014) Identification of unique SUN-interacting nuclear envelope proteins with diverse functions in plants. J Cell Biol 205:677–692. https://doi.org/10.1083/jcb.201401138

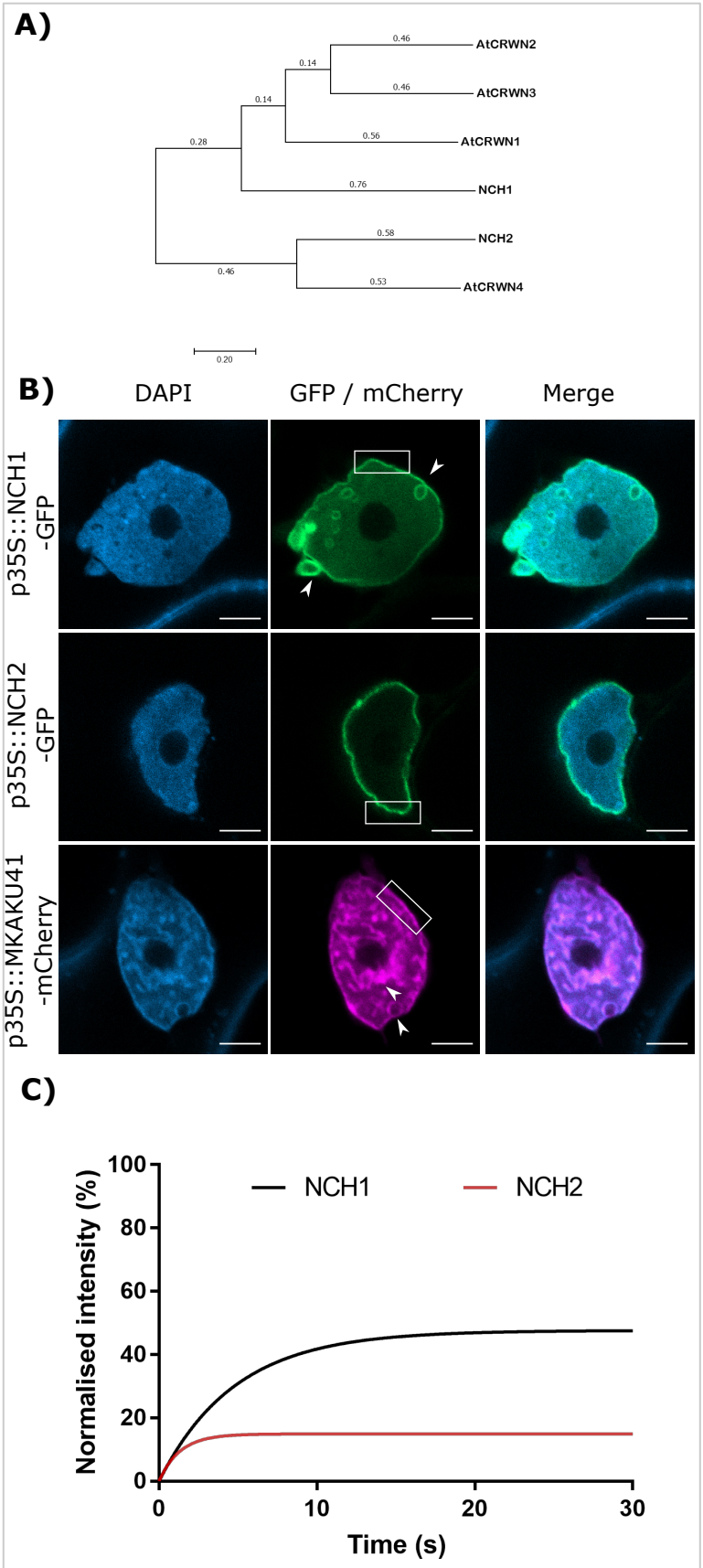

Figure 1 (McKenna, Gumber, et al., submitted Dec. 2020)

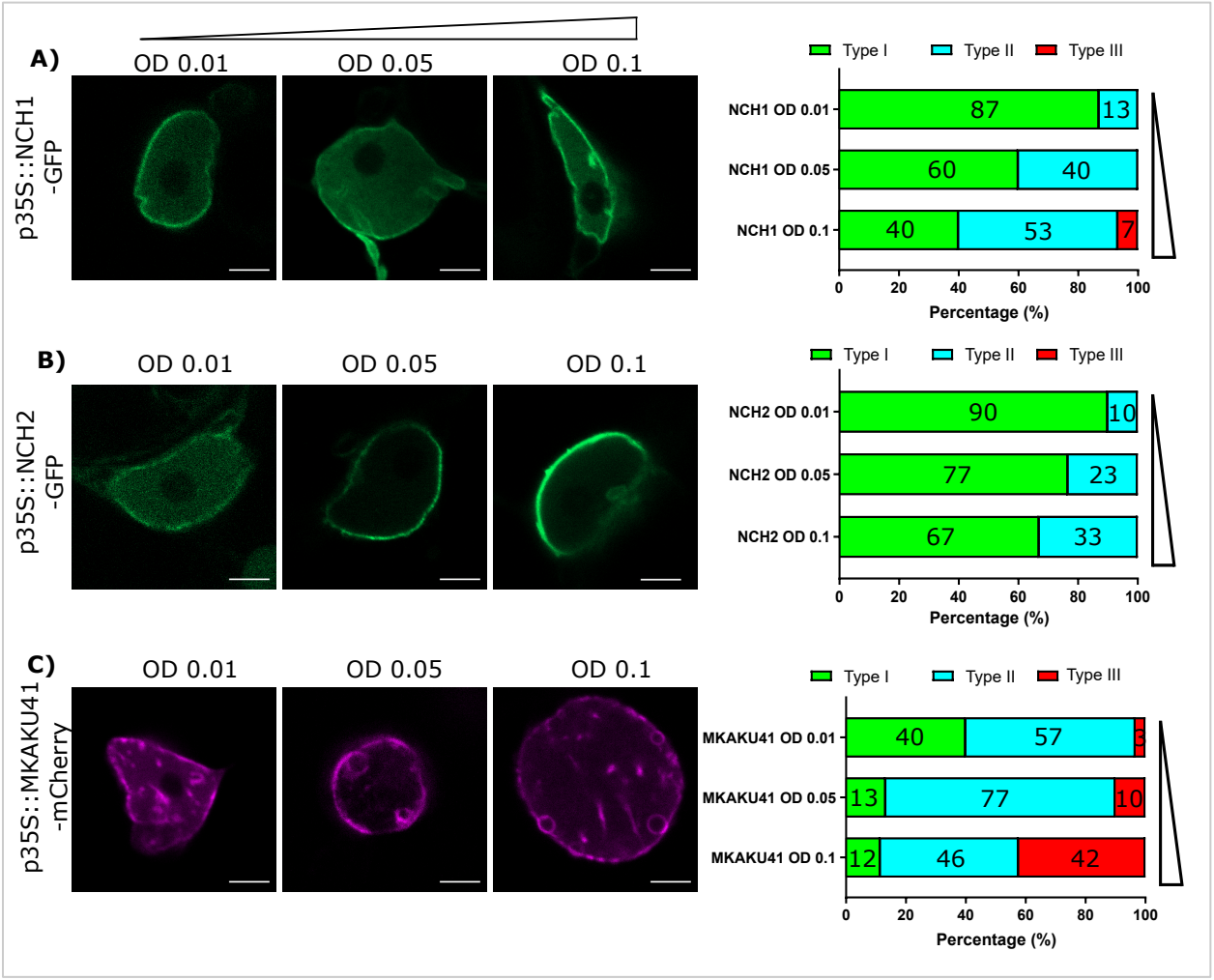

Figure 2

(McKenna, Gumber, et al., submitted Dec. 2020)

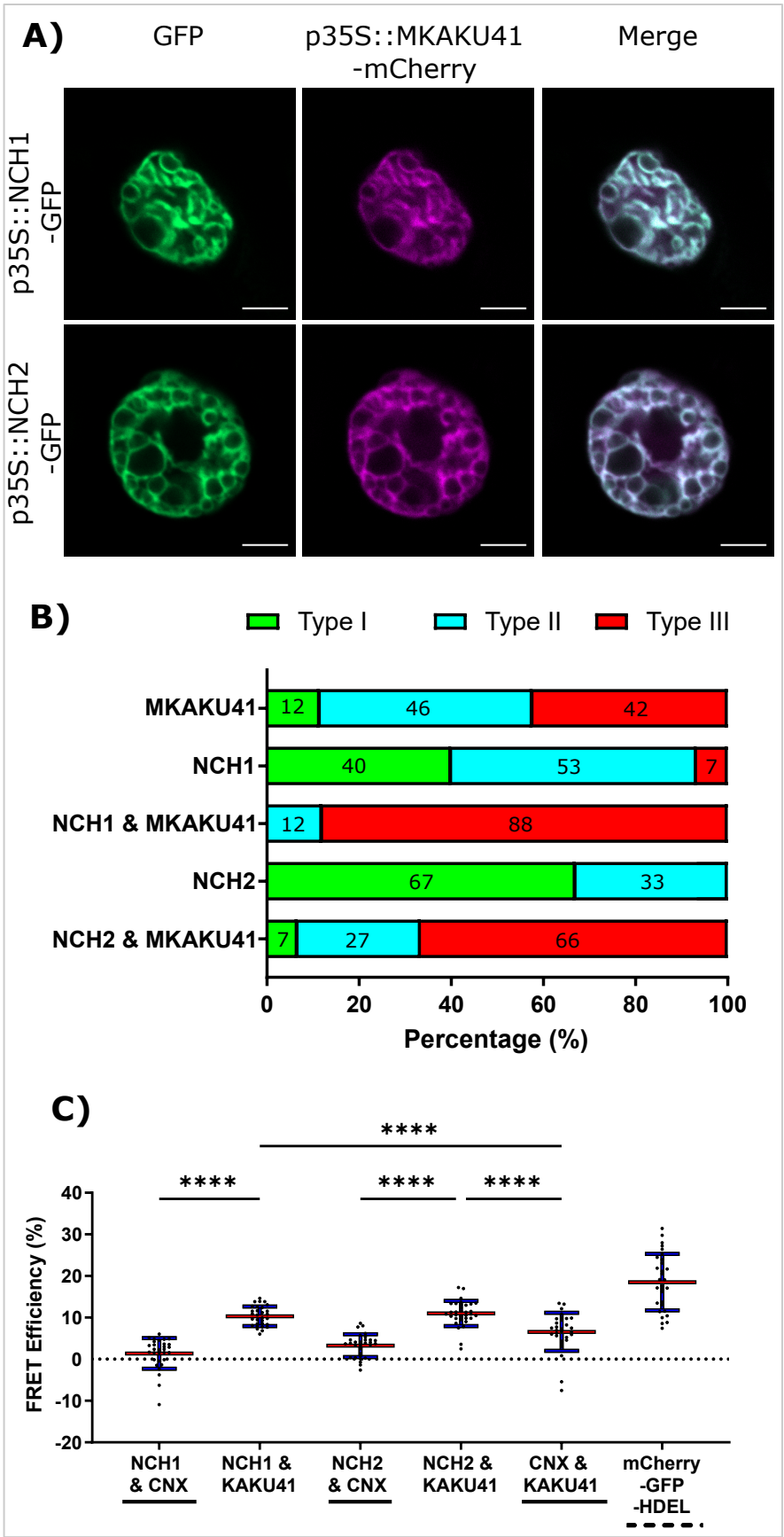

Figure 3 (McKenna, Gumber, et al., submitted Dec. 2020)

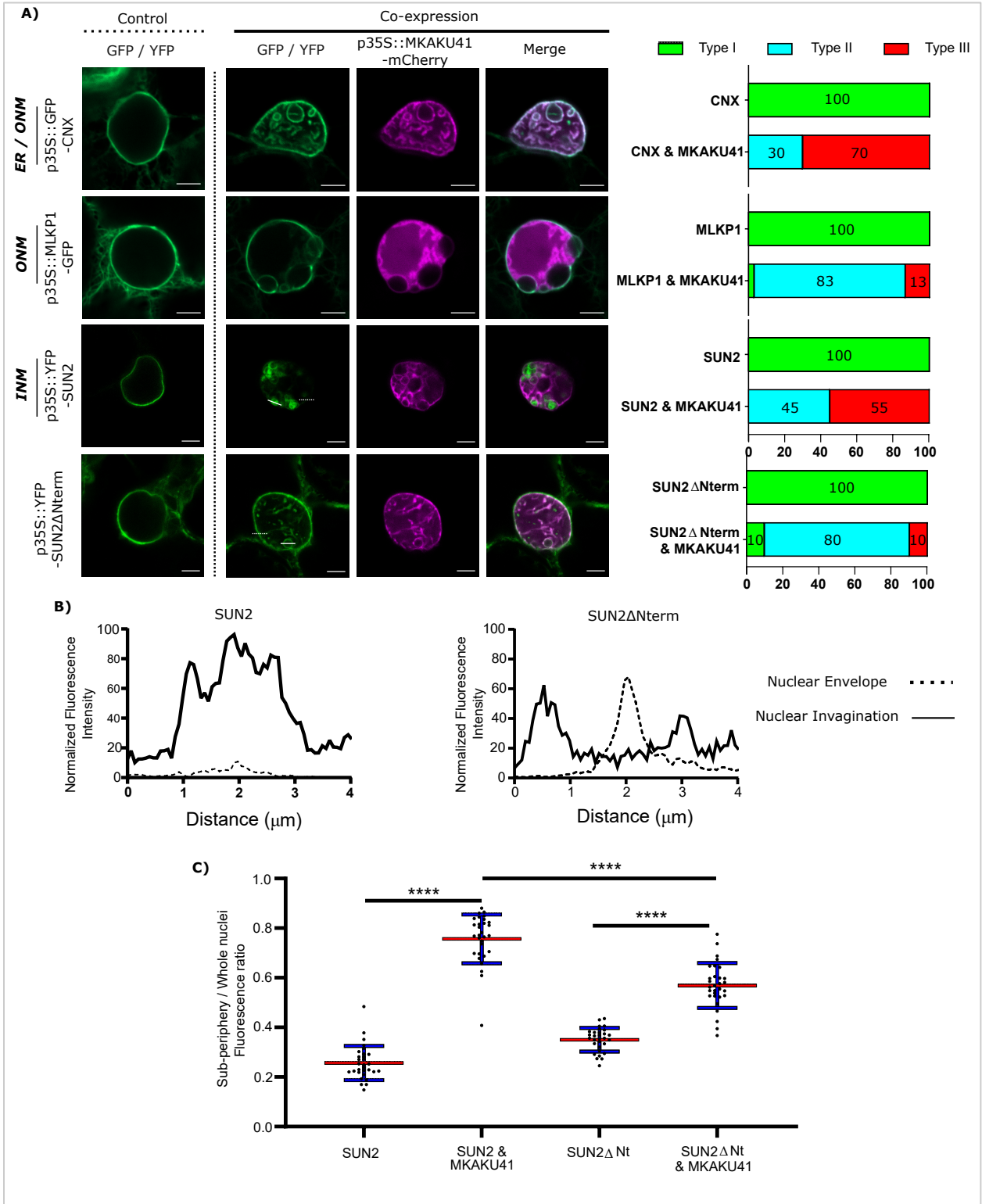

Figure 4

(McKenna, Gumber, et al., submitted Dec. 2020)

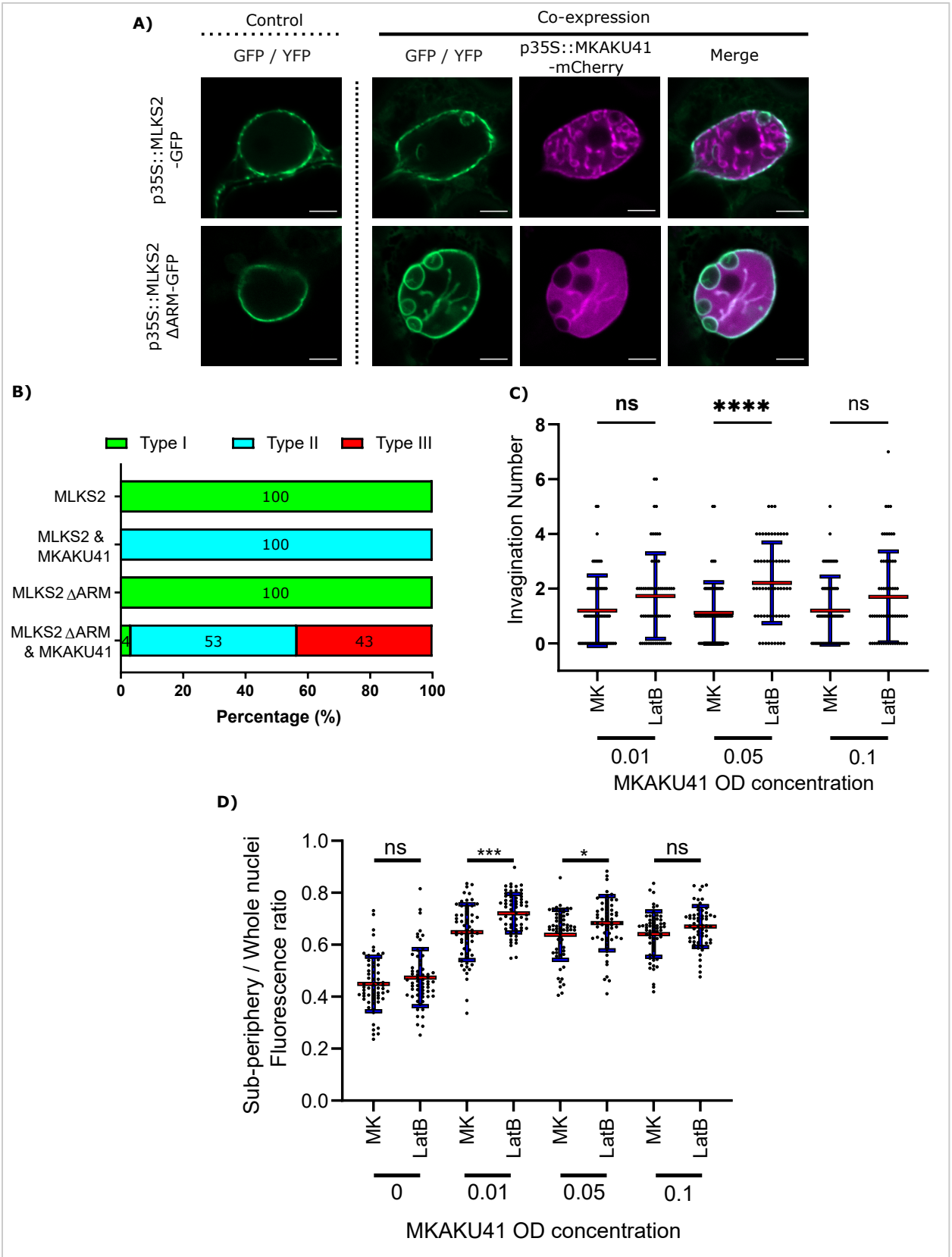

Figure 5

(McKenna, Gumber, et al., submitted Dec. 2020)

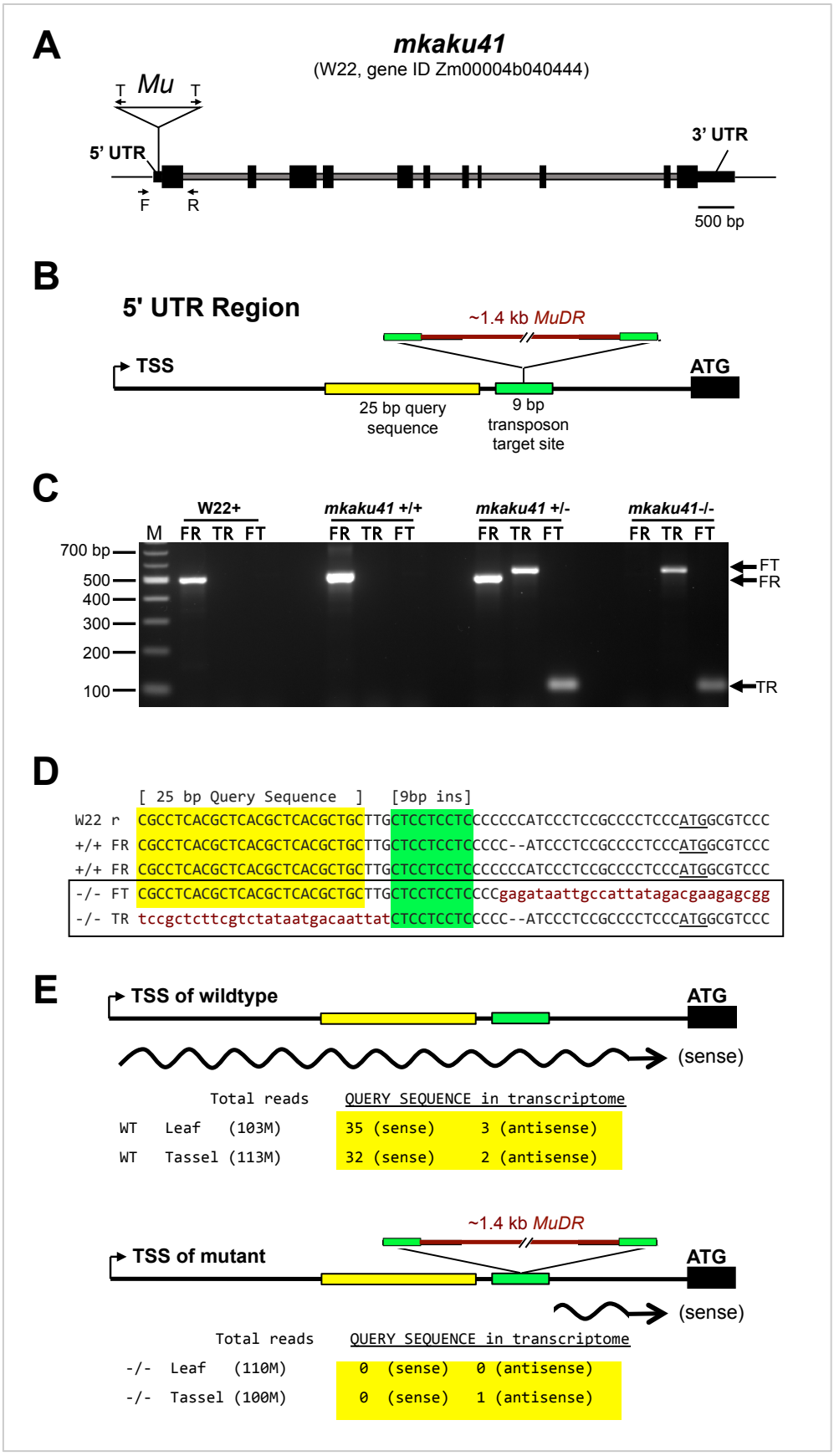

Figure 6 (McKenna, Gumber, et al., submitted Dec. 2020)

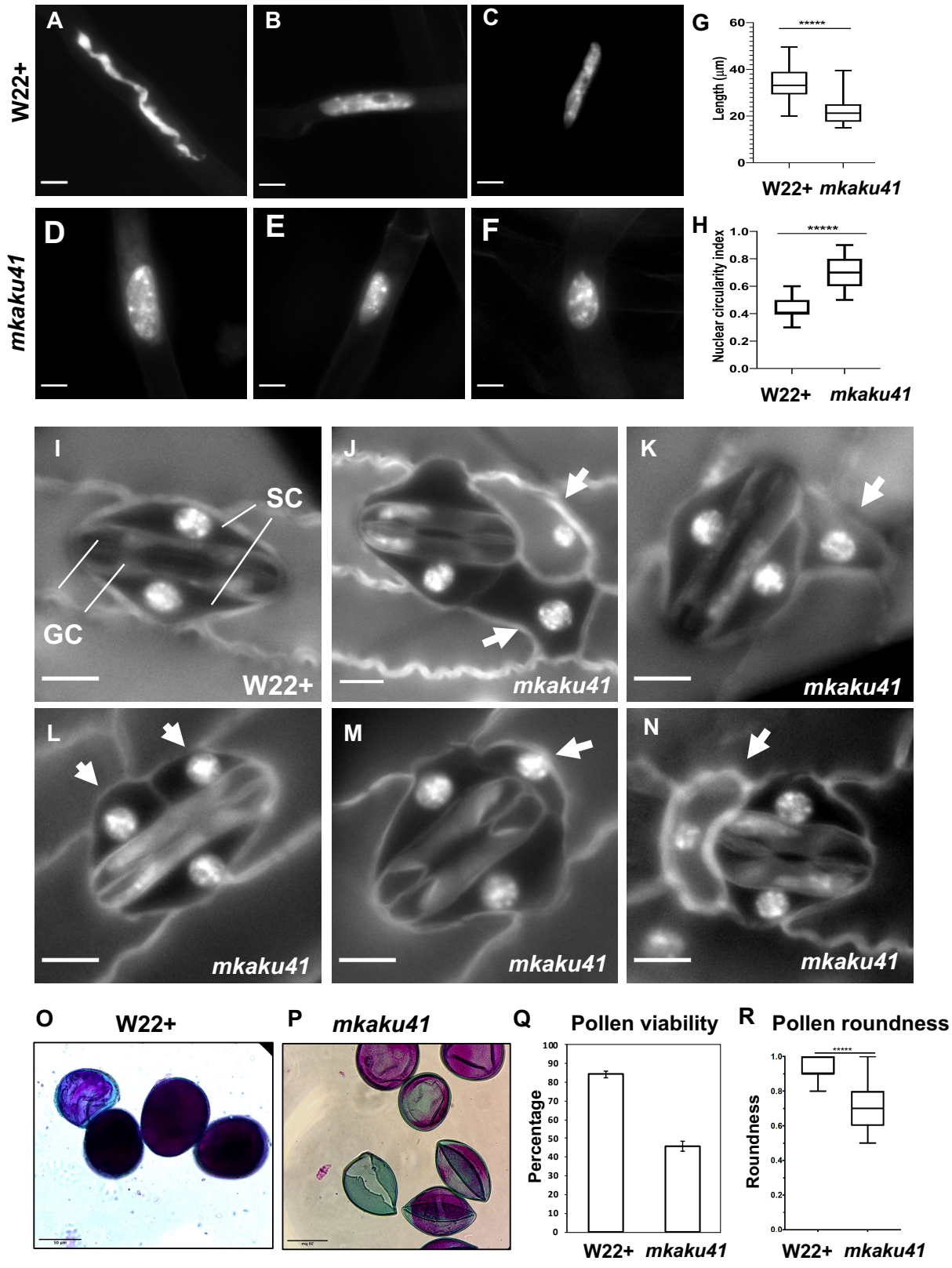

Figure 7

(McKenna, Gumber, et al., submitted Dec. 2020)

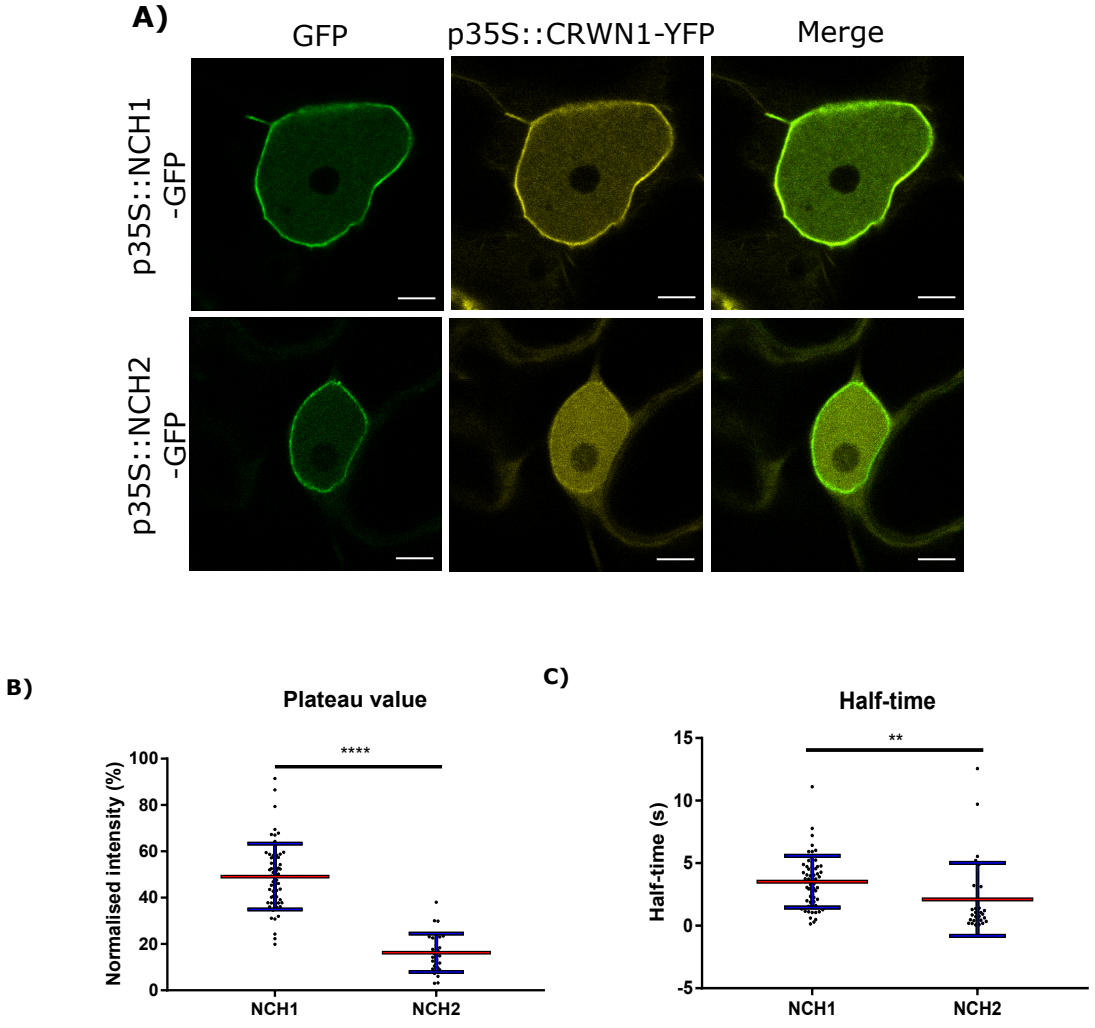

Figure S1

(McKenna, Gumber, et al., submitted Dec. 2020)

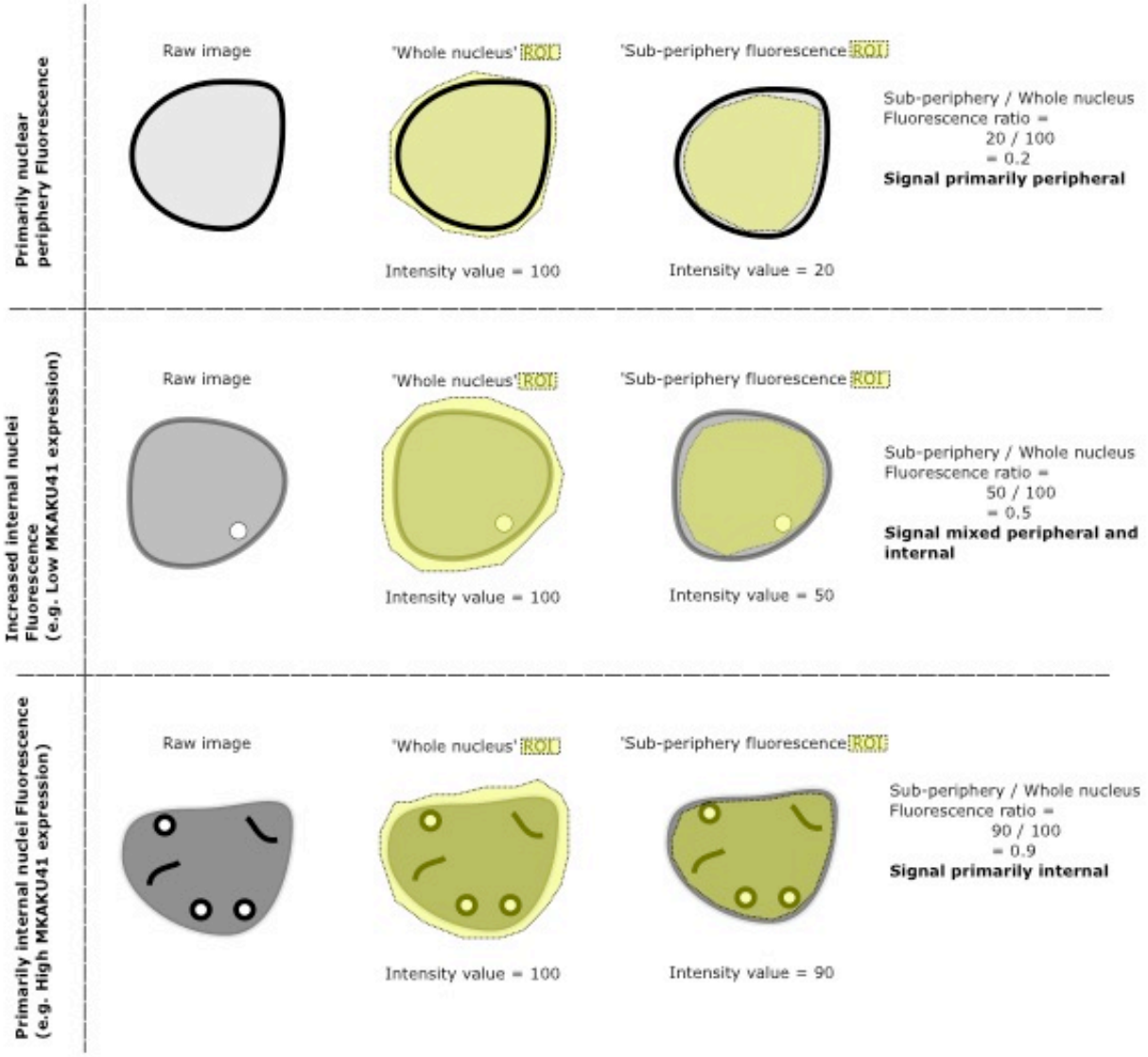

Figure S2

(McKenna, Gumber, et al., submitted Dec. 2020)

A. Gene orientation.

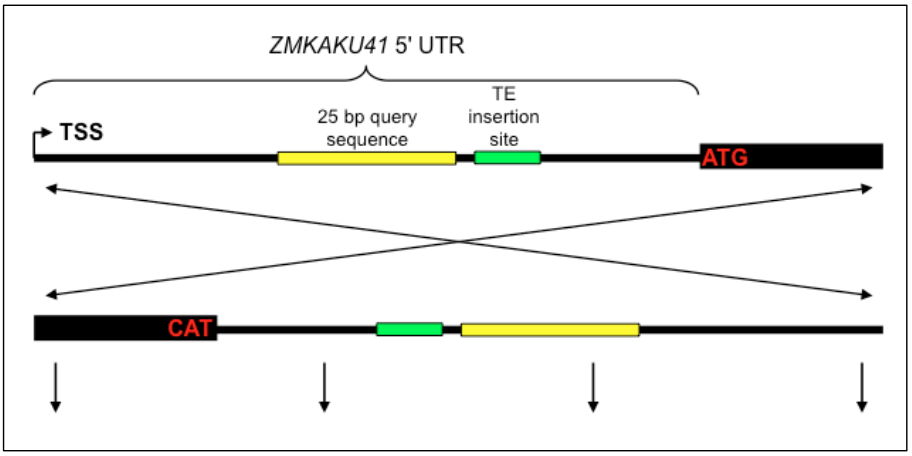

B. Multiple sequence alignment of all transcripts containing the 25 bp query sequence.

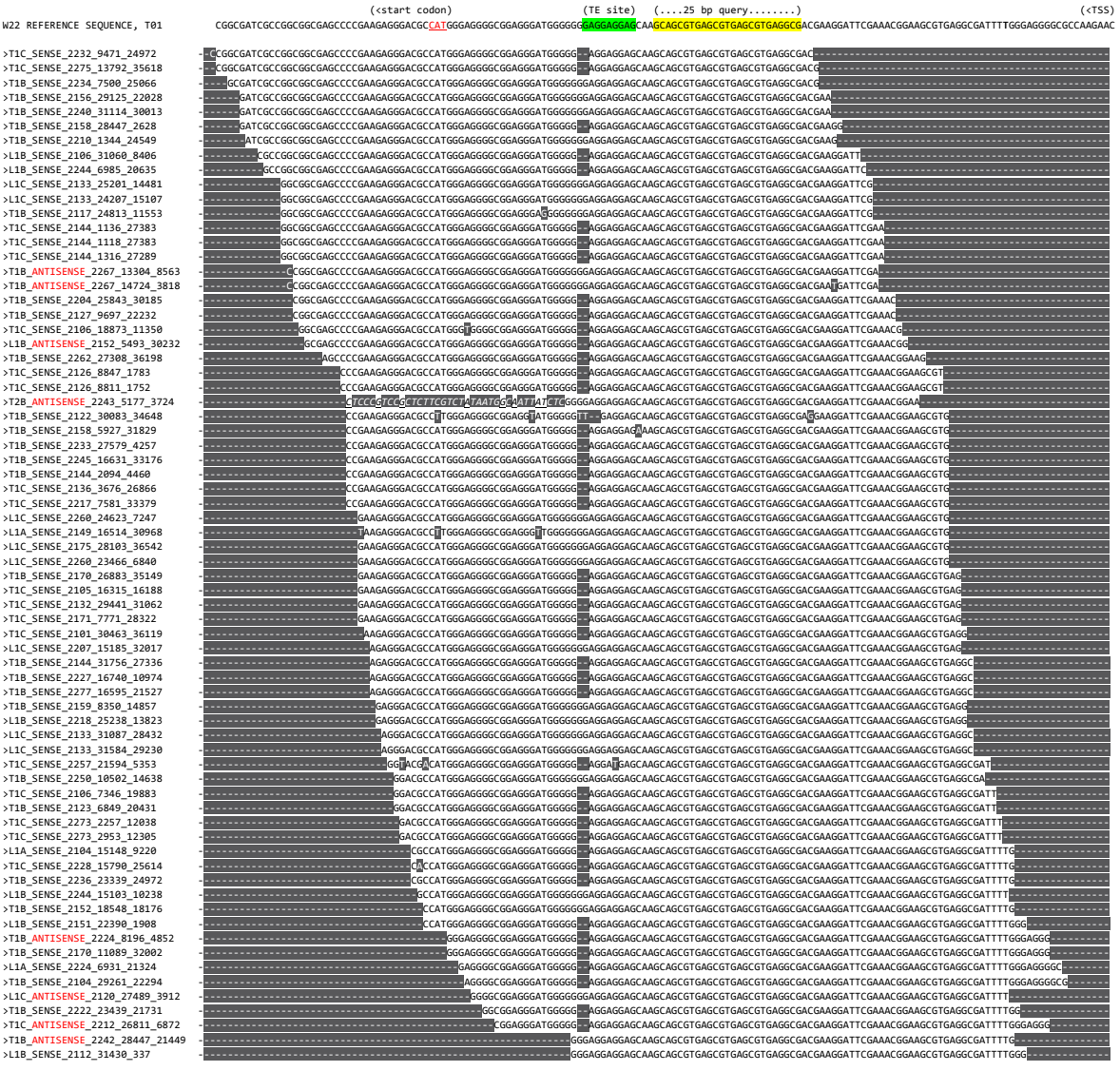

Figure S3 (McKenna, Gumber, et al., submitted Dec. 2020)

Table S1: Values for apFRET efficiency with Internal controls and multiple comparisons of all treatments.

A)	NCH1 & CNX	NCH1 & CNX IC	NCH1 & KAKU41	NCH1 & KAKU41 IC	NCH2 & CNX	NCH2 & CNX IC	NCH2 & KAKU41	NCH2 & KAKU41 IC	CNX & KAKU41	CNX & KAKU41 IC	mCherry -GFP -HDEL	mCherry -GFP -HDEL IC
Number of values	30	30	30	30	30	30	33	33	30	30	30	30
Mean FRET Efficiency (%)	1.4	-0.67	10	-0.94	3.3	-0.86	11	-0.76	6.6	-2.1	19	-0.9
Std. Deviation	3.7	0.53	2.4	0.3	2.7	0.4	3	0.35	4.6	0.63	6.8	1.3
Std. Error of Mean	0.67	0.097	0.43	0.055	0.5	0.074	0.53	0.061	0.84	0.11	1.2	0.23

B)

Tukey's multiple comparisons test	Mean Diff.	95.00% CI of diff.	Below thr	Summary	ed P Value
NCH1 & CNX vs. NCH1 & CNX IC	2.073	-0.4343 to 4.580	No	ns	0.2208
NCH1 & CNX vs. NCH1 & KAKU41	-8.939	-11.45 to -6.432	Yes	****	<0.0001
NCH1 & CNX vs. NCH1 & KAKU41 IC	2.343	-0.1640 to 4.850	No	ns	0.0925
NCH1 & CNX vs. NCH2 & CNX	-1.874	-4.381 to 0.6331	No	ns	0.3694
NCH1 & CNX vs. NCH2 & CNX IC	2.263	-0.2439 to 4.770	No	ns	0.122
NCH1 & CNX vs. NCH2 & KAKU41	-9.607	-12.06 to -7.158	Yes	****	<0.0001
NCH1 & CNX vs. NCH2 & KAKU41 IC	2.163	-0.2862 to 4.612	No	ns	0.1434
NCH1 & CNX vs. CNX & KAKU41	-5.199	-7.706 to -2.692	Yes	****	<0.0001
NCH1 & CNX vs. CNX & KAKU41 IC	3.473	0.9662 to 5.980	Yes	***	0.0004
NCH1 & CNX vs. mCherry -GFP -HDEL	-17.14	-19.65 to -14.64	Yes	****	<0.0001
NCH1 & CNX vs. mCherry -GFP -HDEL IC	2.303	-0.2041 to 4.810	No	ns	0.1065
NCH1 & CNX IC vs. NCH1 & KAKU41	-11.01	-13.52 to -8.505	Yes	****	<0.0001
NCH1 & CNX IC vs. NCH1 & KAKU41 IC	0.2703	-2.237 to 2.777	No	ns	>0.9999
NCH1 & CNX IC vs. NCH2 & CNX	-3.946	-6.453 to -1.440	Yes	****	<0.0001
NCH1 & CNX IC vs. NCH2 & CNX IC	0.1905	-2.316 to 2.697	No	ns	>0.9999
NCH1 & CNX IC vs. NCH2 & KAKU41	-11.68	-14.13 to -9.230	Yes	****	<0.0001
NCH1 & CNX IC vs. NCH2 & KAKU41 IC	0.09053	-2.359 to 2.540	No	ns	>0.9999
NCH1 & CNX IC vs. CNX & KAKU41	-7.272	-9.779 to -4.765	Yes	****	<0.0001
NCH1 & CNX IC vs. CNX & KAKU41 IC	1.401	-1.106 to 3.907	No	ns	0.7958
NCH1 & CNX IC vs. mCherry -GFP -HDEL	-19.22	-21.72 to -16.71	Yes	****	<0.0001
NCH1 & CNX IC vs. mCherry -GFP -HDEL IC	0.2303	-2.277 to 2.737	No	ns	>0.9999
NCH1 & KAKU41 vs. NCH1 & KAKU41 IC	11.28	8.775 to 13.79	Yes	****	<0.0001
NCH1 & KAKU41 vs. NCH2 & CNX	7.065	4.558 to 9.572	Yes	****	<0.0001
NCH1 & KAKU41 vs. NCH2 & CNX IC	11.2	8.695 to 13.71	Yes	****	<0.0001
NCH1 & KAKU41 vs. NCH2 & KAKU41	-0.6675	-3.117 to 1.782	No	ns	0.9991
NCH1 & KAKU41 vs. NCH2 & KAKU41 IC	11.1	8.653 to 13.55	Yes	****	<0.0001
NCH1 & KAKU41 vs. CNX & KAKU41	3.74	1.233 to 6.247	Yes	****	<0.0001
NCH1 & KAKU41 vs. CNX & KAKU41 IC	12.41	9.905 to 14.92	Yes	****	<0.0001
NCH1 & KAKU41 vs. mCherry -GFP -HDEL	-8.204	-10.71 to -5.698	Yes	****	<0.0001
NCH1 & KAKU41 vs. mCherry -GFP -HDEL IC	11.24	8.735 to 13.75	Yes	****	<0.0001
NCH1 & KAKU41 IC vs. NCH2 & CNX	-4.217	-6.724 to -1.710	Yes	****	<0.0001
NCH1 & KAKU41 IC vs. NCH2 & CNX IC	-0.07984	-2.587 to 2.427	No	ns	>0.9999
NCH1 & KAKU41 IC vs. NCH2 & KAKU41	-11.95	-14.40 to -9.500	Yes	****	<0.0001
NCH1 & KAKU41 IC vs. NCH2 & KAKU41 IC	-0.1798	-2.629 to 2.270	No	ns	>0.9999
NCH1 & KAKU41 IC vs. CNX & KAKU41	-7.542	-10.05 to -5.035	Yes	****	<0.0001
NCH1 & KAKU41 IC vs. CNX & KAKU41 IC	1.13	-1.377 to 3.637	No	ns	0.9444
NCH1 & KAKU41 IC vs. mCherry -GFP -HDEL	-19.49	-21.99 to -16.98	Yes	****	<0.0001
NCH1 & KAKU41 IC vs. mCherry -GFP -HDEL IC	-0.04004	-2.547 to 2.467	No	ns	>0.9999
NCH2 & CNX vs. NCH2 & CNX IC	4.137	1.630 to 6.644	Yes	****	<0.0001
NCH2 & CNX vs. NCH2 & KAKU41	-7.733	-10.18 to -5.284	Yes	****	<0.0001
NCH2 & CNX vs. NCH2 & KAKU41 IC	4.037	1.588 to 6.486	Yes	****	<0.0001
NCH2 & CNX vs. CNX & KAKU41	-3.325	-5.832 to -0.8183	Yes	**	0.001
NCH2 & CNX vs. CNX & KAKU41 IC	5.347	2.840 to 7.854	Yes	****	<0.0001
NCH2 & CNX vs. mCherry -GFP -HDEL	-15.27	-17.78 to -12.76	Yes	****	<0.0001
NCH2 & CNX vs. mCherry -GFP -HDEL IC	4.177	1.670 to 6.684	Yes	****	<0.0001
NCH2 & CNX IC vs. NCH2 & KAKU41	-11.87	-14.32 to -9.421	Yes	****	<0.0001
NCH2 & CNX IC vs. NCH2 & KAKU41 IC	-0.09992	-2.549 to 2.349	No	ns	>0.9999
NCH2 & CNX IC vs. CNX & KAKU41	-7.462	-9.969 to -4.955	Yes	****	<0.0001
NCH2 & CNX IC vs. CNX & KAKU41 IC	1.21	-1.297 to 3.717	No	ns	0.9125
NCH2 & CNX IC vs. mCherry -GFP -HDEL	-19.41	-21.91 to -16.90	Yes	****	<0.0001
NCH2 & CNX IC vs. mCherry -GFP -HDEL IC	0.0398	-2.467 to 2.547	No	ns	>0.9999
NCH2 & KAKU41 vs. NCH2 & KAKU41 IC	11.77	9.380 to 14.16	Yes	****	<0.0001
NCH2 & KAKU41 vs. CNX & KAKU41	4.408	1.958 to 6.857	Yes	****	<0.0001
NCH2 & KAKU41 vs. CNX & KAKU41 IC	13.08	10.63 to 15.53	Yes	****	<0.0001
NCH2 & KAKU41 vs. mCherry -GFP -HDEL	-7.537	-9.986 to -5.088	Yes	****	<0.0001
NCH2 & KAKU41 vs. mCherry -GFP -HDEL IC	11.91	9.460 to 14.36	Yes	****	<0.0001
NCH2 & KAKU41 IC vs. CNX & KAKU41	-7.362	-9.812 to -4.913	Yes	****	<0.0001
NCH2 & KAKU41 IC vs. CNX & KAKU41 IC	1.31	-1.139 to 3.759	No	ns	0.8385
NCH2 & KAKU41 IC vs. mCherry -GFP -HDEL	-19.31	-21.76 to -16.86	Yes	****	<0.0001
NCH2 & KAKU41 IC vs. mCherry -GFP -HDEL IC	0.1397	-2.310 to 2.589	No	ns	>0.9999
CNX & KAKU41 vs. CNX & KAKU41 IC	8.672	6.165 to 11.18	Yes	****	<0.0001
CNX & KAKU41 vs. mCherry -GFP -HDEL	-11.94	-14.45 to -9.438	Yes	****	<0.0001
CNX & KAKU41 vs. mCherry -GFP -HDEL IC	7.502	4.995 to 10.01	Yes	****	<0.0001
CNX & KAKU41 IC vs. mCherry -GFP -HDEL	-20.62	-23.12 to -18.11	Yes	****	<0.0001
CNX & KAKU41 IC vs. mCherry -GFP -HDEL IC	-1.17	-3.677 to 1.337	No	ns	0.9296
mCherry -GFP -HDEL vs. mCherry -GFP -HDEL IC	19.45	16.94 to 21.95	Yes	****	<0.0001

*** Note IC = Internal FRET efficiency control**

Supplementary Table S1 is from Mckenna, Gumber, et al., "Maize (Zea mays L.) nucleoskeletal proteins regulate nuclear envelope remodeling…", submitted 12/2020

Table S2: Differentially expressed genes between *mkaku41* mutant versus wildtype plants for maize leaf and tassel.

Table S2 (Tab 1 of 2) LEAF DEGs. All 225 Differentially Expressed Genes from Leaf.

W22v2 GeneID	B73v3 GeneID	B73v4 GeneID	Phytomine description	Uniprot id	Uniprot descriptor	baseMean-LEAF	log2FoldChange (mutant/WT)	lfcSE	stat	pvalue	padj
Zm00004b022952	GRMZM2G079381	Zm00001d052165	(1 of 2) K00366 - ferr	#N/A	#N/A	7467.22838	29.4246738	3.90677062	7.53171267	5.01E-14	4.72E-11
Zm00004b029478	GRMZM2G442804	Zm00001d036738	(1 of 2) 2.1.1.163 - D	B4FF45	S-adenosyl-L-methio	828.430667	13.1270875	3.61827211	3.62799898	0.000286	0.02374659
Zm00004b031378	GRMZM2G163861	Zm00001d039141	(1 of 4) PTHR24055: A	A0A1D6MDU6	Mitogen-activated pr	801.772225	13.0798895	3.63809059	3.59526219	0.000324	0.02627982
Zm00004b032719	GRMZM2G039586	Zm00001d046354	(1 of 2) PTHR10071:	B4F991	GATA transcription fa	675.803091	12.8333192	3.58881725	3.57591882	0.000349	0.02800135
Zm00004b002158	GRMZM2G050961	Zm00001d029997	(1 of 3) PTHR10772: B	4FBN1	Chloroplast chaperor	666.3195	12.8129119	3.61916377	3.54029624	4.00E-04	3.14E-02
Zm00004b031472	GRMZM2G154664	Zm00001d044745	(1 of 1) PTHR11777: A	0A1D6NR62	Alanine--tRNA ligase	442.856807	12.2235394	3.60460055	3.39109402	6.96E-04	4.88E-02
Zm00004b038561	GRMZM2G052036	Zm00001d024241		A0A1D6IYD1	Uncharacterized prot	412.427315	12.1208047	1.25435573	9.6629723	4.33E-22	1.07E-18
Zm00004b024341	GRMZM2G119932	Zm00001d053848	(1 of 5) PF00646//PF	K7U803	Protein SRG1	221.633368	11.2250547	1.22916079	9.13229154	6.71E-20	1.21E-16
Zm00004b040326	GRMZM2G148495	Zm00001d026354		K7TSM1	Uncharacterized prot	155.731123	10.7159853	2.56855691	4.17198672	0.000302	0.00390509
Zm00004b030713	GRMZM2G150471	Zm00001d038361	(1 of 2) PTHR12822:	A0A1D6M5Q9	Protein YIPF	144.117489	10.6047446	1.29299803	8.20167116	2.37E-16	3.35E-13
Zm00004b036977	GRMZM2G000361	Zm00001d021708	(1 of 146) PF13812 -	A0A1D6IE64	Pentatricopeptide rep	91.6284647	9.95055033	2.55206086	3.89902548	0.0000966	0.01021058
Zm00004b002460	GRMZM2G018929	Zm00001d030398	(1 of 2) PTHR24015: A	0A1D6KCE5	Pentatricopeptide rep	73.3024849	9.62871858	2.01775461	4.77199682	0.00000182	0.000344
Zm00004b037691	GRMZM2G020401	Zm00001d022604	(1 of 1) KOG3444 - L	C4J9F3	SNARE-like superfan	65.4345211	9.46628094	1.2787588	7.40271029	1.33E-13	9.78E-11
Zm00004b028573	GRMZM2G133629	Zm00001d035319		A0A1D6LFF8	Uncharacterized prot	61.0798391	9.3646218	1.24462084	7.52407602	5.31E-14	4.78E-11
Zm00004b012339	GRMZM2G048904	Zm00001d014596	(1 of 3) 2.3.1.98 - Ch	A0A1D6GUF2	Alpha-L-fucosidase 2	49.0004256	9.04879444	1.54416675	5.8599853	4.63E-09	0.00000144
Zm00004b012010	GRMZM2G042136	Zm00001d014157	(1 of 6) K03809 - NA	B6SPB2	Flavoprotein wrbA	45.2989985	8.93336195	1.23319652	7.24407002	4.35E-13	2.87E-10
Zm00004b029741	GRMZM2G142443	Zm00001d037085		C4J5G0	Uncharacterized prot	43.6925677	8.88172812	1.25055644	7.10222093	1.23E-12	7.36E-10
Zm00004b030995	GRMZM2G044368	Zm00001d038709	(1 of 5) K07897 - Rar	A0A1D6M9Y7	Ras-related protein F	854.281322	8.80825777	2.49236587	3.534095	0.000409	0.03185181
Zm00004b006605	GRMZM2G129261	Zm00001d002654	(1 of 3) PTHR10593: A	0A1D6E325	Naked endosperm1	793.787161	8.69986561	0.80718841	10.7779863	4.37E-27	2.16E-23
Zm00004b015807	GRMZM2G380319	Zm00001d039492		A0A1D6MHP7	Myb-like transcriptior	892.089428	8.29050629	1.78182041	4.65282935	3.27E-06	0.000573
Zm00004b015016	GRMZM2G090419	Zm00001d017951	(1 of 4) 3.6.1.13//3.6.	B4FG54	Nudix hydrolase 17 n	26.4253106	8.15810576	1.40186465	5.8194675	5.90E-09	1.74E-06
Zm00004b031301	GRMZM2G141252	Zm00001d039054	(1 of 5) PTHR10093	#N/A	#N/A	90.5160879	8.08452683	1.15322615	7.01035681	2.38E-12	1.38E-09
Zm00004b000717	GRMZM2G471253	Zm00001d028138	(1 of 3) PF04481 - Pr	A0A1D6JSB5	Thiamine monophosp	70.5305127	7.71803729	1.08519142	7.11214369	1.14E-12	7.06E-10
Zm00004b036815	GRMZM2G069928	Zm00001d021532	(1 of 1) K01931 - pro	A0A1D6IBW0	RING/U-box superfar	67.482069	7.66883779	1.29122334	5.9392032	2.86E-09	9.89E-07
Zm00004b013399	GRMZM2G177404		(1 of 4) 1.1.1.35//4.2.	#N/A	#N/A	16.2942554	7.46088293	1.8357165	4.0642893	0.0000482	0.00584858
Zm00004b002499	GRMZM5G876022	Zm00001d030507		A0A1D6KCL1	WAT1-related protein	16.1201044	7.44434477	1.29028755	5.76952384	7.95E-09	0.0000023
Zm00004b004054	GRMZM2G413853	Zm00001d032655	(1 of 1) PTHR14950: A	0A1D6KSK7	Dicer-like 102	8.91036307	6.59202137	1.39215016	4.73513676	0.00000219	0.000409
Zm00004b034409	GRMZM2G420926	Zm00001d048336	(1 of 2) PTHR11668: A	0A1D6PJC8	Serine/threonine-prot	268.748915	6.50183669	1.65029566	3.93980112	0.0000815	0.00886601
Zm00004b037350	GRMZM2G312954	Zm00001d022184	(1 of 4) K17964 - leu	A0A1D6IK37	Putative pentatricope	7.96421792	6.43041896	1.59590284	4.02932986	0.0000559	0.00654916
Zm00004b036573	GRMZM2G052474	Zm00001d021248	(1 of 2) PTHR13943: B	7ZZ58	NC domain-containin	7.83785058	6.40412598	1.6734301	3.82694562	0.00013	0.01277228
Zm00004b025146	GRMZM2G112686	Zm00001d008929	(1 of 1) PTHR22835: A	0A1D6FGP9	GDSL esterase/lipas	6.32065121	6.09817703	1.64375468	3.70990701	0.000207	0.01831493
Zm00004b004163	GRMZM2G379656	Zm00001d032784	(1 of 1) PTHR26402: A	0A1D6KTY7	Two-component resp	6.27782711	6.08247491	1.39072809	4.37359033	0.0000122	0.00175244
Zm00004b036551	GRMZM2G017013	Zm00001d021221	(1 of 6) PTHR12329/ B	6TJD1	Protein binding prote	72.3287031	6.00954777	1.72986443	3.47399926	0.000513	0.03814297
Zm00004b018053	GRMZM2G432390	Zm00001d042397	(1 of 15) 3.6.3.43 - P	A0A1D6N3I1	ABC transporter B fa	612.986352	5.99792177	1.29237744	4.64099851	0.00000347	0.000586
Zm00004b000836	GRMZM2G344416	Zm00001d028274	(1 of 3) PTHR10177: A	0A1D6JU49	Cyclin-SDS	5.65464364	5.93097241	1.51373161	3.9181136	0.0000892	0.00954532
Zm00004b024850	GRMZM2G112968	Zm00001d008529	(1 of 7) 3.1.30.1 - Asp	A0A1D6FDT0	Endonuclease 2	178.036732	5.89782245	1.22968922	4.79618944	0.00000162	0.000308
Zm00004b006533	GRMZM2G038851	Zm00001d002570	(1 of 7) K10577 - ubi	A0A1D6E1Y4	SUMO-conjugating e	5.44743536	5.87866026	1.61415843	3.64193511	2.71E-04	2.29E-02
Zm00004b039730	GRMZM2G038934	Zm00001d025670	(1 of 2) PTHR23344/	A0A1D6J8H8	Glycerophosphodiest	5.34966121	5.85600702	1.47791992	3.96233039	7.42E-05	8.23E-03
Zm00004b027306	GRMZM2G091973	Zm00001d011631	(1 of 2) PTHR10994: B	7ZYI3	Reticulon-like protein	5.3177009	5.83749437	1.59890571	3.65093095	0.000261	0.02228524
Zm00004b007542	GRMZM5G858609	Zm00001d003783		#N/A	#N/A	4.99512044	5.75176401	1.53940107	3.73636484	1.87E-04	1.69E-02
Zm00004b009893	GRMZM2G096106	Zm00001d006845	(1 of 2) K14288 - exp	A0A1D6F180	Exportin-T (Exportin(	4.74289835	5.67384186	1.57729911	3.59718828	3.22E-04	0.0261934
Zm00004b021274	GRMZM2G085573	Zm00001d050051	(1 of 3) PTHR23056: A	0A1D6PZJ6	Calcineurin subunit B	4.65262088	5.64877774	1.44916835	3.89794445	0.000097	0.01021058
Zm00004b016770	GRMZM5G895400		(1 of 2) PF07516 - St	#N/A	#N/A	463.230769	5.52897694	1.52920236	3.61559535	0.0003	0.02460305
Zm00004b024230	GRMZM2G000976	Zm00001d053719	(1 of 2) PTHR11062: A	0A1D6QRU0	Exostosin-like	3.6831895	5.30976093	1.53300346	3.46363272	0.000533	0.03920133
Zm00004b037809	GRMZM2G036918	Zm00001d023301	(1 of 20) K13648 - alj	A0A1D6IRJ1	Hexosyltransferase (I	12.9621521	5.24927925	1.29524929	4.05271732	0.0000506	0.00599844
Zm00004b020694	GRMZM2G036829	Zm00001d049343	(1 of 2) PTHR13343: A	0A1D6PTV7	Glutamyl-tRNA reduc	428.130074	5.2109914	0.56562155	9.21285867	3.18E-20	6.28E-17
Zm00004b017828	GRMZM2G170689	Zm00001d042150	(1 of 4) 3.1.2.12 - S-f	A0A1D6N1Q6	S-formylglutathione h	28.6707786	5.05967754	0.88129422	5.74119001	9.40E-09	0.00000266
Zm00004b000729	GRMZM2G047513	Zm00001d028153	(1 of 1) PTHR11700: A	0A1D6JSF1	30S ribosomal protei	214.661897	4.43378056	1.1150952	3.97614531	0.00007	0.00796499
Zm00004b013031	GRMZM2G058252	Zm00001d015460	(1 of 2) K11098 - sms	A0A1D6H288	Putative small nuclea	89.9045646	4.40178796	1.16074364	3.79221374	0.000149	0.01420386
Zm00004b018106	GRMZM2G013016	Zm00001d042472	(1 of 99) PF03514 - G	A0A1D6N495	Protein SCARECRO	7.5468871	4.38419021	1.26130462	3.47591704	0.000509	0.03801417
Zm00004b021544	GRMZM2G068455	Zm00001d050409	(1 of 2) PTHR11540: B	4FFV3	Malate dehydrogenas	154.545715	4.27985353	1.17886939	3.63047303	0.000283	0.02361936
Zm00004b010999	GRMZM5G854045	Zm00001d013012	(1 of 2) PTHR21561: A	0A1D6GEW1	HIT zinc finger	46.8177556	3.90744209	1.03999381	3.75717822	0.000172	0.01574167
Zm00004b036912	GRMZM2G180082	Zm00001d021639	(1 of 1) 1.14.13.184 - A	0A1D6ID92	Taxane 13-alpha-hyd	32.4905967	3.89378865	0.64241747	6.06116561	1.35E-09	4.95E-07
Zm00004b016491	GRMZM2G121404	Zm00001d040311	(1 of 5) K12619 - 5'-3	A0A1D6MQ12	5'-3' exoribonuclease	17.6527176	3.5797071	0.92159871	3.88423621	0.000103	0.01062619
Zm00004b027586	GRMZM2G460566	Zm00001d011938		K7VM12	Uncharacterized prot	474.944398	3.48226135	0.30138449	11.5542157	7.03E-31	6.95E-27
Zm00004b005210	GRMZM2G348578	Zm00001d034124	(1 of 1) PTHR10869: A	0A1D6L5N8	Putative prolyl 4-hyd	13.4450367	3.42875627	0.8513486	4.02744102	5.64E-05	6.56E-03
Zm00004b040037	GRMZM2G322634	Zm00001d026025		A0A1D6JBS5	Uncharacterized prot	40.7950382	3.38071759	0.81575384	4.14428647	3.41E-05	4.32E-03
Zm00004b024374	GRMZM2G155370	Zm00001d053880	(1 of 52) PF06203 - C	A0A1D6QT42	Protein CHLOROPL/	61.9716189	3.36826757	0.88969286	3.78587684	0.000153	0.01443203
Zm00004b038737	GRMZM2G133512	Zm00001d024470	(1 of 1) PTHR20856/ A	0A1D6ZI0	DNA-directed RNA p	60.9752615	3.18589191	0.43383499	7.34355683	2.08E-13	1.42E-10
Zm00004b013023	GRMZM2G109818	Zm00001d015450	(1 of 2) K19347 - SU	A0A1D6H268	SUN domain protein	163.827706	3.0935191	0.8914755	3.47011118	0.00052	0.03841063
Zm00004b032080	GRMZM2G350319	Zm00001d045492	(1 of 164) PF01535//	A0A1D6NWB0	Pentatricopeptide rep	50.0640181	3.04795717	0.72194349	4.22187779	0.0000242	0.00315389
Zm00004b032780	GRMZM2G022275	Zm00001d046445	(1 of 2) K13137 - seri	A0A1D6P2Q2	Transducin/WD40 rep	88.3284389	2.96716841	0.65562993	4.52567567	6.02E-06	0.000976
Zm00004b035113	GRMZM2G410033	Zm00001d019206	(1 of 1) PTHR32195: B	4FDE0	Tryptophan/tyrosine p	18.7119239	2.90922297	0.74995711	3.87918579	0.000105	0.01068974
Zm00004b036531	GRMZM2G043600	Zm00001d021191	(1 of 113) PF00170 - A	A0A1D6I8V4	Basic-leucine zipper	45.4940578	2.76864759	0.69911159	3.96023703	0.000749	0.00823089
Zm00004b028733	GRMZM2G137930	Zm00001d035616	(1 of 3) PTHR10286: B	4FJX6	Soluble inorganic pyr	1152.17637	2.42705929	0.48414472	5.01308634	0.000000536	0.000116
Zm00004b026814	GRMZM2G005350	Zm00001d011037	(1 of 1) PTHR10159/ A	0A1D6FVL3	MAP kinase phospha	139.669477	2.35883218	0.67501116	3.49450842	0.000475	0.03614443
Zm00004b040568	GRMZM2G138870	Zm00001d026625	(1 of 17) PF06749 - I	A0A1D6JI53	Fiber protein Fb34	38.8115476	2.24965091	0.51411253	4.37579478	1.21E-05	1.75E-03
Zm00004b033483	GRMZM2G138987	Zm00001d047289	(1 of 2) PTHR10693/ C	0P7S7	Nuclear transport fac	309.501595	2.23643667	0.5744732	3.89302176	0.000099	0.01036496
Zm00004b000179	GRMZM2G089860	Zm00001d027445	(1 of 3) PTHR12358: B	4FIE8	Sphingoid long-chain	313.055498	2.1844164	0.41009395	5.32662433	0.0000001	0.0000244
Zm00004b030867	GRMZM2G117410	Zm00001d038540	(1 of 1) KOG2896 - L	C0HEV5	Uncharacterized prot	30.93028	2.18269367	0.58520405	3.72979935	1.92E-04	0.01721105
Zm00004b020935	GRMZM2G046804	Zm00001d049641	(1 of 2) PTHR10836/ K	7UBU0	Glyceraldehyde-3-ph	290.988979	1.89219468	0.29262898	6.46619032	1.01E-10	4.61E-08
Zm00004b001825	GRMZM2G171022	Zm00001d029540	(1 of 72) PF12937 - F	A0A1D6K5T7	F-box protein	26.065444	1.65622357	0.45896546	3.60860178	0.000308	0.02517133
Zm00004b028101	AC194405.3_FG021	Zm00001d012575	(1 of 2) PTHR23336: A	0A1D6G9W8	Protein MICRORCHI	43.5892296	1.60749968	0.31253502	5.14342255	0.00000027	0.0000621
Zm00004b038843	GRMZM2G096367	Zm00001d024598	(1 of 1) PTHR21596/ C	0P4G4	Factor of DNA methy	101.92685	1.56813221	0.40416157	3.87996364	0.000104	0.01068974
Zm00004b031527	GRMZM2G435294	Zm00001d044819	(1 of 2) PTHR13140: A	0A1D6NRL8	Myosin-9	220.170163	1.55391523	0.33465225	4.64337307	0.00000343	0.000586
Zm00004b040275	GRMZM2G114182	Zm00001d026295	(1 of 1) KOG0250 - D	A0A1D6JE74	Uncharacterized prot	46.1680683	1.50835262	0.33433076	4.51155799	6.44E-06	0.00103525
Zm00004b040030	GRMZM2G097848	Zm00001d026020	(1 of 2) PTHR36317: A	0A1D6JBQ3	Protein MULTIPLE C	55.809687	1.3965749	0.33510488	4.16757559	0.0000308	0.00395556
Zm00004b032020	GRMZM2G064302	Zm00001d045431	(1 of 8) K01689 - enc	B4FI65	Enolase 1	11601.3236	1.35638718	0.24653673	5.50176521	3.76E-08	0.00000979
Zm00004b037648	GRMZM2G041527	Zm00001d022551	(1 of 1) K01164 - ribc	A0A1D6IP05	Ribonuclease Ps	46.9191013	1.33158372	0.36258589	3.67246425	0.00024	0.02066647
Zm00004b017415	GRMZM2G022298	Zm00001d041635	(1 of 3) PTHR24006: A	0A1D6MXG4	F-box family protein	1133.3013	1.32018091	0.3021743	4.36893847	0.0000125	0.0017646
Zm00004b011111	GRMZM2G028218	Zm00001d013111	(1 of 10) K09503 - Dn	A0A1D6GG02	DnaJ protein	3402.18212	1.31457414	0.3028865	4.34015424	1.42E-05	1.94E-03
Zm00004b029015	GRMZM2G175867	Zm00001d036052	(1 of 1) PTHR24031: #N/A		#N/A	920.642936	1.28068292	0.17925872	7.14432695	9.04E-13	5.77E-10
Zm00004b012112	GRMZM2G377341	Zm00001d014294	(1 of 3) K11262 - ace	A0A1D6GRS8	Acetyl-CoA carboxyla	5379.52762	1.22873173	0.33739947	3.6417714	0.000271	0.02289614
Zm00004b039163	GRMZM2G330635	Zm00001d024963	(1 of 2) PTHR11260/ B	6TL20	Glutathione S-transfe	821.559951	1.12368212	0.25566698	4.39510063	0.0000111	0.00162285
Zm00004b040552	GRMZM2G343149	Zm00001d026606	(1 of 2) KOG0716 - N	C4J426	DNAJ heat shock N-t	175.191177	1.11399665	0.19553823	5.69707843	1.22E-08	0.00000335
Zm00004b006763	GRMZM2G394450	Zm00001d002830	(1 of 3) PF11837 - D	A0A1D6E4N9	Beta-fructofuranosida	510.860825	1.04284275	0.22253867	4.68611918	0.00000278	0.000492
Zm00004b032888	GRMZM2G069630	Zm00001d046571	(1 of 4) PTHR23042/ A	0A1D6P3H5	Putative HLH DNA-b	435.078325	1.01298064	0.15126213	6.69685548	2.13E-11	1.11E-08
Zm00004b028605	GRMZM2G410757	Zm00001d035456		A0A1D6LGG0	Uncharacterized prot	1102.34203	0.94624438	0.24964589	3.79034631	0.00015	0.01424261
Zm00004b023489	GRMZM2G002220	Zm00001d052809	(1 of 4) K09487 - hea	K7V364	Heat shock protein 9	1163.42188	0.94580231	0.15748147	6.00580049	1.90E-09	6.73E-07
Zm00004b030504	GRMZM2G305851	Zm00001d038085	(1 of 10) PF11891 - D	A0A1D6M325	Protein RETICULATA	1188.38199	0.9352027	0.22602528	4.13760226	0.0000351	0.00442314
Zm00004b005417	GRMZM2G074404	Zm00001d034432	(1 of 2) PTHR23291/ B	6TIC8	Bax inhibitor-1 family	424.535285	0.86562979	0.19919175	4.34571109	1.39E-05	1.93E-03
Zm00004b028575	GRMZM2G143788	Zm00001d035321	(1 of 4) PTHR13844: B	6T2N1	SWIB/MDM2 domain	489.708705	0.85679437	0.23070118	3.71387084	0.000204	0.01811114
Zm00004b018769	GRMZM2G173654	Zm00001d043234	(1 of 1) PTHR12612: A	0A1D6N9M7	NTF2-like	282.736689	0.82559477	0.24273462	3.40122386	0.000671	0.04740744
Zm00004b016582	GRMZM2G111014	Zm00001d040416	(1 of 1) K02470 - DN	A0A1D6MQM1	DNA topoisomerase :	573.22022	0.79663319	0.14929919	5.33581713	9.51E-08	2.35E-05
Zm00004b003782	GRMZM2G127396	Zm00001d032334	(1 of 1) PTHR24092: A	0A1D6KQ39	Phospholipid-transpc	307.752055	0.79617809	0.17445876	4.56370378	5.03E-06	8.29E-04
Zm00004b027549	GRMZM2G046558	Zm00001d011891	(1 of 1) K01070 - S-fo	K7V5R6	S-formylglutathione h	527.285315	0.76070436	0.19834295	3.8352982	0.000125	0.01244172
Zm00004b021214	GRMZM2G090241	Zm00001d049956	(1 of 2) K00215 - 4-h	A0A1D6PYZ9	4-hydroxy-tetrahydro	112.382554	0.73587653	0.19995354	3.68023762	0.000233	0.02013407
Zm00004b040222	GRMZM2G129071	Zm00001d026244	(1 of 2) PTHR30222	B7ZYY2	Putrescine-binding pe	282.623632	0.72752977	0.21154612	3.43910705	0.000584	0.04230188
Zm00004b026760	GRMZM2G086766	Zm00001d010969	(1 of 2) KOG3882 - TC	0PGJ5	Tetraspanin-6	207.76703	0.69786407	0.18917115	3.68906184	2.25E-04	1.97E-02
Zm00004b025751	GRMZM2G158818	Zm00001d009719	(1 of 2) PTHR13832: A	0A1D6FLA0	PPM-type phosphata	532.830662	0.63346597	0.17343334	3.65250396	0.00026	0.02224501
Zm00004b038221	GRMZM2G036427	Zm00001d023830	(1 of 1) PTHR31964: B	6TLW3	Fiber protein Fb19	1562.27079	-0.4159396	0.11035905	-3.7689666	1.64E-04	1.52E-02
Zm00004b011092	GRMZM2G007260	Zm00001d013092	(1 of 5) K10573 - ubi	B4FH08	Ubiquitin-conjugating	923.813124	-0.4178773	0.12114084	-3.4495159	0.000562	0.04100456
Zm00004b012273	AC207656.3_FG002	Zm00001d014507	(1 of 17) PF02362//P	A0A1D6GTV0	Auxin response facto	516.855693	-0.4187385	0.12013197	-3.485654	0.000491	0.0369359
Zm00004b036722	AC207722.2_FG009	Zm00001d021435	(1 of 7) K08912 - ligh	B4FNR1	Chlorophyll a-b bindi	170912.219	-0.4331024	0.11385239	-3.8040698	0.000142	0.01373875
Zm00004b023254	GRMZM2G119175	Zm00001d052494	(1 of 2) PTHR11817/	A0A1D6QHK1	Pyruvate kinase (EC	839.32923	-0.475611	0.12467717	-3.8147405	0.000136	0.01322297
Zm00004b012904	GRMZM2G425774	Zm00001d015293	(1 of 2) PTHR21736: A	0A1D6H134	VIN3-like protein 2	197.522432	-0.6919321	0.19597291	-3.5307537	0.000414	0.03202847
Zm00004b019820	GRMZM2G339540	Zm00001d044434	(1 of 16) PF00069//P	A0A1D6NLS2	Putative inactive rece	227.937947	-0.7314427	0.14663392	-4.9882229	0.000000609	0.000131
Zm00004b038201	GRMZM2G001500	Zm00001d023802	(1 of 3) PTHR19375/ A	0A1D6IW15	Heat shock 70 kDa p	390.383872	-0.7427689	0.16663045	-4.4575823	8.29E-06	1.28E-03
Zm00004b040507	GRMZM2G124466	Zm00001d026543	(1 of 14) PF04755 - P	A0A1D6JH82	Putative plastid-lipid-	880.51809	-0.8379358	0.16072008	-5.2136345	0.000000185	0.0000436
Zm00004b024839	GRMZM2G030384	Zm00001d008517	(1 of 8) PTHR19856 A	0A1D6FDQ9	Actin-interacting prot	325.234613	-0.8419972	0.14369917	-5.8594439	4.64E-09	0.00000144
Zm00004b029016	GRMZM2G110983	Zm00001d036054	(1 of 5) K10573 - ubi	A0A1D6LKH9	Ubiquitin-conjugating	428.180372	-0.9107724	0.14663329	-6.2112252	5.26E-10	2.21E-07
Zm00004b031450	GRMZM2G310569	Zm00001d044717	(1 of 2) PTHR10217: K	7VQ87	Potassium outward r	776.082506	-0.9308469	0.17592059	-5.2912904	1.21E-07	2.90E-05
Zm00004b039612	GRMZM2G132875	Zm00001d025533	(1 of 3) PTHR11732: K	7TPL8	NAD(P)-linked oxidor	470.476633	-0.9542234	0.25513441	-3.7400811	0.000184	0.01677435
Zm00004b019130	GRMZM2G158013	Zm00001d043614	(1 of 1) PTHR11814: A	0A1D6NDM6	Putative sulfate trans	220.659598	-0.9996597	0.28788078	-3.4724782	5.16E-04	3.82E-02
Zm00004b021942	GRMZM2G165231	Zm00001d050947	(1 of 1) PTHR23257: C	0P3M4	Protein kinase superf	268.98269	-1.1283649	0.30233028	-3.7322261	1.90E-04	1.71E-02
Zm00004b023416	GRMZM2G097043	Zm00001d052723	(1 of 1663) 2.7.11.1 - A	0A1D6QJ79	Uncharacterized prot	483.959303	-1.1750113	0.3058207	-3.8421574	0.000122	0.01218775
Zm00004b031824	GRMZM2G301860	Zm00001d045204	(1 of 2) PTHR31729: K	7W642	Putative AP2/EREBP	91.8123203	-1.1767874	0.26793309	-4.3920943	1.12E-05	1.63E-03

Table S2a1 (McKenna, Gumber, et al., submitted Dec. 2020)

Zm00004b020891	GRMZM2G145972	Zm00001d049597	(1 of 6) K17871 - NAI	A0A1D6PWC3	External alternative N	425.719275	-1.2024434	0.34440027	-3.4914125	0.00048	0.03636419
Zm00004b014169	GRMZM2G132706	Zm00001d016942	(1 of 1) PTHR11926|	A0A1D6HBD6	Glycosyltransferase (	88.7275892	-1.2785948	0.33703593	-3.7936455	1.48E-04	0.01419039
Zm00004b012181	GRMZM2G035405	Zm00001d014377	(1 of 19) PF02309|P	A0A1D6GSR8	Auxin response facto	150.839573	-1.3074657	0.2772201	-4.7163454	0.0000024	0.00044
Zm00004b028942	GRMZM2G145396	Zm00001d035948	(1 of 1) PF06592 - Pr	A0A1D6LJT8	ATOZI1	154.479925	-1.3600375	0.30840566	-4.409898	0.0000103	0.00155027
Zm00004b025175	GRMZM2G464891	Zm00001d008963	(1 of 2) PTHR12608:	A0A1D6FGW5	GDT1 family protein	130.802281	-1.3936656	0.2822666	-4.9374087	0.00000792	0.000163
Zm00004b040292	GRMZM2G145460	Zm00001d026311	(1 of 3) K12448 - UD	A0A1D6JEI6	NAD(P)-binding Ross	64.5436053	-1.3980243	0.32470084	-4.3055765	0.0000167	0.00225723
Zm00004b000155	GRMZM2G105436	Zm00001d027416	(1 of 1) 1.3.99.22 - C	A0A1D6JM25	Oxygen-independent	71.9333728	-1.4589143	0.32542419	-4.4831158	0.0000736	0.00117383
Zm00004b024901	GRMZM2G477503	Zm00001d008600	(1 of 39) PF00534 - (	A0A1D6FE41	Sulfoquinovosyl trans	135.498723	-1.4788108	0.38764344	-3.8148739	0.000136	0.01322297
Zm00004b001193	GRMZM2G443265	Zm00001d028713	(1 of 2) PTHR11132|B	A4F896	Putative sugar phosp	146.819959	-1.7099847	0.36230074	-4.7197936	0.00000236	0.000437
Zm00004b031260	GRMZM2G318180	Zm00001d039011	(1 of 2) PTHR10168|	A0A1D6MCV5	Grx_l1-glutaredoxin s	55.4235679	-1.728671	0.4362094	-3.9629385	0.000074	0.00823089
Zm00004b021606	GRMZM2G370915	Zm00001d050484	(1 of 4) PTHR10766|	A0A1D6Q1U4	Transmembrane 9 su	24.9518867	-1.7731962	0.51670068	-3.4317667	0.0006	0.04330487
Zm00004b031166	GRMZM2G010349	Zm00001d038894	(1 of 1) PTHR11584::	A0A1D6MBR1	Serine/threonine-prot	7526.21654	-1.8467058	0.44452862	-4.1543013	0.0000326	0.00416527
Zm00004b030125	GRMZM2G009845	Zm00001d037606	(1 of 4) PF00514|PF	C0P5C0	Importin subunit alph	672.163686	-1.8509677	0.41775015	-4.430801	0.00000939	0.00144006
Zm00004b031291	GRMZM2G065757	Zm00001d039043	(1 of 4) PTHR13683:	A0A1D6MD15	Aspartic proteinase A	895.396897	-1.8789325	0.39154149	-4.7988081	0.0000016	0.000307
Zm00004b034200	GRMZM2G113295	Zm00001d048112	(1 of 4) PTHR13139:	C4JAV5	RING/U-box superfar	14.9266987	-1.9881288	0.58232065	-3.4141479	0.00064	0.04570428
Zm00004b031703	GRMZM2G177098	Zm00001d045054	(1 of 2) 4.2.3.123 - Bi	A0A1D6NT87	Sesquiterpene cyclas	563.977223	-2.083258	0.44239875	-4.7090051	0.00000249	0.000452
Zm00004b023346	GRMZM2G091258	Zm00001d052620	(1 of 3) PF15346 - Ar	B4FUY0	Uncharacterized prot	84.8148844	-2.0969343	0.51434005	-4.0769415	0.0000456	0.0056082
Zm00004b009147	GRMZM2G066516	Zm00001d005917	(1 of 18) PF04784 - I	A0A1D6ERJ3	Ternary complex facti	52.1992731	-2.1476846	0.60276371	-3.5630622	3.67E-04	2.91E-02
Zm00004b038557	GRMZM2G134613	Zm00001d024239	(1 of 4) K08341 - GA	A0A1D6IYD0	Autophagy-related pr	220.308776	-2.1764262	0.29327857	-7.42102	1.16E-13	8.84E-11
Zm00004b010118	GRMZM2G473709	Zm00001d007174		A0A1D6F4F7	Uncharacterized prot	72.7028661	-2.2070216	0.60999614	-3.6180911	2.97E-04	2.45E-02
Zm00004b016247	GRMZM2G360023	Zm00001d039993	(1 of 5) 1.11.1.6 - Cal	B6SUS4	Uncharacterized prot	54.6089476	-2.4961955	0.66210963	-3.7700637	0.000163	0.01522807
Zm00004b014100	GRMZM2G113453	Zm00001d016856	(1 of 15) PF07887 - C	A0A1D6HAV0	Calmodulin binding p	896.773245	-2.5156699	0.56352855	-4.4641393	0.00000804	0.00126316
Zm00004b039718	GRMZM2G173878	Zm00001d025660	(1 of 4) K07877 - Rat	#N/A	#N/A	97.9240301	-2.5271222	0.5819074	-4.3428253	0.0000141	0.00194146
Zm00004b009434	GRMZM2G158629	Zm00001d006270	(1 of 2) KOG1206 - FC	C4JA75	Enoyl-CoA hydratase	85.256169	-2.5476031	0.72103652	-3.5332512	0.00041	0.03185181
Zm00004b001295	GRMZM2G076537	Zm00001d028827	(1 of 1) PTHR13058	A0A1D6K021	Exonuclease DPD1 c	11.6682028	-2.589785	0.67760974	-3.8219417	1.32E-04	1.30E-02
Zm00004b011960	GRMZM2G146446	Zm00001d014109	(1 of 1) PTHR14319	A0A1D6GPY5	Transmembrane prot	47.2813877	-2.634432	0.57927246	-4.5478289	5.42E-06	8.86E-04
Zm00004b000177	GRMZM2G090051	Zm00001d027443	(1 of 9) 1.14.13.129 - A	A0A1D6JM56	Hydroxylase8	165.877537	-2.6361802	0.48594064	-5.4249018	0.000000058	0.0000149
Zm00004b018443	GRMZM5G856598	Zm00001d042841	(1 of 2) K08193 - MF	B6SWK6	Putative anion transp	69.729378	-2.6900638	0.43660711	-6.1612919	7.22E-10	2.69E-07
Zm00004b039626	GRMZM2G104603	Zm00001d025549		B4FV84	Putative carboxylesta	16.7476499	-2.7905884	0.70460708	-3.9604887	0.0000748	0.00823089
Zm00004b038619	GRMZM2G315767	Zm00001d024317	(1 of 2) PTHR31642:	A0A1D6IYR6	Transferase	26.921785	-3.006855	0.4854769	-6.1936108	5.88E-10	2.33E-07
Zm00004b000094	GRMZM2G077769	Zm00001d027346	(1 of 61) PF02298 - F	A0A1D6JL89	Early nodulin-like pro	16.7445831	-3.0378518	0.61567127	-4.9342107	8.05E-07	1.64E-04
Zm00004b019474	GRMZM2G004183	Zm00001d044033	(1 of 56) PF13839|P	A0A1D6NHE8	TRICHOME BIREFR	32.4917945	-3.0584748	0.85118053	-3.5932152	3.27E-04	2.64E-02
Zm00004b025514	GRMZM2G387603	Zm00001d009416	(1 of 4) PTHR23244|	A0A1D6FJA2	Jacalin-related lectin	17.2901888	-3.0705361	0.63395466	-4.8434632	1.28E-06	2.50E-04
Zm00004b034863	GRMZM2G074323	Zm00001d018887	(1 of 5) PTHR24411::	A0A1D6HT38	Speckle-type POZ pr	86.5699368	-3.2373495	0.78449684	-4.1266572	0.0000368	0.00460955
Zm00004b018449	GRMZM2G400390	Zm00001d042848	(1 of 1) PTHR11709|	A0A1D6N727	Laccase-7	209.16183	-3.2745927	0.88640694	-3.6942317	0.000221	0.01939589
Zm00004b012332	GRMZM2G168890	Zm00001d014587	(1 of 14) PF07800 - F	B4FED2	C2H2-type domain-c	44.3866773	-3.4437481	1.01336395	-3.3983329	0.000678	0.04774079
Zm00004b001084	GRMZM2G160428	Zm00001d028570	(1 of 2) K08269 - seri	A0A1D6JXN6	Serine/threonine-prot	145.887331	-3.5479438	0.83560926	-4.2459364	0.0000218	0.00287152
Zm00004b005839	GRMZM2G077596	Zm00001d034931	(1 of 3) PTHR31008:	A0A1D6LCN7	COP1-interacting pro	22.8653413	-3.7412166	0.97284789	-3.8456336	0.00012	0.01207723
Zm00004b037811	GRMZM2G004412	Zm00001d023304	(1 of 16) PTHR23155	A0A1D6IRP3	Uncharacterized prot	94.358603	-3.9761305	0.62966583	-6.3146677	2.71E-10	1.16E-07
Zm00004b017793	GRMZM2G037452	Zm00001d042114	(1 of 9) PF12734 - C	B6SGH6	CYSTM domain-cont	80.0975862	-4.0257871	0.6645981	-6.0574761	1.38E-09	4.97E-07
Zm00004b001875	GRMZM2G077316	Zm00001d029594	(1 of 2) 5.3.99.6 - Alle	Q6RW09	Allene oxide cyclase	59.2744867	-4.202648	1.2210899	-3.4417188	5.78E-04	4.20E-02
Zm00004b037351	GRMZM2G017368	Zm00001d022185	(1 of 1) PF00612|PF	A0A1D6IK54	Calmodulin-binding t	134.853653	-4.2552721	1.0466383	-4.0656568	0.0000479	0.00584858
Zm00004b002146	GRMZM2G098208	Zm00001d029978	(1 of 2) PTHR11740|	A0A1D6K8R9	Casein kinase II subu	100.91157	-4.2736018	1.05206984	-4.0620894	0.0000486	0.00586798
Zm00004b018757	GRMZM5G867518	Zm00001d043223	(1 of 4) K02975 - sm	C0HDX5	40S ribosomal protei	43.0334973	-4.4208247	1.00152775	-4.4140811	0.0000101	0.00153221
Zm00004b011289	GRMZM2G312738	Zm00001d013318	(1 of 2) K16278 - E3	A0A1D6GI43	E3 ubiquitin-protein li	65.6800622	-4.5080077	1.14236326	-3.9462121	7.94E-05	8.68E-03
Zm00004b031913	GRMZM2G052562	Zm00001d045302	(1 of 2) PTHR22835|	A0A1D6NV48	Zea nodulation homo	245.889628	-4.5271323	0.99130819	-4.5668263	0.00000495	0.000823
Zm00004b030754	GRMZM2G318992	Zm00001d038407	(1 of 18) PF07765 - K	A0A1D6M671	Protein NETWORKE	45.0447659	-4.6916618	1.37776484	-3.4052704	6.61E-04	4.69E-02
Zm00004b006255	GRMZM2G012628	Zm00001d002244	(1 of 6) PTHR24012:	A0A1D6DYK9	Polyadenylate-bindin	207.03206	-5.2517456	1.36955945	-3.834624	1.26E-04	0.01244172
Zm00004b025060	GRMZM2G112681	Zm00001d008817	(1 of 3) PTHR31079:	A0A1D6FFQ8	NAC domain containi	44.5506993	-5.5508241	1.27422831	-4.3562241	0.0000132	0.00185697
Zm00004b024033	GRMZM2G081644	Zm00001d053447		A0A1D6QPH7	Uncharacterized prot	4.30518018	-5.560515	1.57323927	-3.5344369	4.09E-04	0.03185181
Zm00004b011936	GRMZM2G027135	Zm00001d014080	(1 of 1) PTHR12181|	B4FXM3	Uncharacterized prot	4.38609406	-5.5827533	1.47039337	-3.7967754	0.000147	0.01408052
Zm00004b011171	GRMZM2G033198	Zm00001d013184	(1 of 2) PTHR10438:	A0A096QB26	Thiol disulfide interch	4.48040404	-5.6103985	1.60717577	-3.4908431	0.000481	0.03636419
Zm00004b039392	GRMZM2G151041	Zm00001d025240	(1 of 3) K00164 - 2-o	A0A1D6J5Q7	2-oxoglutarate dehyd	1138.01393	-5.7409501	1.6081364	-3.5699398	0.000357	0.02848875
Zm00004b025158	GRMZM2G161988	Zm00001d008944	(1 of 4) KOG2887 - N	A0A1D6FGT7	Uncharacterized prot	4.97261301	-5.7679222	1.5915362	-3.6241226	2.90E-04	0.0240047
Zm00004b018231	GRMZM2G025703	Zm00001d042613	(1 of 2) PTHR10615|	A0A1D6N5E7	RING/FYVE/PHD-typ	5.558418	-5.931268	1.52727424	-3.8835645	0.000103	0.01062619
Zm00004b015220	GRMZM2G021514	Zm00001d018189	(1 of 1) PF00400|PF	A0A1D6HLB9	Major facilitator supe	5.65292164	-5.9470806	1.54429679	-3.8509959	0.000118	0.01187608
Zm00004b004118	GRMZM2G167438	Zm00001d032728	(1 of 30) K15397 - 3-	B4FQN3	3-ketoacyl-CoA synth	5.68148542	-5.9587649	1.39894683	-4.2594649	0.0000205	0.00273966
Zm00004b009098	GRMZM2G134351	Zm00001d005859	(1 of 1) PTHR13683|	A0A1D6ERB3	Eukaryotic aspartyl p	5.80723206	-5.9856396	1.47557762	-4.0564722	4.98E-05	5.94E-03
Zm00004b030863	GRMZM2G044457	Zm00001d038536	(1 of 3) PTHR10984|	A0A1D6M733	Endoplasmic reticulu	21.3259172	-6.0051667	1.52724447	-3.9320271	0.0000842	0.0091077
Zm00004b038273	GRMZM2G316593	Zm00001d023907		K7TJX6	Uncharacterized prot	6.29336864	-6.1070367	1.73815496	-3.5135168	0.000442	0.03378431
Zm00004b040445	GRMZM2G007477	Zm00001d026489	(1 of 1663) 2.7.11.1 -	K7TP92	OSJNBb0022F16.11	39.149517	-6.3328095	1.31171634	-4.8278803	0.00000138	0.000268
Zm00004b006220	GRMZM2G114861	Zm00001d002186	(1 of 1) PTHR24115::	A0A1D6DXK1	Kinesin-like protein	7.4353572	-6.3452997	1.54048688	-4.1190222	0.000038	0.00473499
Zm00004b039285	GRMZM2G081585	Zm00001d025106	(1 of 9) K04564 - sup	K7U2E7	Superoxide dismutas	7.93221065	-6.4429844	1.37152492	-4.6976794	0.00000263	0.000473
Zm00004b000181	GRMZM2G176585	Zm00001d027447	(1 of 3) PTHR31879:	A0A1D6JM71	Det1 complexing ubic	67.4247474	-6.7039036	1.08801441	-6.1615945	7.20E-10	2.69E-07
Zm00004b034890	GRMZM2G107408	Zm00001d018906		B4FF39	Uncharacterized prot	200.726775	-6.8974602	1.62732124	-4.2385363	0.0000225	0.00294816
Zm00004b038011	GRMZM2G381429	Zm00001d023553	(1 of 2) PTHR23155|	A0A1D6IU36	Disease resistance p	14.1893652	-7.2758491	1.37114923	-5.3063875	0.000000112	0.000027
Zm00004b026342	GRMZM2G157705	Zm00001d010455		A0A1D6FR41	Reticulon-like protein	14.4386388	-7.3062458	1.43186922	-5.102593	0.00000335	0.0000737
Zm00004b038742	GRMZM2G148316	Zm00001d024476		A0A1D6IZI6	UDP-glycosyltransfer	15.6056043	-7.4185534	1.49455082	-4.9637344	0.00000692	0.000146
Zm00004b026136	GRMZM2G149808	Zm00001d010206	(1 of 3) PTHR13286:	B4FT44	SAP30_Sin3_bdg do	16.0010348	-7.4530717	1.89630859	-3.9303053	8.48E-05	9.12E-03
Zm00004b013766	GRMZM2G137495	Zm00001d016440	(1 of 2) PTHR24078|	A0A1D6H7L4	DNAJ heat shock fan	35.5552131	-7.6372363	1.23540564	-6.1819665	6.33E-10	2.46E-07
Zm00004b037949	GRMZM5G839644	Zm00001d023470	(1 of 21) PF00560|P	A0A1D6ITF5	Putative leucine-rich	19.8102521	-7.7609484	1.69935714	-4.5669908	0.00000495	0.000823
Zm00004b001530	GRMZM2G134671	Zm00001d029149	(1 of 52) PF06203 - C	C0PI33	C2C2-CO-like transc	19.836807	-7.763756	1.7767038	-4.3697526	1.24E-05	1.76E-03
Zm00004b039025	GRMZM2G016312	Zm00001d024798		K7TMI5	Uncharacterized prot	19.9227091	-7.7693616	2.19202511	-3.5443762	0.000394	0.03102407
Zm00004b017703	GRMZM5G813403	Zm00001d042016	(1 of 309) 6.3.2.19 -	B6TIZ5	Uncharacterized prot	20.0343	-7.7752321	1.58789062	-4.8965791	0.000000975	0.000193
Zm00004b005561	GRMZM2G347056	Zm00001d034602	(1 of 1) K00297 - met	A0A1D6L979	Brown midrib2	21.7107574	-7.8927693	1.98910339	-3.9680035	7.25E-05	0.0081949
Zm00004b031719	GRMZM2G455243	Zm00001d045080	(1 of 2) K02603 - orig	A0A1D6NTH3	Origin recognition co	24.1413339	-8.0473034	1.29821421	-6.1987485	5.69E-10	0.00000023
Zm00004b037473	GRMZM2G018771	Zm00001d022337	(1 of 2) 3.5.1.88 - Pe	A0A1D6IL69	Peptide deformylase	25.1511161	-8.1065104	1.405358	-5.7682885	8.01E-09	2.30E-06
Zm00004b022114	GRMZM2G418604	Zm00001d051183	(1 of 1) K14327 - reg	A0A1D6Q5H4	Regulator of nonsens	25.6683286	-8.1347867	1.87357723	-4.3418476	0.0000141	0.00194146
Zm00004b018825	GRMZM2G093101	Zm00001d043291	(1 of 1) PTHR22953:	A0A1D6NA73	Purple acid phosphat	29.2236183	-8.3224876	1.26522035	-6.5778958	4.77E-11	2.25E-08
Zm00004b007010	GRMZM2G086486	Zm00001d003117	(1 of 3) PTHR10744|	A0A1D6E6T4	40S ribosomal protei	29.5062216	-8.3337836	1.31279641	-6.3481157	2.18E-10	9.58E-08
Zm00004b005777	GRMZM2G164547	Zm00001d034859		B7ZZ71	Cobalt ion binding	30.292121	-8.3727734	2.14441788	-3.9044504	0.0000944	0.01004666
Zm00004b017733	GRMZM2G059083	Zm00001d042049	(1 of 3) 1.6.99.1 - NA	A0A1D6N0R1	Ferredoxin--NADP re	10464.5512	-8.4011245	1.56595333	-5.3648626	0.000000081	0.0000203
Zm00004b005843	GRMZM2G077222	Zm00001d034935	(1 of 2) KOG3251 - C	A0A1D6LCQ1	Uncharacterized prot	37.6670904	-8.6870873	1.69872918	-5.1138742	0.000000316	0.000071
Zm00004b019700	GRMZM2G070961	Zm00001d044293	(1 of 4) PF00069|PF	A0A1D6NKI4	Protein kinase protei	38.4859778	-8.716857	1.32060373	-6.6006606	4.09E-11	1.98E-08
Zm00004b031672	GRMZM2G447806	Zm00001d045009		A0A1D6NST3	Uncharacterized prot	42.7021894	-8.8681762	1.51122296	-5.8682116	4.41E-09	0.00000141
Zm00004b000867	GRMZM2G043584	Zm00001d028317	(1 of 34) PF00069|P	A0A1D6JUB4	Leucine-rich repeat n	50.3398948	-9.1050678	1.62156852	-5.6149757	1.97E-08	5.26E-06
Zm00004b020252	GRMZM2G468260	Zm00001d048796	(1 of 3) PTHR22763:	A0A1D6PQ59	RING/U-box superfar	53.9469078	-9.2054014	2.53250159	-3.6349045	2.78E-04	2.34E-02
Zm00004b015124	GRMZM2G036418	Zm00001d018057	(1 of 1) PTHR13520|	A0A1D6HKI4	RINT1-like protein Mi	55.1481017	-9.2386971	1.2420628	-7.4381884	1.02E-13	8.08E-11
Zm00004b003465	AC234528.1_FG004	Zm00001d031928	(1 of 1) PF11595 - Pr	B6TZS4	Uncharacterized prot	60.0901134	-9.3602792	1.25718448	-7.4454301	9.66E-14	7.97E-11
Zm00004b030599	GRMZM5G881803	Zm00001d038205	(1 of 4) PTHR31942:	A0A1D6M4I8	MLO-like protein	77.0738763	-9.7205791	1.63722392	-5.9372325	2.90E-09	9.89E-07
Zm00004b006558	GRMZM2G114220	Zm00001d002598	(1 of 1) PTHR12555|	B6T4L6	Ubiquitin fusion degr	82.6579962	-9.8207032	1.42068652	-6.9126462	4.76E-12	2.69E-09
Zm00004b012058	GRMZM2G366638	Zm00001d014207		A0A1D6GR10	Uncharacterized prot	85.6508137	-9.8719883	1.23584383	-7.9880549	1.37E-15	1.36E-12
Zm00004b024150	GRMZM2G171452	Zm00001d053625	(1 of 21) PF01918 - A	B6T175	Alba DNA/RNA-bindi	93.8008006	-10.004327	1.24530628	-8.0336274	9.46E-16	1.01E-12
Zm00004b031781	GRMZM2G023636	Zm00001d045147	(1 of 2) PTHR18934:	A0A1D6NU12	Putative pre-mRNA-s	99.6267326	-10.090917	2.06077138	-4.8966697	0.000000975	0.000193
Zm00004b031625	GRMZM2G088053	Zm00001d044951	(1 of 54) PF00892 - E	B4FTK8	WAT1-related protein	124.401544	-10.411613	1.27855043	-8.1432945	3.85E-16	5.07E-13
Zm00004b024037	GRMZM2G029058	Zm00001d053452	(1 of 5) PF00076|PF	A0A1D6QPS5	Polyadenylate-bindin	203.284528	-11.119527	1.67867824	-6.6239776	3.50E-11	1.77E-08
Zm00004b003203	GRMZM2G386209	Zm00001d031555	(1 of 8) KOG4293 - F	A0A1D6KJM6	Cytochrome b561 an	221.282815	-11.242145	1.39757195	-8.0440548	8.69E-16	1.01E-12
Zm00004b007229	GRMZM2G029001	Zm00001d003394	(1 of 7) PTHR12603:	A0A1D6E920	RING/U-box superfar	221.630087	-11.244202	1.92064065	-5.8544018	4.79E-09	0.00000146
Zm00004b030622	GRMZM2G175676	Zm00001d038248	(1 of 4) K12831 - spli	A0A1D6M4R6	RNA-binding (RRM/F	322.560854	-11.785783	1.82352341	-6.4631924	1.03E-10	4.61E-08
Zm00004b018149	GRMZM2G064914	Zm00001d042512	(1 of 2) PTHR11240::	A0A1D6N4Q6	Ribonuclease 2	421.632858	-12.171961	3.56098798	-3.4181417	0.000631	0.04536639
Zm00004b011184	GRMZM2G114557	Zm00001d013195	(1 of 3) PTHR12383|	A0A1D6GGF2	Thylakoidal processin	443.480025	-12.24485	3.58774162	-3.4129687	0.000643	0.04573738
Zm00004b019678	GRMZM5G848696	Zm00001d044267	(1 of 2) K18121 - glyc	A0A1D6NK13	Glyoxylate/succinic s	469.510211	-12.327109	1.22910896	-10.029306	1.13E-23	3.20E-20
Zm00004b037198	GRMZM2G167932	Zm00001d021999	(1 of 1) PF02136|PF	A0A1D6IIC4	Nuclear transport fac	497.082753	-12.409565	1.38506885	-8.9595291	3.26E-19	4.96E-16
Zm00004b019828	GRMZM2G143128	Zm00001d044445	(1 of 2) K03661 - V-t	#N/A	#N/A	507.068603	-12.438167	3.57743815	-3.4768365	0.000507	0.03801417
Zm00004b003707	GRMZM2G092595	Zm00001d032238	(1 of 1) PTHR11353|	A0A1D6KPG0	Putative 1-phosphati	598.995823	-12.678531	3.6072989	-3.5146883	0.00044	0.03378431
Zm00004b037850	GRMZM2G129804	Zm00001d023340	(1 of 1) K02356 - elo	A0A1D6ISX4	Elongation factor P	830.618221	-13.150242	1.20932357	-10.874048	1.53E-27	1.01E-23
Zm00004b031504	GRMZM2G026833	Zm00001d044785	(1 of 334) PF00249 - K	K7W4V3	G2-like1	1385.73578	-13.888696	1.34835579	-10.300468	7.01E-25	2.77E-21
Zm00004b026230	GRMZM2G086464	Zm00001d010314		A0A1D6FQC3	Uncharacterized prot	1530.26023	-14.031661	3.71963824	-3.7723187	1.62E-04	0.0151673
Zm00004b000190	GRMZM2G177508	Zm00001d027456	(1 of 3) PTHR33222:	B4FTJ9	PBA1 homolog1 (Thr	9043.16785	-16.594887	1.31130707	-12.655226	1.05E-36	2.07E-32

TABLE NOTES:

GENEIDs B73v3 GeneIDs were obtained from the W22 GeneIDs using a MaizeGDB syntelogs lookup table made with SynMap

TRANSCRIPTOME: Trimmed reads were aligned using the splice-aware aligner Hisat2, indices were constructed from known exons and splice sites (W22 annotation Zm00004b & assembly Zm-W22-REFERENCE-NRGENE-2.0 as described in the Methods.

DEG & TABULATION: Differential expression analysis was performed separately per tissue (leaf mutant vs. WT or tassel mutant vs. WT) as described in the Methods

TABLULATION: This entire table, sorted on col-H, log2(fold-change), includes statistically significant differentially expressed (adjusted p-value <0.05) genes and excludes any genes with fewer than 10 counts across sum of all replicates.

COLUMNS G-L: Columns G-L tabulate output values for the baseMean, the log2(fold-change), along with the associated values for standard error (lfcSE), Wald statistic (stat), pvalue, and adjusted pvalue (padj).

PROVENANCE: Supplementary Table S2 from Mckenna, Gumber, et al., "Maize (Zea mays L.) nucleoskeletal proteins regulate nuclear envelope remodeling…", submitted 12/2020

Table S2a2 (McKenna, Gumber, et al., submitted Dec. 2020)

Table S2: Differentially expressed genes between *mkaku41* mutant versus wildtype plants for maize leaf and tassel.

Table S2 (Tab 2 of 2) TASSEL DEGs. All **155** Differentially Expressed Genes from Tassel.

W22v2 GeneID	B73v3 GeneID	B73v4 GeneID	Phytomine description	Uniprot id	Uniprot descriptor	baseMean-LEAF	log2FoldChange (mutant/WT)	lfcSE	stat	pvalue	padj
Zm00004b019058	GRMZM2G031308	Zm00001d043551	(1 of 5) PTHR10994:	B6TGL5	Reticulon-like protein	1116.51594	13.6331752	3.54537242	3.84534362	0.00012	0.01847303
Zm00004b037198	GRMZM2G167932	Zm00001d021999	(1 of 1) PF02136//PF	A0A1D6IIC4	Nuclear transport fac	927.603007	13.3657609	3.51855276	3.79865296	0.000145	0.02157566
Zm00004b040337	GRMZM2G097854	Zm00001d026369	(1 of 3) K08695 - antl	A0A1D6JF45	Anthocyanidin reduct	832.100873	13.2090143	3.56596764	3.70418794	0.000212	0.02892647
Zm00004b016461	GRMZM2G091119	Zm00001d040274	(1 of 4) PF00514//PF	A0A1D6MPN9	Importin subunit alph	766.55018	13.0909023	1.25515948	10.4296725	1.82E-25	6.68E-22
Zm00004b012240	GRMZM2G085967	Zm00001d014467	(1 of 1) PTHR31235:	B6THU9	Peroxidase (EC 1.11.	759.921198	13.0781172	3.49760919	3.7391591	0.000185	0.02582228
Zm00004b030603	GRMZM2G016817	Zm00001d038208	(1 of 4) PTHR12321:	B6TK34	PHD finger protein (F	677.775636	12.9132908	1.50630854	8.5728059	1.01E-17	1.49E-14
Zm00004b012451	GRMZM2G084521	Zm00001d014732	(1 of 1) PTHR11071//	A0A1D6GVX5	Peptidyl-prolyl cis-tra	477.323952	12.4072467	3.43872232	3.60809788	0.000308	0.03962687
Zm00004b034468	GRMZM2G063060	Zm00001d048409	(1 of 5) K13525 - trar	A0A1D6PJZ0	Cell division control p	651.478524	11.8939283	2.18052918	5.45460636	4.91E-08	0.0000155
Zm00004b031400	GRMZM2G099529	Zm00001d039167	(1 of 1) PTHR10381/	B4F9Z4	ATP-dependent Clp p	315.8768	11.8117851	1.25206243	9.4338627	3.95E-21	7.94E-18
Zm00004b022426	GRMZM2G147701	Zm00001d051552	(1 of 2) 1.1.1.102 - 3-	K7U3E5	3-dehydrosphinganin	287.984997	11.6784178	1.54025663	7.58212465	3.40E-14	2.89E-11
Zm00004b003468	GRMZM2G103258	Zm00001d031933	(1 of 2) K09598 - sigr	B6TY57	Signal peptide peptid	170.324314	10.9206558	1.90401389	5.73559672	9.72E-09	0.00000352
Zm00004b002034	GRMZM2G453832	Zm00001d029808	(1 of 3) PTHR13890:	A0A1D6K7V9	Magnesium transport	153.335766	10.7689598	1.36515021	7.88847976	3.06E-15	3.56E-12
Zm00004b014513	GRMZM2G169967	Zm00001d017377	(1 of 83) PF01357//P	A0A1D6HEG4	Beta-expansin 3	145.470907	10.6932269	1.51068068	7.07841642	1.46E-12	9.21E-10
Zm00004b006032	GRMZM2G061745	Zm00001d001966	(1 of 2) K03038 - 26S	A0A1D6DUX4	26S proteasome non	141.170616	10.649926	1.29679144	8.21252027	2.17E-16	2.99E-13
Zm00004b013432	GRMZM2G130425	Zm00001d016034	(1 of 2) K03363 - cell	C0PLV0	Cell division cycle20	521.93026	10.275466	2.88710491	3.55908994	0.000372	0.04619789
Zm00004b032186	GRMZM2G459172	Zm00001d045615	(1 of 2) PTHR12668/	A0A1D6NXR5	Protein FATTY ACID	86.95675	9.95034834	1.28432357	7.74754008	9.37E-15	9.10E-12
Zm00004b036464	GRMZM5G822842	Zm00001d021072	(1 of 3) PF13889 - CI	A0A1D6I880	DUF4210 domain-co	83.2929674	9.88888472	1.23694461	7.9946059	1.30E-15	1.60E-12
Zm00004b025017	GRMZM2G032190	Zm00001d008759	copper ion binding	A0A1D6FF81	Uncharacterized prot	70.5856734	9.64930986	1.60646012	6.0065667	1.89E-09	7.48E-07
Zm00004b001099	GRMZM2G100086	Zm00001d028585	(1 of 4) PTHR30603/	A0A096RK86	RNA polymerase sigr	49.6978463	9.14362423	1.26003287	7.25665535	3.97E-13	2.74E-10
Zm00004b012418	GRMZM2G170805	Zm00001d014692	(1 of 4) PF06094 - Gi	B4FVZ7	AIG2-like protein	266.67295	9.11671684	0.90708367	10.0505799	9.13E-24	2.52E-20
Zm00004b004132	GRMZM2G134747	Zm00001d032736	(1 of 1) 4.2.1.104 - C	A0A1R3MBN3	Cyanate hydratase ((	338.974496	8.80622145	2.35087671	3.74593079	0.00018	0.02545775
Zm00004b037937	GRMZM2G148404	Zm00001d023453		C0HI40	Uncharacterized prot	37.7204071	8.74631485	1.56432485	5.59111163	2.26E-08	0.00000755
Zm00004b023615	GRMZM2G397281	Zm00001d052963		A0A1D6QL57	EGF-like domain-con	34.783636	8.6294773	1.42645668	6.04958947	1.45E-09	6.05E-07
Zm00004b039332	GRMZM2G139407	Zm00001d025165	(1 of 4) PTHR10693/	K7TNM4	Nuclear transport fac	342.380481	8.38816455	1.93661663	4.33135004	0.0000148	0.00289799
Zm00004b013393	GRMZM2G019553	Zm00001d015988	(1 of 1) K02200 - cyt	B6SU73	Cytochrome c-type b	27.3880869	8.28329824	2.02586486	4.08877137	0.0000434	0.00772796
Zm00004b027287	GRMZM2G030284	Zm00001d011615	(1 of 13) K16732 - pr	B4F8V2	65-kDa microtubule-a	167.362819	7.92131804	2.00239446	3.95592287	0.0000762	0.01266669
Zm00004b032576	GRMZM2G083841	Zm00001d046170	(1 of 3) PTHR30523/	Q43267	PEP carboxylase (Ph	18.6138473	7.72779073	1.43542165	5.38363813	7.30E-08	0.0000218
Zm00004b040223	GRMZM2G415229	Zm00001d026245	(1 of 6) PTHR10032:	A0A1D6JDK2	Trihelix transcription	18.160057	7.69219139	1.58572195	4.85090805	0.00000123	0.000289
Zm00004b036145	GRMZM2G127537	Zm00001d020670	(1 of 2) PF00046//PF	B4FH59	HB transcription factc	17.7078164	7.65622705	1.41089273	5.42651252	5.75E-08	0.0000179
Zm00004b018381	GRMZM5G831584	Zm00001d042762	(1 of 2) 3.1.1.89 - Pr	A0A1D6N6L2	Catalytic/ hydrolase	84.6504735	7.56126644	1.36363839	5.54492049	2.94E-08	0.0000097
Zm00004b039799	GRMZM2G005939	Zm00001d025752		A0A1D6J9A3	Transcription factor b	83.7504033	7.52422242	1.202317	6.25810199	3.90E-10	1.83E-07
Zm00004b011538	GRMZM5G822180	Zm00001d013598	(1 of 65) PF14368 - F	B4G0Q2	Lipid binding protein	30.752681	7.48199367	1.31879864	5.67334044	1.40E-08	0.0000491
Zm00004b028398	GRMZM2G032315	Zm00001d035087	(1 of 3) K02942 - larg	B6T361	60S acidic ribosomal	9.57098821	6.76511433	1.79409873	3.77075922	0.000163	0.02340051
Zm00004b039943	GRMZM2G017815	Zm00001d025911	(1 of 11) PTHR14221	K7U5C2	Transducin/WD40 rep	62.494728	6.76470472	1.9033603	3.55408523	0.000379	0.04654892
Zm00004b019310	GRMZM2G316223	Zm00001d043819	(1 of 1) PF00415//PF	A0A1D6NF99	Uncharacterized prot	9.45026789	6.74829124	1.45030119	4.65302745	0.00000327	0.00073
Zm00004b005589	GRMZM2G155329	Zm00001d034635	(1 of 1) K01859 - cha	B6TJA9	Chalcone-flavonone i	2498.54833	6.712817	1.6798008	3.99619824	0.0000644	0.01094105
Zm00004b018181	GRMZM2G328795	Zm00001d042558	(1 of 1) PTHR31791:	A0A1D6N567	TPR repeat-containir	8.74339242	6.63790001	1.75838949	3.77498844	0.00016	0.02340051
Zm00004b037112	GRMZM2G092669	Zm00001d021879	(1 of 11) PF14365 - [	B4G0L1	NEP-interacting prote	449.338405	6.52571887	1.54959928	4.21122992	0.0000254	0.00479683
Zm00004b027462	GRMZM2G167758	Zm00001d011799	(1 of 1) PTHR34213:	K7V1E4	Nuclear transport fac	7.40410104	6.39553672	1.61471115	3.96079307	0.0000747	0.0125051
Zm00004b009299	GRMZM2G179002	Zm00001d006102	(1 of 4) PTHR22883/	A0A1D6ESW0	Uncharacterized prot	355.743669	6.22902942	0.6923039	8.99753627	2.31E-19	3.92E-16
Zm00004b026474	GRMZM5G827266	Zm00001d010614	(1 of 3) K02976 - sm	A0A1D6FSC6	40S ribosomal protei	4312.26968	6.11457177	1.01798407	6.00654957	1.90E-09	7.48E-07
Zm00004b014767	GRMZM2G428233	Zm00001d017658	(1 of 11) PF08458 - F	A0A1D6HG97	Uncharacterized prot	5.23476558	5.8965248	1.65059434	3.5723646	0.000354	0.04467034
Zm00004b033022	GRMZM2G180863	Zm00001d046742	(1 of 1) PTHR10210/	B7ZZ73	Ribose-phosphate py	199.077229	5.86648046	1.33522799	4.39361704	0.0000111	0.00223943
Zm00004b008843	GRMZM2G346865	Zm00001d005544	(1 of 2) PTHR19316:	A0A1D6ENR8	ARM repeat superfar	46.3742592	5.855099	1.26125486	4.64228063	0.00000345	0.000761
Zm00004b026907	AC207342.3_FG007	Zm00001d011145	(1 of 3) PF13474 - Sr	B4FET0	F-box protein SKIP8	66.4771194	5.81106553	1.48313606	3.91809333	0.0000893	0.01429134
Zm00004b025652	GRMZM2G058913	Zm00001d009591	(1 of 4) PTHR12758:	A0A1D6FKE6	GBF-interacting prote	72.2310448	5.80719248	1.51786221	3.82590228	0.00013	0.01958575
Zm00004b017977	GRMZM2G119650	Zm00001d042309	(1 of 2) PTHR32133:	A0A1D6N2R0	F-box only protein 6	190.959684	5.45833106	1.22510187	4.45540997	0.00000837	0.00174552
Zm00004b033705	GRMZM2G462803	Zm00001d047540	(1 of 1) PF06920//PF	A0A1D6PBF4	Guanine nucleotide e	134.054619	5.44016169	1.23490804	4.40531726	0.0000106	0.00216119
Zm00004b014532	GRMZM2G068340	Zm00001d017392	(1 of 2) PTHR10026:	A0A1D6HEM4	Cyclin-T1-3	198.893809	5.38931983	1.45077883	3.71477699	0.000203	0.02798318
Zm00004b018190	GRMZM2G070562	Zm00001d042569	(1 of 1) K03108 - sigr	A0A1D6N584	Signal recognition pa	717.560538	5.37996285	0.62550463	8.60099611	7.90E-18	1.25E-14
Zm00004b025991	GRMZM2G102745	Zm00001d010023	(1 of 2) K15115 - sol	A0A1D6FNM8	Nicotinamide adenine	56.4004262	4.96359461	1.39255218	3.5643868	0.000365	0.04578948
Zm00004b034487	GRMZM2G115674	Zm00001d048431	(1 of 3) PF15365 - Pr	K7VQD7	Uncharacterized prot	96.1690586	4.93403936	1.29122851	3.82119766	0.000133	0.01982835
Zm00004b015186	GRMZM2G072300	Zm00001d018131	(1 of 173) PTHR2407	A0A096R205	Chaperone protein dr	21.6294645	4.72947748	1.13382031	4.17127603	0.0000303	0.0056245
Zm00004b032905	GRMZM2G105167	Zm00001d046592	(1 of 2) KOG3306 - F	K7VW99	ER membrane protei	206.287168	4.7211818	1.15860049	4.07490058	0.000046	0.00813771
Zm00004b030094	GRMZM2G034622	Zm00001d037557	(1 of 1) K10589 - ubi	A0A1D6LYY6	E3 ubiquitin-protein li	519.15557	4.71657044	0.80201653	5.88088928	4.08E-09	0.00000155
Zm00004b030898	GRMZM2G020150	Zm00001d038585	(1 of 213) PF00847 - A	A0A1D6M7D1	Putative AP2/EREBP	56.826908	4.70792367	0.73702313	6.38775562	1.68E-10	8.09E-08
Zm00004b021954	GRMZM2G006672	Zm00001d050965	(1 of 5) K00030 - isoc	A0A1D6O461	Isocitrate dehydroger	16.045869	4.53410659	1.20156413	3.77350362	0.000161	0.02340051
Zm00004b028599	GRMZM2G036908	Zm00001d035447	(1 of 3) K14689 - sol	A0A1D6LGF5	Metal tolerance prote	409.16687	4.46231855	0.59555026	7.49276567	6.74E-14	5.32E-11
Zm00004b012681	GRMZM5G806358	Zm00001d014998	(1 of 1) PTHR13980	C0PP15	FACT complex subur	1291.20935	4.46041724	0.58607138	7.61070651	2.73E-14	2.41E-11
Zm00004b034033	GRMZM2G101001	Zm00001d047912		C0P8K4	Translation initiation f	472.429917	4.30781299	1.1409786	3.77554232	0.00016	0.02340051
Zm00004b023245	GRMZM2G059381	Zm00001d052485	(1 of 2) PTHR24096:	B6SWE6	AMP-binding protein	239.813652	4.19842567	1.15390827	3.6384397	0.000274	0.03586446
Zm00004b033266	GRMZM2G116327	Zm00001d047063	(1 of 2) PTHR28259:	B6SKI7	Camphor resistance (	230.168414	4.14211418	0.70868349	5.84480126	5.07E-09	0.00000187
Zm00004b018529	GRMZM2G359234	Zm00001d042943	(1 of 4) PTHR10366/	A0A1D6N7M5	UDP-glucuronic acid	427.784759	3.8668841	0.60111732	6.43282757	1.25E-10	6.29E-08
Zm00004b015462	GRMZM5G824600	Zm00001d018468	(1 of 1) 1.2.1.1 - Tran	A0A1D6HP90	Formaldehyde dehyd	2308.1842	3.76544431	0.24689454	15.2512258	1.62E-52	3.57E-48
Zm00004b025644	GRMZM2G413652	Zm00001d009580	(1 of 1) K03189 - ure	A0A1D6FKC6	Urease accessory pr	299.32788	3.73454777	0.9269234	4.02897131	0.000056	0.00967114
Zm00004b026151	GRMZM6G741620	Zm00001d010220		A0A1D6FPV2	40S ribosomal protei	966.613911	3.73185328	0.76847807	4.85616107	0.0000012	0.000284
Zm00004b004862	GRMZM2G346263	Zm00001d033654	(1 of 1) PTHR18959	A0A1D6L178	Opaque endosperm1	20.3271731	3.22962957	0.83761752	3.85573308	0.000115	0.01795511
Zm00004b037008	GRMZM2G050933	Zm00001d021745	(1 of 1) K18812 - cyc	B6TAD6	CYCD6	1010.40449	3.1479061	0.53784676	5.85279362	4.83E-09	0.00000181
Zm00004b014508	GRMZM2G420469	Zm00001d017371	(1 of 11) PTHR14221	A0A1D6HED4	Signal transducer	167.893909	2.89874952	0.80718669	3.59117606	0.000329	0.04180513
Zm00004b038905	GRMZM2G393742	Zm00001d024677	(1 of 2) PTHR10799:	A0A1D6J0X9	Protein CHROMATIN	108.712563	2.89269635	0.56788595	5.09379809	3.51E-07	0.0000881
Zm00004b037289	GRMZM2G038303	Zm00001d022109	(1 of 3) PTHR12632/	A0A1D6IJ95	Nuclear transcription	122.841214	2.5689457	0.39349329	6.52856299	6.64E-11	3.49E-08
Zm00004b022846	GRMZM2G032163	Zm00001d052050	(1 of 4) 5.3.3.2 - Isop	A0A1D6QCE2	Nudix hydrolase 3	1146.62228	2.30053508	0.38821183	5.92597885	3.10E-09	0.0000012
Zm00004b034305	GRMZM5G882285			#N/A	#N/A	56.4083527	2.29386867	0.62983361	3.64202326	0.000271	0.03557928
Zm00004b014191	GRMZM5G861269	Zm00001d016977	(1 of 3) PTHR11886:	A0A1D6HBJ3	Dynein light chain	70.3348279	2.11193342	0.4571777	4.61950225	0.00000385	0.000842
Zm00004b030010	GRMZM2G125054	Zm00001d037438		A0A1D6LXU8	Uncharacterized prot	252.813869	2.07092393	0.29085411	7.12014676	1.08E-12	7.01E-10
Zm00004b009281	GRMZM5G866100	Zm00001d006084	(1 of 3) K00876 - uric	B6T7J2	Uridine kinase (EC 2.	1543.09642	2.01148265	0.26371773	7.62740763	2.40E-14	2.21E-11
Zm00004b002266	GRMZM2G430710	Zm00001d030143	(1 of 44) PF01535//P	A0A1D6KA87	Tetratricopeptide repe	30.942965	1.95994914	0.53979606	3.63090669	0.000282	0.03671056
Zm00004b002292	GRMZM2G159992	Zm00001d030173	(1 of 2) PTHR27003:	A0A1D6KAS3	Calmodulin-binding r	696.971619	1.52357862	0.2028397	7.51124466	5.86E-14	4.79E-11
Zm00004b027487	GRMZM2G133926	Zm00001d011828	(1 of 2) K14325 - RN	A0A1D6G432	Serine/arginine-rich s	253.228795	1.43514915	0.2521224	5.69227152	1.25E-08	0.00000447
Zm00004b007010	GRMZM2G086486	Zm00001d003117	(1 of 3) PTHR10744/	A0A1D6E6T4	40S ribosomal protei	402.744292	1.36119528	0.29127527	4.67322644	0.00000297	0.000669
Zm00004b037480	GRMZM2G429231	Zm00001d022346	(1 of 2) KOG1860 - N	A0A1D6ILB3	SAC3 family protein I	590.373325	1.31006904	0.3493059	3.75049219	0.000176	0.02516033
Zm00004b033038	GRMZM2G378653	Zm00001d046759	(1 of 2) PTHR12565:	A0A1D6P4V3	Putative HLH DNA-bi	281.65404	1.04740925	0.20418933	5.12959831	0.00000029	0.0000737
Zm00004b002665	GRMZM2G086887	Zm00001d030774	(1 of 11) KOG0123 -	A0A1D6KEA9	RNA-binding (RRM/F	2147.22187	0.99069478	0.16462362	6.01793825	1.77E-09	7.23E-07
Zm00004b037183	GRMZM2G411916	Zm00001d021972	(1 of 7) K01530 - phc	A0A1D6II79	Phospholipid-transpo	599.743563	0.91273641	0.17158889	5.31932126	1.04E-07	0.0000291
Zm00004b005747	GRMZM2G056393	Zm00001d034826	(1 of 1) PTHR23115:	A0A1D6LBQ9	Elongation factor G, (	962.317187	0.88687693	0.24287944	3.65151094	0.000261	0.03491353
Zm00004b005063	GRMZM2G033135	Zm00001d033935	(1 of 2) K08873 - PI-	A0A1D6L3E8	Serine/threonine-prot	905.356031	0.8536198	0.23391793	3.64922778	0.000263	0.03496643
Zm00004b018233	GRMZM2G034639	Zm00001d042615	(1 of 1) PF08729 - HI	A0A1D6N5F5	Wound-responsive fa	672.996245	0.68630198	0.15886115	4.32013723	0.0000156	0.00302249
Zm00004b025122	GRMZM2G472625	Zm00001d008893	(1 of 2) PTHR24057:	B4FE45	Shaggy-related prote	1487.53332	0.67939668	0.12409803	5.47467734	4.38E-08	0.0000142
Zm00004b038192	GRMZM2G331368	Zm00001d023795	(1 of 3) K10592 - E3	A0A1D6IVN3	E3 ubiquitin-protein li	4755.10766	0.65216734	0.15818723	4.12275591	0.0000374	0.00678063
Zm00004b022902	GRMZM2G449909	Zm00001d052110	(1 of 1) PTHR13140:	A0A1D6QDE1	Opaque endosperm1	1134.47856	0.55751927	0.14787332	3.77024932	0.000163	0.02340051
Zm00004b020700	GRMZM2G026459	Zm00001d049349	(1 of 2) PTHR11654//	A0A1D6PTX6	Protein NRT1/ PTR F	791.740497	-0.6716858	0.16230397	-4.1384435	0.000035	0.00638567
Zm00004b011043	GRMZM2G115612	Zm00001d013046	(1 of 3) PTHR14969:	A0A1D6GF85	Lipid phosphate phos	714.795212	-0.8131227	0.20154562	-4.0344349	0.0000547	0.00952326
Zm00004b017318	GRMZM2G098397	Zm00001d041511	(1 of 5) K07964 - hep	A0A1D6MWN0	Heparanase-like prot	763.079646	-0.9465329	0.22192695	-4.2650651	0.00002	0.00380686
Zm00004b022535	GRMZM2G012814	Zm00001d051687	(1 of 2) PTHR10980:	K7U856	Rho GDP-dissociatio	102.730112	-1.3999356	0.36476726	-3.8378871	0.000124	0.0189116
Zm00004b020861	GRMZM5G870572	Zm00001d049563	(1 of 1) K03141 - trar	A0A1D6PW70	Putative RNA polyme	249.64317	-1.6236128	0.22531901	-7.2058404	5.77E-13	3.86E-10
Zm00004b033123	GRMZM2G058162	ubiquitin-conjugating enzyr	(1 of 3) PTHR24067:	#N/A	#N/A	690.415242	-2.0449529	0.37385177	-5.4699566	4.50E-08	0.0000144

Table S2b1 (McKenna, Gumber, et al., submitted Dec. 2020)

Zm00004b000914	GRMZM2G157177	Zm00001d028372	(1 of 4) PTHR22952/	A0A1D6JVI5	BZIP transcription fac	71.0752415	-2.0593793	0.30429553	-6.7676948	1.31E-11	7.81E-09
Zm00004b030613	GRMZM2G153075	Zm00001d038224	(1 of 2) K03875 - F-b	B4F7T2	F-box protein FBL2 (I	218.253808	-2.0984351	0.57522464	-3.648027	0.000264	0.03496643
Zm00004b034784	GRMZM2G012031	Zm00001d018795	(1 of 1) PTHR24365/	A0A1D6HSC5	187-kDa microtubule	1281.82697	-2.5686201	0.38603854	-6.6537919	2.86E-11	1.62E-08
Zm00004b029454	GRMZM5G829955	Zm00001d036709	(1 of 1) K12857 - Prp	A0A1D6LQJ4	Transducin/WD40 rep	72.5753958	-2.5762318	0.34823181	-7.398037	1.38E-13	9.85E-11
Zm00004b037334	GRMZM2G371721	Zm00001d022168	(1 of 5) PTHR24078:	Q5GAN9	AT hook-containing M	66.8457668	-2.7007364	0.36102147	-7.4808194	7.39E-14	5.63E-11
Zm00004b011381	GRMZM2G090172	Zm00001d013431	(1 of 2) PTHR24067:	A0A1D6GJ80	Ubiquitin-conjugating	178.729135	-2.7762387	0.68518628	-4.0518014	0.0000508	0.0089133
Zm00004b016600	GRMZM2G305264	Zm00001d040445	(1 of 2) PTHR22763/	C0PF84	RING/U-box superfar	134.364196	-3.1863228	0.66813468	-4.7689828	0.00000185	0.000426
Zm00004b005951	GRMZM2G040115	Zm00001d001858	(1 of 45) PF03000 - N	B8A094	BTB/POZ domain-co	95.666743	-3.2570704	0.84535642	-3.852896	0.000117	0.01803748
Zm00004b006866	GRMZM2G176677	Zm00001d002945	(1 of 151) PF02365 - A	A0A1D6E5L0	Ras-related protein18	359.948291	-3.3304859	0.61989729	-5.3726415	7.76E-08	0.0000227
Zm00004b007683	AC235541.1_FG002	Zm00001d003948	(1 of 3) PTHR24078/	C4J193	DNAJ heat shock N-t	109.280361	-3.4489189	0.97099931	-3.5519273	0.000382	0.04654892
Zm00004b032487	GRMZM2G057743	Zm00001d046033	(1 of 2) PTHR10288/	K7W8X7	RNA-binding KH dom	35.6783799	-3.4498949	0.56344471	-6.1228631	9.19E-10	3.98E-07
Zm00004b030589	GRMZM2G133021	Zm00001d038194	(1 of 127) PF00646 -	C0P6L8	F-box/FBD/LRR-repe	212.536727	-3.4882886	0.6674719	-5.2261206	1.73E-07	0.0000461
Zm00004b019813	GRMZM5G812270	Zm00001d044429	(1 of 44) 5.3.4.1 - Prc	B6TH36	Thioredoxin superfan	158.728386	-3.5236272	0.97410544	-3.6172955	0.000298	0.03846912
Zm00004b001427	GRMZM2G312661	Zm00001d029028	(1 of 2) PTHR10891/	C0P445	Calcium-binding prot	49.7443658	-3.5317195	0.67313631	-5.2466631	1.55E-07	0.0000417
Zm00004b001119	GRMZM2G087600	Zm00001d028612		A0A1D6JY27	Uncharacterized prot	255.883023	-3.5347045	0.67840253	-5.210335	1.88E-07	0.000049
Zm00004b034015	GRMZM2G013814	Zm00001d047894	(1 of 7) PF11833 - Pr	B6TKC3	Protein CHAPERONI	119.776564	-3.546751	0.54232152	-6.5399414	6.15E-11	3.32E-08
Zm00004b037413	GRMZM2G180568	Zm00001d022256	(1 of 46) PF03634 - T	A0A060CZ25	TCP transcription fac	126.838844	-4.1765009	0.41628918	-10.032691	1.09E-23	2.69E-20
Zm00004b014162	GRMZM2G075637	Zm00001d016935	(1 of 2) K11290 - tem	Q94F78	Nucleosome/chromat	774.018655	-4.3893148	0.65387115	-6.712813	1.91E-11	1.11E-08
Zm00004b031562	GRMZM2G058560	Zm00001d044866	(1 of 1) K17605 - ser	A0A1D6NRY3	Serine/threonine-prot	158.722343	-4.6022265	0.85675423	-5.3716998	7.80E-08	0.0000227
Zm00004b011362	GRMZM2G152328	Zm00001d013410	(1 of 2) PTHR11937/	#N/A	#N/A	1408.63065	-4.8578728	0.62713761	-7.7461035	9.48E-15	9.10E-12
Zm00004b005296	GRMZM2G170727	Zm00001d034254	(1 of 3) KOG3381 - L	A0A1D6L6F1	Protein AE7-like 1	88.6494724	-5.7478947	1.45627857	-3.9469747	0.0000791	0.01305123
Zm00004b000303	GRMZM2G009014	Zm00001d027588		A0A1D6JN74	Uncharacterized prot	47.4651127	-6.0922781	1.65823335	-3.6739571	0.000239	0.03217847
Zm00004b036142	GRMZM5G832772	Zm00001d020666	(1 of 58) 3.6.3.44 - X	A0A1D6I5K5	Multidrug resistance	85.8988549	-6.1525908	1.13848309	-5.4042004	6.51E-08	0.00002
Zm00004b040245	GRMZM2G018462	Zm00001d026259	(1 of 2) PTHR33972:	A0A1D6JDS9	Uncharacterized prot	69.2136647	-6.6238048	1.70248072	-3.8906783	0.0001	0.01577795
Zm00004b039476	GRMZM2G095826	Zm00001d025352	(1 of 2) PTHR19370:	B4FYW4	Ferredoxin	163.683221	-6.6902767	0.64379504	-10.391936	2.70E-25	8.52E-22
Zm00004b038507	GRMZM2G094452	Zm00001d024212	(1 of 7) K00901 - diac	A8QM11	diacylglycerol kinase	14.1787349	-7.2001486	1.36678595	-5.2679417	1.38E-07	0.0000376
Zm00004b013692	GRMZM2G029559	Zm00001d016358	(1 of 1) PF00043//PF	A0A1D6H6X9	Putative elongation fa	528.862948	-7.3168313	1.9781414	-3.6988414	0.000217	0.02936134
Zm00004b003529	GRMZM2G084583	Zm00001d032024	(1 of 2) PTHR10641/	A0A1D6KN59	Myb transcription fac	15.7016476	-7.351001	1.59883276	-4.5977298	0.00000427	0.000925
Zm00004b032897	GRMZM5G805627	Zm00001d046583	(1 of 5) K02955 - sm	A0A1D6P3R8	40S ribosomal protei	2049.55018	-7.3664354	1.37568503	-5.3547398	8.57E-08	0.0000243
Zm00004b004185	GRMZM2G144782	Zm00001d032810	(1 of 1) PTHR21319/	A0A1D6KU49	CHY-type/CTCHY-typ	16.6392848	-7.4346907	1.64434719	-4.5213631	0.00000614	0.00130548
Zm00004b017739	GRMZM2G162250	Zm00001d042055	(1 of 3) PTHR31326:	A0A1D6N0T2	ARGOS6	18.9738992	-7.6208123	1.68744911	-4.5161731	0.0000063	0.00132513
Zm00004b011561	GRMZM2G038801	Zm00001d013639	(1 of 2) PTHR15852:	A0A1D6GL71	DnaJ/Hsp40 cysteine	19.1338892	-7.6335474	2.14431334	-3.5599029	0.000371	0.04619789
Zm00004b013627	GRMZM2G121309	Zm00001d016277	(1 of 32) K14484 - au	A0A1D6H6I5	Auxin-responsive pro	20.9605007	-7.7652893	2.16172134	-3.5921787	0.000328	0.04180513
Zm00004b039120	GRMZM2G174671	Zm00001d024908	(1 of 1) K01476 - arg	A0A1D6J2P7	Arginase 1 mitochon	124.634851	-7.8105926	2.01527474	-3.8756962	0.000106	0.01666212
Zm00004b038454	GRMZM2G062585	Zm00001d024155	(1 of 2) 3.1.3.21 - Gl	B4FM45	(DL)-glycerol-3-phos	22.7030084	-7.8802551	1.29576777	-6.0815335	1.19E-09	5.06E-07
Zm00004b007737	GRMZM2G027272	Zm00001d004022	(1 of 3) K13456 - RP	A0A1D6ED15	RPM1-interacting prc	85.7103695	-7.9584404	2.12649259	-3.7425197	0.000182	0.02564156
Zm00004b033732	GRMZM5G872256	Zm00001d047582	(1 of 3) 2.4.1.123 - In	Q7XYY1	Hexosyltransferase (I	31.5946066	-8.3574989	1.55936046	-5.3595683	8.34E-08	0.0000239
Zm00004b015097	GRMZM2G028325	Zm00001d018037	(1 of 5) PTHR19139/	A0A1Q1ADS4	NOD26-like membra	37.5124823	-8.6059927	1.76417839	-4.8781873	0.00000107	0.000257
Zm00004b029343	GRMZM2G126920	Zm00001d000360		#N/A	#N/A	48.7785425	-8.9851403	1.817047	-4.9449135	7.62E-07	0.000185
Zm00004b018250	GRMZM2G135743	Zm00001d042627	(1 of 8) 2.4.1.17 - Gl	A0A1D6N5J7	Hexosyltransferase (I	982.742606	-9.016643	0.77835005	-11.584303	4.95E-31	5.47E-27
Zm00004b036596	GRMZM2G048165	Zm00001d021280	(1 of 1) PTHR22298:	A0A1D6I9L5	Endoglucanase (EC :	50.8729068	-9.0456557	1.81462784	-4.9848545	0.00000062	0.000152
Zm00004b011870	GRMZM2G001887	Zm00001d013999	(1 of 5) K01527 - nas	A0A1D6GPC3	Basic transcription fa	53.8848989	-9.1296606	1.47437162	-6.1922384	5.93E-10	2.67E-07
Zm00004b039616	GRMZM2G097499	Zm00001d025538		A0A1D6J7M0	Uncharacterized prot	61.4228893	-9.3179732	2.14512664	-4.343787	0.000014	0.00276306
Zm00004b003293	GRMZM2G452523	Zm00001d031691	(1 of 2) PF04055//PF	A0A1D6KKQ0	Biotin synthase	122.070016	-9.3438471	1.50000812	-6.2291977	4.69E-10	2.16E-07
Zm00004b040319	GRMZM2G150950	Zm00001d026348	(M=2) PF02178 - AT	K7TSL3	AT hook motif family	66.1902783	-9.4249272	2.11675509	-4.4525355	0.00000849	0.00175252
Zm00004b000181	GRMZM2G176585	Zm00001d027447	(1 of 3) PTHR31879:	A0A1D6JM71	Det1 complexing ubi	66.744177	-9.4374569	2.07279808	-4.5530035	0.00000529	0.00113457
Zm00004b009722	GRMZM2G099239	Zm00001d006626	(1 of 32) PF03763 - R	A0A1D6EZ75	Remorin family prote	134.038381	-9.4798187	2.21758152	-4.2748456	0.0000191	0.00367521
Zm00004b031639	GRMZM2G142072	Zm00001d044971	(1 of 3) K15172 - tra	A0A1D6NSG9	Transcription elongat	85.8177719	-9.7999257	1.58831871	-6.1699996	6.83E-10	3.02E-07
Zm00004b036768	GRMZM2G131275	Zm00001d021489	(1 of 23) PF03759 - R	A0A1D6IBJ1	Rop guanine nucleoti	92.4669284	-9.9071476	1.42087283	-6.9725786	3.11E-12	1.91E-09
Zm00004b029791	GRMZM2G048194	Zm00001d037151	(1 of 3) PTHR23354:	A0A1D6LUX5	Erwinia induced prote	503.899342	-9.9154886	0.93584643	-10.595209	3.14E-26	2.31E-22
Zm00004b015296	GRMZM2G095778	Zm00001d018278	(1 of 2) PTHR28039:	B4F9M5	Fatty-acid-binding pr	96.9447582	-9.9763143	1.54298423	-6.4655971	1.01E-10	5.19E-08
Zm00004b011028	AC210013.4_FG014	Zm00001d013030	(1 of 3) PTHR24349/	B4FF99	Calcium-dependent p	100.245209	-10.023864	1.99183346	-5.0324812	4.84E-07	0.00012
Zm00004b026211	GRMZM2G007384	Zm00001d010294	(M=25) PF00627 - UI	A0A1D6FQ91	Ubiquitin-associated/	109.832559	-10.155952	2.31126258	-4.3941144	0.0000111	0.00223943
Zm00004b035448	GRMZM2G515595	Zm00001d019671	(1 of 1) PTHR13527:	A0A1D6HZP9	Ubiquitin family prote	128.430769	-10.382079	1.33796142	-7.7596254	8.52E-15	8.96E-12
Zm00004b031625	GRMZM2G088053	Zm00001d044951	(1 of 54) PF00892 - E	B4FTK8	WAT1-related protein	132.976976	-10.431711	1.93391696	-5.3940843	6.89E-08	0.0000208
Zm00004b012800	GRMZM2G017229	Zm00001d015138		A0A1D6GZI4	Uncharacterized prot	263.006615	-11.415653	2.71423684	-4.2058427	0.000026	0.00487091
Zm00004b004985	GRMZM2G143238	Zm00001d033839	(1 of 10) PF07714//P	C4J1X5	Putative LRR recepto	443.323259	-12.16883	3.42896934	-3.5488303	0.000387	0.04672324
Zm00004b033257	GRMZM2G144730	Zm00001d047054	(1 of 2) PTHR11817/	K7VGL4	Pyruvate kinase (EC	580.352579	-12.557533	1.30571317	-9.6173746	6.75E-22	1.49E-18
Zm00004b037132	GRMZM2G374969	Zm00001d021902	(1 of 1) PTHR16220	B6T966	Transducin/WD40 rep	723.238902	-12.875086	1.22507056	-10.509669	7.80E-26	3.45E-22
Zm00004b039391	GRMZM2G159675	Zm00001d025239	(1 of 1) K12625 - U6	B4FCE3	Sm-like protein LSM6	856.966885	-13.119928	1.24673117	-10.523462	6.74E-26	3.45E-22

TABLE NOTES:

GENEIDs B73v3 GeneIDs were obtained from the W22 GeneIDs using a MaizeGDB syntelogs lookup table made with SynMap

TRANSCRIPTOME: Trimmed reads were aligned using the splice-aware aligner Hisat2, indices were constructed from known exons and splice sites (W22 annotation Zm00004b & assembly Zm-W22-REFERENCE-NRGENE-2.0 as described in the Methods.

DEG & TABULATION: Differential expression analysis was performed separately per tissue (leaf mutant vs. WT or tassel mutant vs. WT) as described in the Methods

TABULATION: This entire table, sorted on col-H, log2(fold-change), includes statistically significant differentially expressed (adjusted p-value <0.05) genes and excludes any genes with fewer than 10 counts across sum of all replicates.

COLUMNS G-L: Columns G-L tabulate output values for the baseMean, the log2(fold-change), along with the associated values for standard error (lfcSE), Wald statistic (stat), pvalue, and adjusted pvalue (padj).

PROVENANCE: Supplementary Table S2 from Mckenna, Gumber, et al., "Maize (Zea mays L.) nucleoskeletal proteins regulate nuclear envelope remodeling…", submitted 12/2020

Table S2b2 (McKenna, Gumber, et al., submitted Dec. 2020)

Figure S3: Multiple Seq Alignment of Transcripts.

Addgene gene ID	Plasmid name	Plasmid type	N-terminal Tag	Backbone Name	Bacterial Resistance
131014	MKAKU41ec	entry vector	mCherry-FLAG-HA	pDONR221	Kanamycin
131015	MKAKU41exp	expression vector	mCherry-FLAG-HA	pH7WG2	Spectinomycin
131016	NCH1ec	entry vector	eGFP-FLAG-HA	pDONR221	Kanamycin
131017	NCH1exp	expression vector	eGFP-FLAG-HA	pH7WG2	Streptomycin
131018	NCH2ec	entry vector	eGFP-FLAG-HA	pDONR221	Kanamycin
131019	NCH2exp	expression vector	eGFP-FLAG-HA	pH7WG2	Spectinomycin
159097	p35S::mCherry-GFP-H	expression vector	mCherry-GFP	pB7FWG2	Spectinomycin

Table S3 is from Mckenna, Gumber, et al., "Maize (Zea mays L.) nucleoskeletal proteins…", submitted 12/2020